# Technische Universität München
# Physik-Department

# Resummation of logarithmic contributions in MSSM Higgs-boson mass calculations

Master Thesis
of
Henning Bahl

written at the
Max-Planck-Institut für Physik, München
3. Juli 2015

Supervisor:
Prof. Dr. Wolfgang Hollik

Max-Planck-Institut für Physik
(Werner-Heisenberg-Institut)

**Abstract**

One of the most promising models for Beyond Standard Model physics is the Minimal Supersymmetric Standard Model (MSSM). It is a distinct feature of the MSSM that the mass of the lightest Higgs boson is calculable in terms of the model parameters. Identifying this Higgs boson with the recently discovered Higgs boson at the LHC, a precision calculation is necessary to fully profit theoretically from the accurateness reached in the measurement of the Higgs boson's mass. Existing Feynman-diagrammatic calculations are already quite accurate for low masses of supersymmetric particles. For heavy supersymmetric particles however, the result contains large logarithms, which need to be resummed. This can be achieved in an effective field theory approach using renormalization group equations. To profit also from the explicit diagrammatic calculation, both methods have to be combined taking care of the different employed renormalization schemes and avoiding double-counting of one- and two-loop terms. This thesis refines this approach by extending it to electroweak contributions and implementing a chargino/neutralino as well as a gluino threshold. Corrections up to $\sim 5$ GeV are found for heavy spectra. In addition, short overviews over supersymmetry, the MSSM and the calculation of the lightest Higgs bosons mass in the different approaches are presented.

# Contents

# Chapter 1

# Introduction

The Standard Model (SM) of particle physics has been developed in the second half of the last century. It is remarkably successful in describing the interactions of fundamental particles. Precise calculations agree astonishingly well with experiments (e.g. the anomalous magnetic moment of the electron, see [1] for an experimental value and [2] for a theoretical prediction) confirming the underlying model. Nevertheless, until recently, one part of the model was missing. The Higgs boson, respectively the Higgs field and therefore the Higgs mechanism developed in the 60s [3–5], is needed to implement mass terms consistently into the SM. Its discovery 3 years ago by ATLAS [6] and CMS [7] was an important breakthrough in particle physics. In a combined analysis [8], they determined the Higgs-boson mass $M_h$ to be

$$M_h = 125.09 \pm 0.21 \pm 0.11 \text{ GeV}. \tag{1.1}$$

Despite of this success, the SM leaves some questions of both experimental and theoretical nature open. Measurements of some observables show deviations of the predicted values (e.g. the anomalous magnetic moment of the muon [9]) or are not explainable in the SM (e.g. observation of neutrino mixing [10, 11]). On the other hand there are several theoretical shortcomings of the SM. The main issues is maybe that it is not able to incorporate gravity in a meaningful way. A more advanced theoretical framework is needed to derive a theory describing all four fundamental forces. Another issues is the so-called hierarchy problem. Quantum effects raise the mass of the Higgs boson to non-acceptable values. This can only be avoided by extremely fine-tuning the SM, which is considered as unnatural.

Several theoretical frameworks have been developed to adress at least some of these problems. One promising candidate is the concept of Supersymmetry (SUSY) relating bosons to fermions. The simplest phenomenologically viable model realising this concept is called Minimal Supersymmetric Standard Model (MSSM). It predicts a bunch of new particles, i.e. each SM-particle gets a superpartner with the same couplings and quantum numbers but for the spin, which is shifted by 1/2. Moreover, the Higgs sector of the MSSM is extended. It consists out of two Higgs doublets. These correspond to 5 physical Higgs bosons, 2 CP-even neutral bosons $h$, $H$ (of which one plays the role of the already discovered SM-like Higgs boson), 1 neutral CP-odd boson $A$, as well as two charged bosons $H^{\pm}$.

So far none of these additional SUSY-particles has been discovered. This does not disprove the MSSM, since due to SUSY-breaking the superpartners can get large masses in comparison to their SM counterparts (albeit this certainly affects the naturalness of the MSSM) making them undetectable with current collider experiments. A second way to constrain the MSSM

are indirect measurements. Through virtual effects the superpartners enter in the calculation of precision observables. Thereby, a comparison between theoretical evaluations and experimental results allows to restrict the parameter space of the model.

Typical precision observables are e.g. the mass of the W-boson $M_W$, the mass of the Z-boson $M_Z$, the electroweak mixing angle $\sin^2 \theta_w$ or the anomalous magnetic moment of the muon $a_\mu$. If examining the MSSM, the Higgs-boson mass can be added to this list. The reason is that the mass of the lightest CP-even Higgs boson is calculable in the MSSM in dependence of the model parameters. At tree-level it is given by $M_h^2 = M_Z^2 \cos^2 2\beta$ (with $\tan \beta$ being the ratio of the vacuum expectation values of the two Higgs doublets). So, the lightest Higgs-boson mass is bounded by $M_Z$ at tree-level, which is clearly in contradiction to the results of the LHC. However, the Higgs-boson mass is significantly raised by loop contributions with the dominant correction being the one-loop top-superpartner contribution. To match the experimental accuracy also other contributions have to be known. The current status is that the complete one-loop [12–14] as well as the dominant two-loop contributions $\propto \mathcal{O}(\alpha_s \alpha_t, \alpha_s \alpha_b, \alpha_t^2, \alpha_t \alpha_b, \alpha_b^2)$ [15–29] are known. They are implemented e.g. in the publicly available program `FeynHiggs` [30].

It has been recognized in the last years that for heavy SUSY-spectra even higher-order contributions are relevant [31]. Since full direct Feynman-diagrammatic (FD) calculations are quite hard already at the two-loop level, effective field theory (EFT) techniques become more and more important to obtain the dominant higher-order contributions. One of them is the use of renormalization group equations (RGEs). They allow to identify and resum logarithmically enhanced terms.

The method has first been applied in [32] and was refined in [26, 33]. The authors of [34] explained apparent mismatches with the result of explicit Feynman-diagrammatic calculations. Further refinements including an all-order resummation have been worked out by [35–38]. In all of the mentioned publications the calculation is performed using only effective field theories. To benefit also from the result of explicit diagrammatic calculations, both approaches have to be combined. This has been already been achieved by the authors of [39] for logarithms appearing in the stop-sector. Their results have been implemented into the program `FeynHiggs`.

It is the subject of this thesis to extend the result of [39] to the electroweak sector, namely to logarithms proportional to the weak gauge couplings. In addition two variable thresholds are considered, above which neutralinos/charginos, respectively gluinos, contribute to the renormalization group running. All results obtained using the RGE approach are consistently combined with the Feynman-diagrammatic calculation.

The thesis is structured as follows. A short introduction to the SM is given in Chapter 2 and to Supersymmetry in Chapter 3. Chapter 4 outlines the MSSM and details on the various particle sectors with a particular emphasis on the Higgs sector and its renormalization. In Chapter 5 the necessary steps in the calculation of the lightest Higgs boson's mass using a FD approach and an EFT approach are explained and the question how both approaches can be combined is discussed. The FD calculation and the corresponding extraction of logarithms needed in this thesis is described in Chapter 6. Chapter 7 details on the resumming of logarithms using RGEs in the EFT approach. The derivation of the scheme conversion formulas is described in Chapter 8. Numerical results are presented in Chapter 9. A conclusion as well as an outlook is given in Chapter 10. In the appendix lengthy equations are written down explicitly and some technical details relevant for the calculations are explained more closely.

# Chapter 2

# The Standard Model

## 2.1 General structure and particle content

The Standard Model (SM) of particle physics is a gauge theory based on the gauge group $SU(3)_C \times SU(2)_L \times U(1)_Y$. The $SU(3)$ subgroup is the origin of the strong interaction, whereas the $SU(2)_L \times U(1)_Y$ subgroup is responsible for the electroweak interactions. The corresponding gauge bosons are

- gluons $G_\mu^a$ for $SU(3)_C$ ($a \in \{1, ..., 8\}$) with the gauge coupling $g_3$

- W-bosons $W_\mu^a$ for $SU(2)_L$ ($a \in \{1, 2, 3\}$) with the gauge coupling $g$

- B-boson $B_\mu$ for $U(1)_Y$ with the gauge coupling $g'$.

In this thesis, $\alpha_s \equiv g_3^2/4\pi$ is sometimes used instead of $g_3$. The W- and B-Bosons correspond to the physical mass eigenstates $W_\mu^\pm$, $Z_\mu$ and the photon $A_\mu$, which can be obtained through rotation of the original states.

The matter fields of the SM are grouped into three generations. In addition to this overlaying structure, the fermion fields can be grouped according to their behaviour under the SM gauge-group transformations:

| | | |
|---|---|---|
| left-handed quark doublets | : | $(\mathbf{3}, \mathbf{2})_{1/6}$ |
| right-handed u-type quarks | : | $(\mathbf{3}, \mathbf{1})_{2/3}$ |
| right-handed d-type quarks | : | $(\mathbf{3}, \mathbf{1})_{-1/3}$ |
| left-handed lepton doublets | : | $(\mathbf{1}, \mathbf{2})_{-1/2}$ |
| right-handed lepton singlets | : | $(\mathbf{1}, \mathbf{1})_{-1}$ |

The first number in the round brackets corresponds to $SU(3)_C$ (triplet or singlet), the second one to $SU(2)_L$ (doublet or singlet) and the subscript to the $U(1)_Y$ quantum number (hypercharge).

In addition to the particles listed above, also so-called Faddeev-Popov ghosts exist in the theory. They are unphysical and enter only as virtual particles into Feynman amplitudes. Their introduction is necessary to cancel the effects of the unphysical timelike and longitudinal polarizations of the gauge bosons in a non-Abelian theory and thus to conserve unitarity [40].

Furthermore, a Higgs sector is needed for the generation of masses.

## 2.2 Higgs sector

Most of the SM particles are massive. This is an apparent problem for the theory, since a mass term in the SM-Lagrangian violates the gauge symmetry. The Higgs mechanism solves this problem by breaking the $SU(2) \times U(1)$ symmetry of the SM spontaneously down to the $U(1)_{\text{em}}$ symmetry of quantum electodynamics (QED). Spontaneous symmetry breaking occurs, if the vacuum state of the theory is less symmetric than the Lagrangian.

The Higgs mechanism is incorporated by introducing a scalar isospin-doublet $\Phi$ with a hypercharge of 1. The Higgs field is coupled to the gauge bosons through the covariant derivative

$$\mathcal{L}_{\text{Higgs,kin.}} = \frac{1}{2}(D_\mu \Phi)^\dagger D^\mu \Phi, \tag{2.1}$$

$$\text{with} \qquad D_\mu = \partial_\mu - ig I_a W^a_\mu + i\frac{g'}{2}B_\mu \tag{2.2}$$

with $I_a$ being the weak isospin of the field on which the covariant derivative acts. The Higgs scalar potential can be parametrized as follows

$$\mathcal{L}_{\text{Higgs,pot.}} = -\mu^2 \Phi^\dagger \Phi + \frac{\lambda}{4}(\Phi^\dagger \Phi)^2. \tag{2.3}$$

To ensure spontaneous symmetry breaking, both $\mu$ and $\lambda$, must be greater than zero. The corresponding non-zero vacuum expectation value (vev) of $\Phi$ can be written as follows

$$\Phi_0 = \begin{pmatrix} 0 \\ v \end{pmatrix} \tag{2.4}$$

$$\text{with} \qquad v = \frac{\sqrt{2}\mu}{\lambda} \approx 174 \text{ GeV [41]}. \tag{2.5}$$

The Higgs-field has to be expanded around the vev to examine the physics of the theory in the phase of the spontaneously broken symmetry,

$$\Phi(x) = \begin{pmatrix} \phi^+(x) \\ v + \frac{1}{\sqrt{2}}(H(x) + i\chi(x)) \end{pmatrix}. \tag{2.6}$$

The newly introduced fields $H$, $\chi$ and $\phi^+$ are defined to have a zero vev. By choosing a specific gauge (namely the unitary gauge) the fields $\chi$ and $\phi^+$ can be eliminated signaling that they are unphysical. The corresponding degrees of freedom are absorbed into the now massive vector boson fields $W$ and $Z$ as longitudinal modes.

The $W$- and $Z$-masses are given by

$$m_W^2 = \frac{v^2}{2}g^2, \tag{2.7}$$

$$m_Z^2 = \frac{v^2}{2}(g^2 + g'^2). \tag{2.8}$$

The corresponding on-shell masses are denoted by $M_W$ and $M_Z$.

For renormalization it is, however, advantageous to work in general gauge. In this case the additional degrees of freedom enter the calculation in the form of non-physical fields named Goldstone bosons.

Also the Higgs field itself gets massive, $m_h^2 = 2\lambda v^2$.

## 2.3   Fermion masses

Fermion masses are obtained by introducing Yukawa terms to the Lagrangian coupling the Higgs-field to the fermions, i.e.

$$\mathcal{L}_{\text{Yuk,quarks}} = -h_d \bar{Q}_L \cdot \Phi d_R - h_u \epsilon^{ab} \bar{Q}_{La} \Phi_b^\dagger u_R + h.c..  \tag{2.9}$$

where $h_u, h_d$ are the Yukawa couplings for the u- and down-type quarks and $Q$ is the corresponding $SU(2)_L$ quark doublet. Plugging in the expansion of $\Phi$ around its vev, the mass of a fermion $f$ is obtained as

$$m_f = h_f v.  \tag{2.10}$$

Instead of the top-Yukawa coupling $h_t$, sometimes $\alpha_t \equiv h_t^2/4\pi$ is used.

## 2.4   Problems of the Standard Model

The Standard Model is well tested in various different physical setups. In nearly all of them it yields very precise predictions for physical observables. Despite this success, there are unsolved problems of both theoretical and experimental nature which remain unsolved in the Standard Model.

The most common ones are listed below.

- The SM fails to predict a suitable candidate for dark matter. Also the measured dark energy density of the universe can not be obtained within the SM. Additionally, the necessary amount of CP-violation to explain the observed baryon-antibaryon assymmetry of the universe is not provided by the SM. Furthermore, neutrino oscillations are not explainable within the SM.

- The fundament force of gravity is not invoked in the SM. General Relativity, the theory of gravity, is not quantiziable in a straightforward manner. At very high energies above the Planck scale $M_{Pl} \approx 10^{19}$ GeV however, quantum effects of gravity become important. A theory of quantum gravity is needed. Therefore, the SM has to be regarded as incomplete. It is seen as a low energy effective theory of a more fundamental underlying theory.

- The loop corrections to the Higgs-boson mass are quadratically divergent. In the simplest case the cut-off scale of the SM is the Planck-scale $M_{Pl}$ leading to the expectation that the Higgs-boson mass is of the same order. To retain it at the electroweak scale extreme fine-tuning regarded as unnatural is necessary. This is called the hierarchy problem.

- The CP-violating $\Theta$-term in the QCD-Lagrangian is measured to be unnaturally small (strong CP-problem).

- In grand unified theories, it is expected that the running gauge couplings unify at one scale called $M_{GUT}$. Using SM renormalization group equations this is not the case.

# Chapter 3

# Supersymmetry

## 3.1 Motivation

Supersymmetry (SUSY) is able to solve some of the issues of the SM.

- Supersymmetry relates fermions to bosons. In this way, the quadratic divergences in the corrections of the Higgs boson mass through SM-particles are cancelled by the contributions of their corresponding superpartners. In other words, the Higgs-boson mass is protected by SUSY. In this way the hierarchy problem is solved (at least if the SUSY breaking scale is not too high).

- Supersymmetric theories provide a candidate for dark matter in the form of the lightest supersymmetric particle (LSP).

- The additional supersymmetric degrees of freedom alter the renormalization group equations such that a much better unification of the three fundamental gauge couplings is obtained at the scale $Q = M_{GUT}$.

## 3.2 General structure

Supersymmetry is a symmetry relating bosons to fermions. Following the No-Go-theorem of Mandula [42], the Poincaré-symmetry can only be extended truly, which means that the extension does not factorize out as a subgroup in form of a gauge group, by a fermionic symmetry meaning that its generators obey anticommutation relations. The authors of [43] showed that the maximal extension can be given by introducing fermionic operators $Q^i_\alpha$ ($0 \leq i < N$) with the algebra (here for $N = 1$)

$$\{Q_\alpha, \bar{Q}_{\dot{\alpha}}\} = 2\sigma^\mu_{\alpha\dot{\beta}}P_\mu, \tag{3.1a}$$

$$\{Q_\alpha, Q_\beta\} = \{\bar{Q}_{\dot{\alpha}}, \bar{Q}_{\dot{\beta}}\} = 0, \tag{3.1b}$$

$$[Q_\alpha, P_\mu] = [\bar{Q}_{\dot{\alpha}}, P_\mu] = 0, \tag{3.1c}$$

where $\sigma^\mu$ are the Pauli-matrices and $P_\mu$ is the Poincaré-generator of translations. $\alpha, \beta \in \{1, 2\}$, the dotted components transform as right-handed Weyl-spinors, the undotted ones as left-handed

Weyl-spinors. Eq. (3.1a) expresses that the application of SUSY-operators can lead to a translation in normal spacetime. This shows the interweavement of SUSY and normal spacetime-symmetry.

The action of the supersymmetry generators $Q$ can be interpreted geometrically by introducing the so-called superspace parametrized by the normal spacetime coordinates $x_\mu$ as well as the additional variables $\theta_\alpha$ and $\bar{\theta}_{\dot{\alpha}}$. The action of $Q_\alpha$, $\bar{Q}_{\dot{\alpha}}$ corresponds to a translation in the $\theta$, $\bar{\theta}$ directions in superspace. It follows out of Eq. 3.1 that $\theta_\alpha$ and $\bar{\theta}_{\dot{\alpha}}$ have to be anticommuting Grassmann-numbers.

Correspondingly, superfields can be defined, which are an extension of the normal fields living in Minkowski space to the superspace. They depend not only on the spacetime coordinates $x_\mu$ but also on the supervariables $\theta_\alpha$, $\bar{\theta}_{\dot{\alpha}}$. The anticommuting character of the $\theta_\alpha$, $\bar{\theta}_{\dot{\alpha}}$ allows to expand a general superfield $S(x_\mu, \theta_\alpha, \theta_{\dot{\alpha}})$ (sums over spinorindices are surpressed in the notation), i.e.

$$S(x_\mu, \theta_\alpha, \bar{\theta}_{\dot{\alpha}}) = \varphi(x) + \theta\psi(x) + \bar{\theta}\bar{\chi}(x) + \theta\theta M(x) + \bar{\theta}\bar{\theta}N(x) + (\theta\sigma^\mu\bar{\theta})V_\mu(x) \tag{3.2}$$
$$+ (\theta\theta)\bar{\theta}\bar{\lambda}(x) + (\bar{\theta}\bar{\theta})\theta\rho(x) + (\theta\theta)(\bar{\theta}\bar{\theta})D(x). \tag{3.3}$$

Using a gerneralized covariant derivative

$$D_\alpha = \partial_\alpha - i\sigma^\mu_{\alpha\dot{\beta}}\bar{\theta}^{\dot{\beta}}\partial_\mu, \tag{3.4}$$
$$\bar{D}^{\dot{\alpha}} = \bar{\partial}^{\dot{\alpha}} - i\bar{\sigma}^{\dot{\alpha}\beta}_\mu\theta_\beta\partial^\mu \tag{3.5}$$

commuting with $Q_\alpha$, $\bar{Q}_{\dot{\alpha}}$, special types of superfields can be defined.

$$\text{left chiral superfield} \ \to \bar{D}^{\dot{\alpha}}\Phi = 0 \tag{3.6}$$
$$\text{right chiral superfield} \ \to D_\alpha\Phi^\dagger = 0 \tag{3.7}$$
$$\text{vector superfield} \ \to V^\dagger = V \tag{3.8}$$

Out of the vector superfields super-fieldstrengths

$$W^a_\alpha \equiv -\frac{1}{4}(\bar{D}\bar{D})D_\alpha V^a \tag{3.9}$$

can be built.

To build a general supersymmetric Lagrangian one observes that only the terms proportional to a maximum number of Grassmann variables (e.g. $D(x)$ in Eq. 3.2) transform under a global supersymmetric transformation such that the corresponding action remains unchanged (see [44], Section 4.6). An integration over the superspace variables $\theta_\alpha$ can be used to project out these components due to the integration rules for Grassmann-numbers (see [44], Section 4.1).

So the most general, supersymmetric and renormalizable Lagrangian containing chiral superfields $\Phi_i$ and vector superfields $V^a$ with a gauge symmetry (generators $T^a$) is given by

$$\mathcal{L}_{SUSY} = \left[\int d^2\theta \left(\frac{1}{4}W^{a,\alpha}W^a_\alpha + \mathcal{W}(\Phi_i)\right) + h.c.\right] + \int d^4\theta \Phi^\dagger_i e^{2g_a T^a V^a}\Phi_i \tag{3.10}$$

with the holomorphic superpotential $\mathcal{W}(\Phi_i) = c_i\Phi_i + \frac{1}{2}m_{ij}\Phi_i\Phi_j + \frac{1}{6}y_{ijk}\Phi_i\Phi_j\Phi_k$.

## 3.3 R-parity

In principle, SUSY-theories allow for baryon- and lepton-number violation. Experimental constraints, like for the lifetime of the proton, require the respective couplings to be very small. Introducing a discrete $\mathbb{Z}_2$-symmetry called R-parity forbids the respective terms. It is defined as

$$R = (-1)^{3(B-L)+2s}, \tag{3.11}$$

where B is baryon number, L is lepton number and s is spin. For SM particles it is $+1$, for sparticles $-1$. As an immediate consequence, a single sparticle can not decay only into SM particles. In other words the lightest supersymmetric particle (LSP) is stable. For realistic spectra the LSP is normally not charged under $SU(3)_C$ and $U(1)_{em}$ and thus provides a perfect dark matter candidate.

## 3.4 Breaking of supersymmetry

If nature realized SUSY as an exact symmetry, the superpartners and their correspond SM particle would have the same mass. Since no sparticle has been discovered so far, SUSY has to be broken. The breaking mechanism is not known so far. Many models of spontaneous symmetry breaking have been proposed, e.g. gravity-mediated breaking [45] or gauge-mediated breaking [46].

For phenomenological studies it is convenient to simply parametrize our ignorance of SUSY breaking by introducing terms into the Lagrangian which explicitly break SUSY. These terms are required to have positive mass dimension in order to give not rise to quadratically divergent corrections to the Higgs boson's mass. Due to this property, they are called soft-breaking terms. They are thought of to be generated by an unknown breaking mechanism.

The possible soft-breaking terms in the Lagrangian of a general supersymmetric theory respecting gauge invariance as well as renormalizability are

$$\mathcal{L}_{\text{soft-breaking}} = -\left(\frac{1}{2}M_a\lambda^a\lambda^a + \frac{1}{6}a_{ijk}\phi_i\phi_j\phi_k + \frac{1}{2}b_{ij}\phi_i\phi_j + c_i\phi_i + \text{h.c.}\right) - m^2_{ij}\phi^*_i\phi_j, \tag{3.12}$$

with $\phi$ being a scalar and $\lambda^a$ being a left-chiral Weyl spinor (see for example [44]).

An immediate consequence of the soft-breaking terms is that the sparticles have a higher mass than their SM-partners. To maintain naturalness the soft-breaking parameters should not be heavier than a few TeV. Otherwise fine-tuning would be become necessary again.

# Chapter 4

# The Minimal Supersymmetric Standard Model

Out of the ingredients described in the previous Section phenomenological supersymmetric models can be built. The simplest physically viable model is a $N = 1$ supersymmetric extension of the SM called Minimal Supersymmetric Standard Model (MSSM), in which the SM fermions of the SM are described by Weyl spinors contained in chiral superfields and SM gauge bosons by vector fields contained in vector superfields. The additional components of the superfields are called superpartners and ensure that the number of fermionic and bosonic degrees of freedom are equal.

## 4.1  Particle content

In the MSSM each particles of the SM gets a superpartner (a tilde is used to denote the superpartner $\tilde{a}$ of a SM particle $a$). Particle and superpartner are grouped in superfields.

The gauge fields of the SM (spin 1) get fermionic superpartners called gauginos (spin 1/2) (see Table 4.1). The specific gauginos are named Bino, Wino and Gluino.

| superfield | particle | superparticle | gauge group |
|:---:|:---:|:---:|:---:|
| $V_Y$ | $B_\mu$ | $\tilde{B}$ | $U(1)_Y$ |
| $V_w$ | $W_\mu$ | $\tilde{W}_\mu$ | $SU(2)_L$ |
| $V_c$ | $G_\mu$ | $\tilde{G}$ | $SU(3)_C$ |

Table 4.1: Gauge sector of the MSSM.

Similary, each SM fermion $f$ ($f = e, \mu, \tau, u, d, c, s, t, b$) gets a scalar superpartner $\tilde{f}$ (spin 0) called like the SM-fermion with a 's' in front. E.g., the superpartner of a top-quark is a stop. The Higgs sector of the MSSM differs from the SM Higgs sector. It consists out of two Higgs doublets ($\mathcal{H}_1$ with $Y = -1$ and $\mathcal{H}_2$ with $Y = +1$). Two doublets are needed to implement Yukawa-couplings for up- ($\mathcal{H}_2$) and down-type quarks ($\mathcal{H}_1$) into the holomorpic superpotential (the holomorphicity of the superpotential ensure that the action is invariant under SUSY-transformations). In addition, in the MSSM gauge anomalies $\propto \mathrm{Tr}\{Y^3\}$ exists (see Figure 4.1). Without the introduction of a second Higgs doublet with opposite hypercharge these anomalies would not cancel. The two Higgs doublets are accomodated by two fermionic $SU(2)_L$

doublets, namely the Higgsinos $\tilde{\mathcal{H}}_1, \tilde{\mathcal{H}}_2$. Higgs and Higgsino doublets are grouped together into the superfields $H_1$ and $H_2$. The matter content of the MSSM is summarized in Table 4.2:

| superfield | components | quantum numbers |
|:---:|:---:|:---:|
| $Q_i$ | $q_{i,L}, \tilde{q}_{i,L}$ | $(\mathbf{3}, \mathbf{2})_{1/3}$ |
| $U_i^C$ | $u_{i,R}^C, \tilde{u}_{i,R}^C$ | $(\bar{\mathbf{3}}, \mathbf{1})_{-4/3}$ |
| $D_i^C$ | $d_{i,R}^C, \tilde{d}_{i,R}^C$ | $(\bar{\mathbf{3}}, \mathbf{1})_{2/3}$ |
| $L_i$ | $l_{i,L}, \tilde{l}_{i,L}$ | $(\mathbf{1}, \mathbf{2})_{-1}$ |
| $E_i^C$ | $e_{i,R}^C, \tilde{e}_{i,R}^C$ | $(\mathbf{1}, \mathbf{1})_2$ |
| $H_1$ | $\mathcal{H}_1, \tilde{\mathcal{H}}_1$ | $(\mathbf{1}, \mathbf{2})_{-1}$ |
| $H_2$ | $\mathcal{H}_2, \tilde{\mathcal{H}}_2$ | $(\mathbf{1}, \mathbf{2})_1$ |

Table 4.2: Matter content of the MSSM.

The superfield content and the gauge group determine most of the structure of the MSSM. Missing pieces like the Yukawa coupling are incorporated in the superpotential. Suppressing generation indices, it is given by

$$\mathcal{W}_{\text{MSSM}} = \mu H_1 \cdot H_2 - \mathbf{h}_e (H_1 \cdot L) E^C - \mathbf{h}_d (H_1 \cdot Q) D^C - \mathbf{h}_u (Q_i \cdot H_2) U^C, \tag{4.1}$$

where $\mathbf{h}_{e,d,u}$ are Yukawa-coupling matrices and $\mu$ is the Higgsino mass parameter (since the corresponding term in the superpotential is necessary to give mass to the Higgsinos). The product of two superfields doublets is defined by ($\epsilon$ is the Levi-Civita-tensor with $\epsilon^{12} = 1$)

$$\Phi_1 \cdot \Phi_2 = \epsilon_{ij} \Phi_1^i \Phi_2^j. \tag{4.2}$$

Specifying the gauge group, the superfield content as well as the superpotential, the Lagrangian is fixed. Most of the mass matrices appearing in the non-SM part of the Lagrangian are not diagonal. The corresponding mass eigenstates are listed in Table 4.3.

| name | spin | gauge eigenstate | mass eigenstate |
|:---:|:---:|:---:|:---:|
| Higgs bosons | 0 | $\mathcal{H}_{1,2}$ | $h, H, A, H^{\pm}$ |
| Goldstone bosons | 0 | $\mathcal{H}_{1,2}$ | $G, G^{\pm}$ |
| squarks | 0 | $\tilde{q}_{L,R}$ | $\tilde{q}_{1,2}$ |
| sleptons | 0 | $\tilde{e}_{L,R}, \tilde{\mu}_{L,R}, \tilde{\tau}_{L,R}, \tilde{\nu}_{e_{L,R}, \mu_{L,R}, \tau_{L,R}}$ | $\tilde{e}_{1,2}, \tilde{\mu}_{1,2}, \tilde{\tau}_{1,2}, \tilde{\nu}_{e_{1,2}, \mu_{1,2}, \tau_{1,2}}$ |
| neutralinos | 1/2 | $\tilde{B}, \tilde{\mathcal{H}}_{1,2}, \tilde{W}^0$ | $\tilde{\chi}_{1,2,3,4}^0$ |
| charginos | 1/2 | $\tilde{\mathcal{H}}_{1,2}^{\pm}, \tilde{W}^{\pm}$ | $\tilde{\chi}_{1,2}^{\pm}$ |
| gluino | 1/2 | $\tilde{g}$ | $\tilde{g}$ |

Table 4.3: Mass eigenstates of the MSSM.
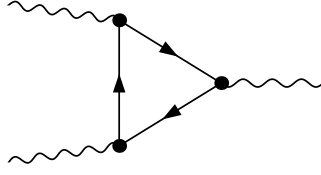
Figure 4.1: Gauge anomaly in the MSSM $\propto \mathrm{Tr}\{Y^3\}$.

## 4.2 Soft-breaking in the MSSM

As discussed in Section 3.4 soft-breaking terms are used to parametrize the ignorance of the SUSY breaking mechanism. Specifying Eq. 3.12 for the MSSM yields ($i, j$ are gneration indices)

$$
\begin{aligned}
\mathcal{L}_{\text{soft-breaking}}^{\text{MSSM}} = &-\frac{1}{2}\left(M_3 \tilde{g}\tilde{g} + M_2 \tilde{W}\tilde{W} + M_1 \tilde{B}\tilde{B} + \text{h.c.}\right) \\
&-\tilde{m}_1 \mathcal{H}_1^\dagger \mathcal{H}_1 - \tilde{m}_2 \mathcal{H}_2^\dagger \mathcal{H}_2 - (b_{\mathcal{H}_1 \mathcal{H}_2} \mathcal{H}_1 \cdot \mathcal{H}_2 + \text{h.c.}) \\
&- \Big[ (\mathbf{h}_u \mathbf{A}_u)_{ij}(\tilde{q}_{L,i} \cdot \mathcal{H}_2)\tilde{u}_{R,j}^* + (\mathbf{h}_d \mathbf{A}_d)_{ij}(\mathcal{H}_1 \cdot \tilde{q}_{L,i})\tilde{d}_{R,j}^* \\
&\quad + (\mathbf{h}_e \mathbf{A}_e)_{ij}(\mathcal{H}_1 \cdot \tilde{l}_{L,i})\tilde{e}_{R,j}^* + \text{h.c.}\Big] \\
&-(m_{\tilde{q}}^2)_{ij}\tilde{q}_{L,i}^*\tilde{q}_{L,j} - (m_{\tilde{u}}^2)_{ij}\tilde{u}_{R,i}^*\tilde{u}_{R,j} - (m_{\tilde{d}}^2)_{ij}\tilde{d}_{R,i}^*\tilde{d}_{R,j} \\
&-(m_{\tilde{l}}^2)_{ij}\tilde{l}_{L,i}^*\tilde{l}_{L,j} - (m_{\tilde{e}}^2)_{ij}\tilde{e}_{R,i}^*\tilde{e}_{R,j}.
\end{aligned}
\tag{4.3}
$$

In principle, some of these terms are flavor-violating. Throughout this thesis flavor violation is neglected. Consequently, the Yukawa coupling matrices $\mathbf{h}$, the trilinear coupling matrices $\mathbf{A}$ as well as the mass-breaking matrices $m_{\tilde{q},\tilde{u},\tilde{d},\tilde{e},\tilde{l}}$ are diagonal.

To extract dominant contributions certain assumptions are made in this thesis. First, all sfermion mass-breaking parameters are assumed to be equal, i.e. ($f = (e, \mu, \tau, u, d, c, s, t, b)$)

$$
m_{\tilde{f},L} = m_{\tilde{f},R} \equiv M_{Susy}.
\tag{4.4}
$$

Second, all lepton and quark mass with the exception of the top-quark mass are neglected ($m_f \simeq 0$ for $f \neq t$). This automatically implies that the off-diagonal entries of the squark/slepton mass matrices (4.6) are set to zero. Therefore, sfermion mixing is neglected (with exception of stop mixing).

Third, the soft-breaking parameters appearing in the electroweak gaugino sector and the Higgsino mass parameter $\mu$ are set equal, i.e.

$$
M_1 = M_2 = \mu \equiv M_\chi.
\tag{4.5}
$$

Forth, all parameters are assumed to be real. Also all other parameters appearing in the MSSM Lagrangian apart of soft-breaking parameters (e.g. the Higgsino mass parameter $\mu$) are assumed to be real.

After specifying the soft-breaking terms in the MSSM, the particular sectors are examined more closely following the notations of [47].

## 4.3 Squark/slepton sector

For each quark $q$ two squarks $\tilde{q}_L$, $\tilde{q}_R$ exist. Their mass matrix is given by

$$\mathbf{M}_{\tilde{q}}^2 = \begin{pmatrix} m_{\tilde{q}_L}^2 + m_q^2 + M_Z^2 \cos 2\beta (I_3^q - Q_q s_w^2) & m_q X_q \\ m_q X_q & m_{\tilde{q}_R}^2 + m_q^2 + M_Z^2 \cos 2\beta Q_q s_w^2 \end{pmatrix}, \tag{4.6}$$

where $I_3^q$ is the isospin, $Q_q$ the electric charge and $m_q$ the mass of the corresponding quark.

The off-diagonal mixing parameter $X_q$ is given in terms of the soft-breaking trilinear coupling parameter $A_q$, the Higgsino mass parameter $\mu$ and the ratio of the vacuum expectation values of the two Higgs doublets $\tan \beta = v_2/v_1$ (see Section 4.6) by

$$X_q \equiv A_q - \mu \{\cot \beta, \tan \beta\}, \tag{4.7}$$

where $\cot \beta$ applies for up-type quarks, respectively $\tan \beta$ for down-type quarks. For the stop squarks this matrix reads

$$\mathbf{M}_{\tilde{t}}^2 = \begin{pmatrix} m_{\tilde{t}_L}^2 + m_t^2 + \cos 2\beta (\frac{1}{2} - \frac{2}{3}s_w^2)M_Z^2 & m_t X_t \\ m_t X_t & m_{\tilde{t}_R}^2 + m_t^2 + \frac{2}{3}\cos 2\beta s_w^2 M_Z^2 \end{pmatrix} \tag{4.8}$$

with $X_t \equiv A_t - \mu \cot \beta$.

These mass matrices are diagonalized by the unitary matrices $\mathbf{U}_{\tilde{q}}$ ($\mathbf{U}_{\tilde{q}}\mathbf{U}_{\tilde{q}}^\dagger = \mathbb{1}$). The masses of the squark mass eigenstates $\tilde{q}_1, \tilde{q}_2$ are then given by

$$m_{\tilde{q}_{1,2}}^2 = m_q^2 + \frac{1}{2}\left[ M_{\tilde{q}_L}^2 + M_{\tilde{q}_R}^2 + I_3^q M_Z^2 \cos 2\beta \right. \tag{4.9}$$

$$\left. \mp \sqrt{[M_{\tilde{q}_L}^2 - M_{\tilde{q}_R}^2 + M_Z^2 \cos 2\beta (I_3^q - 2Q_q s_w^2)]^2 + 4m_q^2 X_q^2} \right]. \tag{4.10}$$

In this thesis, with the exception of stop mixing, squark mixing is neglected. In the case of stop mixing, the masses and entries of the mixing matrix can be expanded in $M_Z/X_t$ in the limit $\mathcal{O}(M_Z) \ll M_{Susy} \equiv M_{\tilde{q}_L} = M_{\tilde{q}_R} \approx X_t$. The analytic results can be found in App. C.1.

## 4.4 Chargino sector

The charginos $\chi_{1,2}^\pm$ are the mass eigenstates of the charged gauginos. Their masses can be obtained out of the mass matrix

$$\mathbf{X} = \begin{pmatrix} M_2 & \sqrt{2}\sin\beta M_W \\ \sqrt{2}\cos\beta M_W & \mu \end{pmatrix}. \tag{4.11}$$

The mass eigenstates are determined by diagonalizing the matrix $\mathbf{X}$ using two unitary 2x2 matrices $\mathbf{U}$ and $\mathbf{V}$. The matrices $\mathbf{U}$ and $\mathbf{V}$ rotate the original wino and higgsino states to the mass states

$$\begin{pmatrix} \tilde{\chi}_1^+ \\ \tilde{\chi}_2^+ \end{pmatrix} = \mathbf{V}\begin{pmatrix} \tilde{W}^+ \\ \tilde{\mathcal{H}}_2^+ \end{pmatrix}, \qquad \begin{pmatrix} \tilde{\chi}_1^- \\ \tilde{\chi}_2^- \end{pmatrix} = \mathbf{U}\begin{pmatrix} \tilde{W}^- \\ \tilde{\mathcal{H}}_1^- \end{pmatrix}. \tag{4.12}$$

The rotation is chosen in a way such that the resulting mass matrix

$$\begin{pmatrix} m_{\tilde{\chi}_1^\pm} & 0 \\ 0 & m_{\tilde{\chi}_2^\pm} \end{pmatrix} = \mathbf{U}^* \mathbf{X} \mathbf{V}^\dagger \tag{4.13}$$
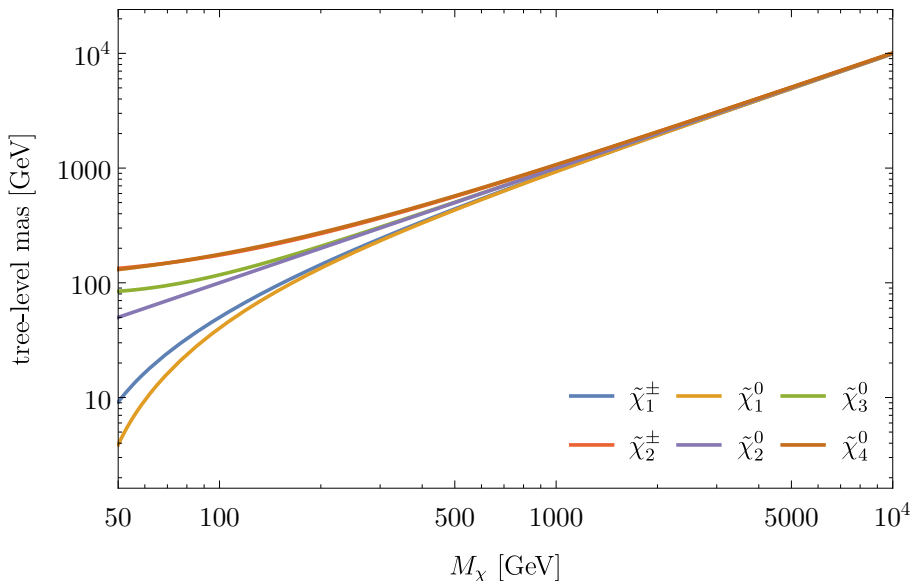
Figure 4.2: Tree-level masses of charginos and neutralinos versus the common mass scale $M_\chi$

is diagonal. Mathematically this corresponds to a singular value decomposition with the masses being the singular values.

In principle analytic expressions for the masses and mixing matrices can be given. Since these expressions are quite complicated and therefore difficult to handle, an approximation is used. The common scale $M_1 = M_2 = \mu \equiv M_\chi$ is assumed to be much larger than $M_Z$ (for a numeric result see Figure 4.2). Therefore the the derived complicated expressions can be expanded in the variable $x_\chi \equiv M_Z/M_\chi$. The resulting expression are listed in App. C.2.

## 4.5 Neutralino sector

The neutralino sector is similar to the chargino sector. In the neutralino sector the matrix

$$\mathbf{Y} = \begin{pmatrix} M_1 & 0 & -M_Z s_w \cos\beta & M_Z s_w \sin\beta \\ 0 & M_2 & M_Z c_w \cos\beta & -M_Z c_w \sin\beta \\ -M_Z s_w \cos\beta & M_Z c_w \cos\beta & 0 & -\mu \\ M_Z s_w \sin\beta & -M_Z c_w \sin\beta & -\mu & 0 \end{pmatrix} \tag{4.14}$$

has to be diagonalized to obtain the mass eigenstates. The abbreviations

$$s_\gamma \equiv \sin\gamma, \qquad c_\gamma \equiv \cos\gamma, \qquad t_\gamma \equiv \tan\beta \tag{4.15}$$

are introduced to keep the expressions short. The electroweak mixing angle $\theta_w$ is abbreviated with the subscript $w$, i.e.

$$c_w = \cos\theta_w = M_W/M_Z. \tag{4.16}$$

The diagonalization is done by using a Takagi transformation [48] such that the resulting mass matrix of the rotated states

$$
\begin{pmatrix} \tilde{\chi}_1^0 \\ \tilde{\chi}_2^0 \\ \tilde{\chi}_3^0 \\ \tilde{\chi}_4^0 \end{pmatrix} = \mathbf{N} \begin{pmatrix} \tilde{B}^0 \\ \tilde{W}^0 \\ \tilde{H}_1^0 \\ \tilde{H}_2^0 \end{pmatrix}
\tag{4.17}
$$

is diagonal, i.e.

$$
\begin{pmatrix} m_{\tilde{\chi}_1^0} & 0 & 0 & 0 \\ 0 & m_{\tilde{\chi}_2^0} & 0 & 0 \\ 0 & 0 & m_{\tilde{\chi}_3^0} & 0 \\ 0 & 0 & 0 & m_{\tilde{\chi}_4^0} \end{pmatrix} = \mathbf{M}_{diag} = \mathbf{N}^* \mathbf{Y} \mathbf{N}^\dagger .
\tag{4.18}
$$

The Takagi factorization can be simplified by first switching to the new basis (this discussion follows [49])

$$
\begin{pmatrix} \tilde{\gamma} \\ \tilde{Z}^0 \\ \tilde{\mathcal{H}}_a^0 \\ \tilde{\mathcal{H}}_b^0 \end{pmatrix} = \mathbf{A} \begin{pmatrix} \tilde{B}^0 \\ \tilde{W}^0 \\ \tilde{\mathcal{H}}_1^0 \\ \tilde{\mathcal{H}}_2^0 \end{pmatrix} = \begin{pmatrix} c_w & s_w & 0 & 0 \\ -s_w & c_w & 0 & 0 \\ 0 & 0 & c_\beta & -s_\beta \\ 0 & 0 & s_\beta & c_\beta \end{pmatrix} \begin{pmatrix} \tilde{B}^0 \\ \tilde{W}^0 \\ \tilde{\mathcal{H}}_1^0 \\ \tilde{\mathcal{H}}_2^0 \end{pmatrix} .
\tag{4.19}
$$

In this basis the (new) mass matrix $\mathbf{Y}_{rot}$ takes the form

$$
\mathbf{Y}_{rot} = \mathbf{A} \mathbf{Y} \mathbf{A}^T = M_\chi \begin{pmatrix} 1 & 0 & 0 & 0 \\ 0 & 1 & x_\chi & 0 \\ 0 & x_\chi & s_{2\beta} & -c_{2\beta} \\ 0 & 0 & -c_{2\beta} & -s_{2\beta} \end{pmatrix}
\tag{4.20}
$$

with $x_\chi = M_Z / M_\chi$.

This matrix is diagonal in the first component. Therefore the original problem of diagonalizing a 4x4 matrix is reduced to the problem of diagonalizing a 3x3 matrix. The new mixing matrix $\mathbf{N}_{rot}$, which diagonalizes $\mathbf{Y}_{rot}$, is now decomposed in a possibly complex Majorana part $\mathbf{M}$ and a real part $\mathbf{D}$ (both are unitary matrices),

$$
\mathbf{N}_{rot} = \mathbf{M}\mathbf{D}, \qquad \mathbf{D}^\dagger \mathbf{D} = \mathbb{1}, \qquad \mathbf{M}^\dagger \mathbf{M} = \mathbb{1},
\tag{4.21}
$$

$$
\mathbf{M}_{diag} = \mathbf{N}_{rot}^* \mathbf{Y}_{rot} \mathbf{N}_{rot}^\dagger
\tag{4.22}
$$

with

$$
\mathbf{M} = \begin{pmatrix} e^{i\alpha_1} & 0 & 0 & 0 \\ 0 & e^{i\alpha_2} & 0 & 0 \\ 0 & 0 & e^{i\alpha_3} & 0 \\ 0 & 0 & 0 & e^{i\alpha_4} \end{pmatrix} .
\tag{4.23}
$$

In the next step the squared mass matrix is considered,

$$
\mathbf{M}_{diag} \mathbf{M}_{diag}^\dagger = \mathbf{D}^* \mathbf{Y}_{rot} \mathbf{Y}_{rot}^\dagger \mathbf{D}^T .
\tag{4.24}
$$

The entries of the matrix $\mathbf{M}_{diag}$ can now be identified with the square roots of the eigenvalues of $\mathbf{M}_{diag}\mathbf{M}_{diag}^\dagger$. The square roots are required to be positive. This is ensured by the matrix $\mathbf{M}$. Its phases can be derived from the equation (following from Eqs. (4.21), (4.22))

$$\mathbf{M}^2\mathbf{M}_{diag} = \mathbf{D}^*\mathbf{Y}_{rot}\mathbf{D}^\dagger. \tag{4.25}$$

In this way the problem of finding the Takagi factorization of the original mass matrix $\mathbf{Y}$ is reduced to finding the eigenvalues and eigenvectors of $\mathbf{Y}_{rot}\mathbf{Y}_{rot}^\dagger$. The original transformation matrix $\mathbf{N}$ is connected to $\mathbf{N}_{rot}$ via

$$\mathbf{N} = \mathbf{N}_{rot}\mathbf{A}. \tag{4.26}$$

In principle, this procedure can be used to derive exact analytic expressions. But even under the assumption $M_1 = M_2 = \mu = M_\chi$ the resulting expressions (for a numeric result see Figure 4.2) are too complex to be used directly. Therefore an expansion in the variable $x_\chi = M_Z/M_\chi$ is employed. The corresponding expressions can be found in App. C.3.

## 4.6 Higgs sector

This Section follows in large parts the discussion in [47].

Since the superpotential must be holomorphic, two Higgs-doublets are needed. Conventionally they are decomposed as follows,

$$\mathcal{H}_1 = \begin{pmatrix} v_1 + \frac{1}{\sqrt{2}}(\phi_1 - i\chi_1) \\ -\phi_1^- \end{pmatrix}, \qquad \mathcal{H}_2 = \begin{pmatrix} \phi_2^+ \\ v_2 + \frac{1}{\sqrt{2}}(\phi_2 + i\chi_2) \end{pmatrix}, \tag{4.27}$$

where $\phi_i$, $\chi_i$ and $\phi^\pm$ are real scalar fields and $v_1, v_2$ are the vacuum expectation values of the doublets. The ratio $v_2/v_1$ is called $\tan\beta$ ($\tan\beta \equiv v_2/v_1$).

In its general form the Higgs potential $V_H$ is given as follows (including the soft breaking terms $m_1^2$, $m_2^2$, $m_{12}^2$ as well as the Higgsino mass parameter $\mu$, which are assumed to be real in this thesis)

$$\begin{aligned} V_H = & m_1^2\mathcal{H}_1^\dagger\mathcal{H}_1 + m_2^2\mathcal{H}_2^\dagger\mathcal{H}_2 + m_{12}^2(\mathcal{H}_1 \cdot \mathcal{H}_2 + \text{h.c.}) + \\ & + \frac{1}{8}(g_1^2 + g_2^2)(\mathcal{H}_1^\dagger\mathcal{H}_1 - \mathcal{H}_2^\dagger\mathcal{H}_2)^2 + \frac{1}{2}g_2^2|\mathcal{H}_1^\dagger\mathcal{H}_2|^2, \end{aligned} \tag{4.28}$$

where $m_{1,2}^2 = \tilde{m}_{1,2}^2 + |\mu|^2$ amd $m_{12}^2 = b_{\mathcal{H}_1\mathcal{H}_2}$.

Plugging in the expressions for $\mathcal{H}_1$ and $\mathcal{H}_2$ yields the Higgs potential in terms of $\phi_i$, $\chi_i$ and $\phi^\pm$,

$$V_H = \text{const.} - T_{\phi_1}\phi_1 - T_{\phi_2}\phi_2 + \frac{1}{2}\left(\phi_1, \phi_2, \chi_1, \chi_2\right)\mathbf{M}_{\phi\phi\chi\chi}\begin{pmatrix} \phi_1 \\ \phi_2 \\ \chi_1 \\ \chi_2 \end{pmatrix} \tag{4.29}$$

$$+ \left(\phi_1^-, \phi_2^+\right)\mathbf{M}_{\phi^\pm\phi^\pm}\begin{pmatrix} \phi_1^+ \\ \phi_2^- \end{pmatrix} + \text{coupling terms.} \tag{4.30}$$

The coefficients $T_{\phi_1}, T_{\phi_2}$, also called tadpoles, are

$$T_{\phi_1} = -\sqrt{2}\left(m_1^2 v_1 - m_{12}^2 v_2 + \frac{1}{4}(g_1^2 + g_2^2)(v_1^2 - v_2^2)v_1\right), \tag{4.31}$$

$$T_{\phi_2} = -\sqrt{2}\left(m_2^2 v_2 - m_{12}^2 v_1 - \frac{1}{4}(g_1^2 + g_2^2)(v_1^2 - v_2^2)v_2\right). \tag{4.32}$$

The mass matrices $\mathbf{M}_{\phi\phi\chi\chi}$ and $\mathbf{M}_{\phi^\pm\phi^\pm}$ are given by

$$\mathbf{M}_{\phi\phi\chi\chi} = \begin{pmatrix} \mathbf{M}_\phi & 0 \\ 0 & \mathbf{M}_{\chi\chi} \end{pmatrix}, \tag{4.33}$$

$$\mathbf{M}_\phi = \begin{pmatrix} m_1^2 + \frac{1}{4}(g_1^2 + g_2^2)(3v_1^2 - v_2^2) & -m_{12}^2 - \frac{1}{2}(g_1^2 + g_2^2)v_1 v_2 \\ -m_{12}^2 - \frac{1}{2}(g_1^2 + g_2^2)v_1 v_2 & m_2^2 + \frac{1}{4}(g_1^2 + g_2^2)(3v_2^2 - v_1^2) \end{pmatrix}, \tag{4.34}$$

$$\mathbf{M}_\chi = \begin{pmatrix} m_1^2 + \frac{1}{4}(g_1^2 + g_2^2)(v_1^2 - v_2^2) & -m_{12}^2 \\ -m_{12}^2 & m_2^2 + \frac{1}{4}(g_1^2 + g_2^2)(v_2^2 - v_1^2) \end{pmatrix}, \tag{4.35}$$

$$\mathbf{M}_{\phi^\pm\phi^\pm} = \begin{pmatrix} m_1^2 + \frac{1}{4}g_1^2(v_1^2 - v_2^2) + \frac{1}{4}g_2^2(v_1^2 + v_2^2) & -m_{12}^2 - \frac{1}{2}g_2^2 v_1 v_2 \\ -m_{12}^2 - \frac{1}{2}g_2^2 v_1 v_2 & m_2^2 + \frac{1}{4}g_1^2(v_2^2 - v_1^2) + \frac{1}{4}g_2^2(v_1^2 + v_2^2) \end{pmatrix}. \tag{4.36}$$

The mass eigenstates can be obtained by an unitary transformation of the $\phi, \chi$ basis:

$$\begin{pmatrix} h \\ H \\ A \\ G \end{pmatrix} = \mathbf{U}_n \cdot \begin{pmatrix} \phi_1 \\ \phi_2 \\ \chi_1 \\ \chi_2 \end{pmatrix}, \qquad \begin{pmatrix} H^\pm \\ G^\pm \end{pmatrix} = \mathbf{U}_c \cdot \begin{pmatrix} \phi_1^\pm \\ \phi_2^\pm \end{pmatrix} \tag{4.37}$$

The unitary matrices $\mathbf{U}_n$ and $\mathbf{U}_c$ can be parametrized using the angles $\alpha$, $\beta_n$ and $\beta_c$, i.e.

$$\mathbf{U}_n = \begin{pmatrix} -\sin\alpha & \cos\alpha & 0 & 0 \\ \cos\alpha & \sin\alpha & 0 & 0 \\ 0 & 0 & -\sin\beta_n & \cos\beta_n \\ 0 & 0 & \cos\beta_n & \sin\beta_n \end{pmatrix}, \qquad \mathbf{U}_c = \begin{pmatrix} -\sin\beta_c & \cos\beta_c \\ \cos\beta_c & \sin\beta_c \end{pmatrix}. \tag{4.38}$$

In this new basis the Higgs-potential reads

$$\begin{aligned} V_H =& \text{const.} - T_h \cdot h - T_H \cdot H \\ &+ \frac{1}{2}(h, H, A, G) \cdot \begin{pmatrix} m_h^2 & m_{hH}^2 & 0 & 0 \\ m_{hH}^2 & m_H^2 & 0 & 0 \\ 0 & 0 & m_A^2 & m_{AG}^2 \\ 0 & 0 & m_{AG}^2 & m_G^2 \end{pmatrix} \cdot \begin{pmatrix} h \\ H \\ A \\ G \end{pmatrix} + \\ &+ (H^-, G^-) \cdot \begin{pmatrix} m_{H^\pm}^2 & m_{H^-G^+}^2 \\ m_{G^-H^+}^2 & m_{G^\pm}^2 \end{pmatrix} \cdot \begin{pmatrix} H^+ \\ G^+ \end{pmatrix} + \\ &+ \text{coupling terms.} \end{aligned} \tag{4.39}$$

Using the modified mass formulas for the massive gauge bosons ($v^2 \to v_1^2 + v_2^2$ in the MSSM)

$$M_Z^2 = \frac{1}{2}(g_1^2 + g_2^2)(v_1^2 + v_2^2), \tag{4.40}$$

$$M_W^2 = \frac{1}{2} g_2^2 (v_1^2 + v_2^2), \tag{4.41}$$

the masses $m_x^2$ can be expressed in terms of $s_w, c_w, M_Z^2, M_W^2, \tan\beta$, the tadpoles $T_x$, the angles $\alpha, \beta_c, \beta_n$ and either $m_A$ or $m_{H^\pm}$ (here $m_A$ is chosen). The entries involving CP-even Higgs bosons read

$$
\begin{aligned}
m_h^2 = & \; M_Z^2 \sin^2(\alpha + \beta) \\
& + m_A^2 \cos^2(\alpha - \beta) / \cos^2(\beta - \beta_n) \\
& + \frac{e}{2 M_Z s_w c_w} T_H \cos(\alpha - \beta) \sin^2(\alpha - \beta_n) / \cos^2(\beta - \beta_n) \\
& + \frac{e}{2 M_Z s_w c_w} T_h \frac{1}{2} \sin(\alpha - \beta_n)(\cos(2\alpha - \beta - \beta_n) + 3\cos(\beta - \beta_n)) / \cos^2(\beta - \beta_n),
\end{aligned}
\tag{4.42a}
$$

$$
\begin{aligned}
m_{hH}^2 = & - M_Z^2 \sin(\alpha + \beta) \cos(\alpha + \beta) \\
& + m_A^2 \sin(\alpha - \beta) \cos(\alpha - \beta) / \cos^2(\beta - \beta_n) \\
& + \frac{e}{2 M_Z s_w c_w} T_H \sin(\alpha - \beta) \sin^2(\alpha - \beta_n) / \cos^2(\beta - \beta_n) \\
& - \frac{e}{2 M_Z s_w c_w} T_h \cos(\alpha - \beta) \cos^2(\alpha - \beta_n) / \cos^2(\beta - \beta_n),
\end{aligned}
\tag{4.42b}
$$

$$
\begin{aligned}
m_H^2 = & \; M_Z^2 \cos^2(\alpha + \beta) \\
& + m_A^2 \sin^2(\alpha - \beta) / \cos^2(\beta - \beta_n) \\
& + \frac{e}{2 M_Z s_w c_w} T_H \frac{1}{2} \cos(\alpha - \beta_n)(\cos(2\alpha - \beta - \beta_n) - 3\cos(\beta - \beta_n)) / \cos^2(\beta - \beta_n) \\
& + \frac{e}{2 M_Z s_w c_w} T_h \sin(\alpha - \beta) \cos^2(\alpha - \beta_n) / \cos^2(\beta - \beta_n).
\end{aligned}
\tag{4.42c}
$$

Out of requirement that $v_1$ and $v_2$ are indeed the vacuum expectation values of the Higgs potential follows that the tadpoles vanish at lowest order. To obtain diagonal mass matrices (in Eq. (4.39)), the corresponding off-diagonal elements have to vanish. It follows that (at tree-level)

$$\beta_c = \beta_n = \beta. \tag{4.43}$$

The mixing angle $\alpha$ can be calculated by demanding that $m_{hH}^2$ should be zero. Alternatively, one can diagonalize the matrix $\mathbf{M}_\phi$ (4.34) directly. Both ways result in the tree-level prediction

$$m_h^2 = \frac{1}{2} \left( m_A^2 + M_Z^2 - \sqrt{(m_A^2 + M_Z^2)^2 - 4 m_A^2 M_Z^2 \cos^2 2\beta} \right), \tag{4.44}$$

$$m_H^2 = \frac{1}{2} \left( m_A^2 + M_Z^2 + \sqrt{(m_A^2 + M_Z^2)^2 - 4 m_A^2 M_Z^2 \cos^2 2\beta} \right), \tag{4.45}$$

$$m_{H^\pm}^2 = m_A^2 + M_W^2 \tag{4.46}$$

for the masses of the Higgs bosons. The mixing angle $\alpha$ reads

$$\alpha = \arctan\left[ -\frac{(m_A^2 + M_Z^2) \sin\beta \cos\beta}{M_Z^2 \cos^2\beta + m_A^2 \sin^2\beta - m_h^2} \right]. \tag{4.47}$$
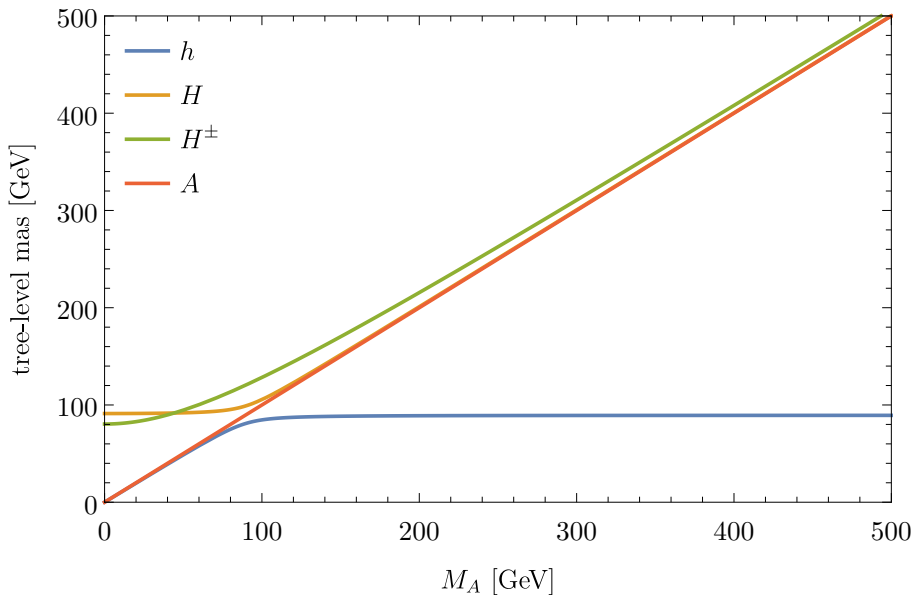
Figure 4.3: Tree-level Higgs-boson masses in dependence of $M_A$ for $\tan\beta = 10$.

Conventionally, one choose $-\frac{\pi}{2} < \alpha < 0$. Alternatively one can write

$$\frac{\tan 2\alpha}{\tan 2\beta} = \frac{m_A^2 + M_Z^2}{m_A^2 - M_Z^2}. \tag{4.48}$$

In contrast to the tree-level Higgs-boson masses, a Higgs-boson mass is denoted with a capitalized $M$, if higher-order corrections are included. In this notation $m_A = M_A$, since the tree-level mass $m_A$ does not receive any higher-order corrections in the used on-shell scheme (see Section 4.7).

Figure 4.3 shows the tree-level masses in dependence of the mass of the $A$-boson. For rising $M_A$ the masses of the $H$- and $H^\pm$-bosons rise too. In particular the mass of the $H$-boson converges to $M_A$. In contrast the mass of the lightest CP-even Higgs $M_h$ remains constant ($m_h \leq M_Z$). In other words the lightest CP-even Higgs decouples from the other Higgs bosons (the limit $M_A \gg M_Z$ is also called decoupling limit). This means that for energies $\sim M_Z$ the Higgs sector of the MSSM is hardly distinguishable from the one of the SM, if $M_A \gg M_Z$.

## 4.7 Renormalization of the MSSM Higgs sector

The tree-level prediction for $M_h$ (Eq. (4.44)) receives large quantum corrections. Computing them naively leads to divergent terms. To avoid these divergences, the MSSM and i.e. the Higgs sector of the MSSM have to be renormalized. The notation in this Section follows closely the conventions of [47].

### 4.7.1 Renormalization schemes

In principle, renormalization can be carried out in various ways. The most important requirement is that after renormalization all divergences appearing in Green's functions are canceled.

To reach this cancellation, counterterms have to be introduced into the Lagrangian by expressing each unrenormalized, 'bare' quantity $g$ through the sum of a renormalized finite quantity $g_{\text{ren}}$ and a counterterm $\delta g$, i.e.

$$g \to g_{\text{ren}} + \delta g. \tag{4.49}$$

Also the fields have to be renormalized,

$$\phi \to \sqrt{Z_\phi}\phi = \sqrt{1 + \delta Z_\phi}\phi. \tag{4.50}$$

In this way

$$\mathcal{L}_{\text{bare}} \to \mathcal{L}_{\text{ren}} + \mathcal{L}_{\text{counterterms}}. \tag{4.51}$$

The counterterms have to be chosen such that all appearing divergences cancel in the final result.

The first step in this procedure is to regularize the appearing divergent loop integrals. In this thesis, dimensional regularization (DREG) is chosen as regularization scheme. In dimensional regularization the dimension of the loop integrals is shifted from 4 to $D = 4 - 2\epsilon$ ($\epsilon > 0$),

$$\int \frac{d^4 k}{(2\pi)^4} \to \mu^{4-D} \int \frac{d^D k}{(2\pi)^D}. \tag{4.52}$$

The at first hand arbitrary renormalization scale $\mu$ (mass dimension 1) has to be introduced to preserve the overall mass dimension of the integral. After shifting the integral to dimension $D$, it can be calculated analytically. The result can be expanded in $\epsilon$. Terms proportional to an inverse power of $\epsilon$ reflect the original divergence. In this way, the divergences are parametrized in an analytic form, which allows to choose the counterterms such that these divergences cancel in the final result.

In the simplest scheme, the minimal subtraction (MS) scheme, the counterterms are chosen such that only the divergent terms are canceled. In the slightly modified $\overline{\text{MS}}$-scheme, also the additionally appearing terms $\propto \ln 4\pi - \gamma_E$ ($\gamma_E = -\Gamma'(1)$) are absorbed meaning that all terms proportional to

$$\Delta = \frac{1}{\epsilon} + \ln 4\pi - \gamma_E \tag{4.53}$$

are removed by choosing the counterterms accordingly. A list of one- and two-point one-loop integrals calculated using DREG can be found in App. D.

In DREG all four dimensional objects are shifted to $D$ dimensions. This implies that the number of bosonic and fermionic degrees of freedom are changed asymmetrical. In other words, DREG breaks supersymmetry. Therefore, in supersymmetric theories dimensional reduction (DRED) is used for the regularization of loop integrals. DRED resembles DREG in the way that it shifts the dimension of momenta and loop integral measures to $D$-dimensions. But, all other four-dimensional objects are left untouched. Thus, supersymmetry is conserved. The DRED renormalization-scheme corresponding to $\overline{\text{MS}}$ in DREG is called $\overline{\text{DR}}$ (for a detailed description of $\overline{\text{DR}}$, see [50]).

A particular scheme well-suited for calculating physical observables is the on-shell scheme. Basically, it is defined such that the pole of a loop-corrected propagator corresponds to the physical mass of the propagating particle. This corresponds to the condition that the renormalized

one-particle irreducible two-point function (the hat marks a renormalized and therefore finite quantity)

$$\hat{\Gamma}(p^2) = i(p^2 - M^2) + i\hat{\Sigma}(p^2), \tag{4.54}$$

where $M$ is the renormalized mass, is zero for $p^2 = M^2$. The quantity

$$\hat{\Sigma}(p^2) = \Sigma(p^2) + \text{ counterterms} \tag{4.55}$$

is the sum of one-particle irreducible loop diagrams with two external legs. This sum is called self-energy. Out of the condition $\hat{\Gamma}(p^2 = M^2) = 0$ follows immediately that

$$\text{Re } \hat{\Sigma}(p^2 = M^2) = 0. \tag{4.56}$$

has to be fulfilled. This condition has only to be fulfilled for the real part, since strictly speaking just the real part of the denominator of the propagator has to be zero for $p^2 = M^2$, whereas $\hat{\Sigma}$ can be complex in general (i.e. above particle thresholds). This is the on-shell renormalization condition. It can be extended by demanding that the field renormalization constants should be fixed such that the residues of all propagators are equal to 1.

### 4.7.2 Counterterms

Applying this procedure for the parameters in the Higgs potential of the the MSSM, counterterms have to be introduced in the first step,

$$M_Z^2 \to M_Z^2 + \delta M_Z^2, \tag{4.57a}$$
$$M_W^2 \to M_W^2 + \delta M_W^2, \tag{4.57b}$$
$$T_h \to T_h + \delta T_h, \tag{4.57c}$$
$$T_H \to T_H + \delta T_H, \tag{4.57d}$$
$$T_A \to T_A + \delta T_A, \tag{4.57e}$$
$$\tan\beta \to \tan\beta + \delta\tan\beta. \tag{4.57f}$$

This implies that the mass matrices get counterterm contributions,

$$\mathbf{M}_{hHAG} \to \mathbf{M}_{hHAG} + \delta\mathbf{M}_{hHAG} = \begin{pmatrix} \delta m_h^2 & \delta m_{hH}^2 & 0 & 0 \\ \delta m_{hH}^2 & \delta m_H^2 & 0 & 0 \\ 0 & 0 & \delta m_A^2 & \delta m_{AG}^2 \\ 0 & 0 & \delta m_{AG}^2 & \delta m_G^2 \end{pmatrix}, \tag{4.58}$$

$$\mathbf{M}_{H^\pm G^\pm} \to \mathbf{M}_{H^\pm G^\pm} + \delta\mathbf{M}_{H^\pm G^\pm} = \begin{pmatrix} \delta m_{H^\pm}^2 & \delta m_{H^- G^+}^2 \\ \delta m_{G^- H^+}^2 & \delta m_{G^\pm}^2 \end{pmatrix}. \tag{4.59}$$

Eqs. (4.42a)-(4.42c) relate the counterterms to each other such that only the counterterms given in Eq. (4.57a)-(4.57f) and $\delta m_A^2$ remain. E.g., the mass-counterterms of the CP-even entries of the neutral Higgs-boson mass matrix defined in Eq. (4.58) read

$$\delta m_h^2 = \delta m_A^2 \cos^2(\alpha - \beta) + \delta M_Z^2 \sin^2(\alpha + \beta)$$
$$+ \frac{e}{2M_Z s_w c_w} \left( \delta T_H \cos(\alpha - \beta) \sin^2(\alpha - \beta) + \delta T_h \sin(\alpha - \beta)(1 + \cos^2(\alpha - \beta)) \right)$$
$$+ \delta \tan \beta \sin \beta \cos \beta \left( m_A^2 \sin 2(\alpha - \beta) + M_Z^2 \sin 2(\alpha + \beta) \right), \tag{4.60a}$$

$$\delta m_{hH}^2 = \frac{1}{2} \left( \delta m_A^2 \sin 2(\alpha - \beta) - \delta M_Z^2 \sin 2(\alpha + \beta) \right)$$
$$+ \frac{e}{2M_Z s_w c_w} \left( \delta T_H \sin^3(\alpha - \beta) - \delta T_h \cos^3(\alpha - \beta) \right)$$
$$- \delta \tan \beta \sin \beta \cos \beta \left( m_A^2 \cos 2(\alpha - \beta) + M_Z^2 \cos 2(\alpha + \beta) \right), \tag{4.60b}$$

$$\delta m_H^2 = \delta m_A^2 \sin^2(\alpha - \beta) + \delta M_Z^2 \cos^2(\alpha + \beta)$$
$$- \frac{e}{2M_Z s_w c_w} \left( \delta T_H \cos(\alpha - \beta)(1 + \sin^2(\alpha - \beta)) + \delta T_h \sin(\alpha - \beta) \cos^2(\alpha - \beta) \right)$$
$$- \delta \tan \beta \sin \beta \cos \beta \left( m_A^2 \sin 2(\alpha - \beta) + M_Z^2 \sin 2(\alpha + \beta) \right). \tag{4.60c}$$

In addition to the mass renormalization, also the fields have to be renormalized to guarantee the finiteness of all appearing Green's functions,

$$\mathcal{H}_1 \to \left( 1 + \frac{1}{2} \delta Z_{\mathcal{H}_1} \right) \mathcal{H}_1, \tag{4.61}$$

$$\mathcal{H}_2 \to \left( 1 + \frac{1}{2} \delta Z_{\mathcal{H}_2} \right) \mathcal{H}_2. \tag{4.62}$$

Corresponding to Eq. 4.58, field renormalization constants for the mass eigenstates are defined, i.e.

$$\begin{pmatrix} h \\ H \\ A \\ G \end{pmatrix} \to \begin{pmatrix} 1 + \frac{1}{2} \delta Z_{hh} & \frac{1}{2} \delta Z_{hH} & 0 & 0 \\ \frac{1}{2} \delta Z_{hH} & 1 + \frac{1}{2} \delta Z_{HH} & 0 & 0 \\ 0 & 0 & 1 + \frac{1}{2} \delta Z_{AA} & \frac{1}{2} \delta Z_{AG} \\ 0 & 0 & \frac{1}{2} \delta Z_{AG} & 1 + \frac{1}{2} \delta Z_{GG} \end{pmatrix} \cdot \begin{pmatrix} h \\ H \\ A \\ G \end{pmatrix}. \tag{4.63}$$

For the mass matrix of the charged Higgs this reads

$$\begin{pmatrix} H^\pm \\ G^\pm \end{pmatrix} \to \begin{pmatrix} 1 + \frac{1}{2} \delta Z_{H^\pm H^\pm} & \frac{1}{2} \delta Z_{H^\pm G^\pm} \\ \frac{1}{2} \delta Z_{H^\pm G^\pm} & 1 + \frac{1}{2} \delta Z_{G^\pm G^\pm} \end{pmatrix} \cdot \begin{pmatrix} H^\pm \\ G^\pm \end{pmatrix}. \tag{4.64}$$

These counterterms are related to the field renormalization constants of the overall doublets (Eqs. (4.61) and (4.62)) by the rotation to the mass eigenstate basis (see Eq. (4.37)). It follows e.g. for the CP-even entries that

$$\delta Z_{hh} = s_\alpha^2 \delta Z_{\mathcal{H}_1} + c_\alpha^2 \delta Z_{\mathcal{H}_2}, \tag{4.65a}$$
$$\delta Z_{hH} = s_\alpha c_\alpha (Z_{\mathcal{H}_2} - Z_{\mathcal{H}_1}), \tag{4.65b}$$
$$\delta Z_{HH} = c_\alpha^2 \delta Z_{\mathcal{H}_1} + s_\alpha^2 \delta Z_{\mathcal{H}_2}. \tag{4.65c}$$

Corresponding formulas for the CP-odd entries can be found in [47].

### 4.7.3 Renormalization conditions

To fix the counterterms, renormalization conditions have to be chosen. Here, the scheme of [47], which is basically an OS-scheme apart of the $\overline{\text{DR}}$-renormalization of the Higgs fields, is chosen (this is also the scheme used for the corrections implemented into `FeynHiggs`).

For the massive gauge bosons $Z$ and $W$, the on-shell condition reads (see [51])

$$\text{Re } \hat{\Sigma}_{ZZ}(M_Z^2) = 0, \quad \text{Re } \hat{\Sigma}_{WW}(M_W^2) = 0, \tag{4.66}$$

where $\hat{\Sigma}_{ZZ}$ is the renormalized $Z$ self-energy and $\hat{\Sigma}_{WW}$ is the renormalized $W$ self-energy (see Figure 6.2 for $Z$ self-energy diagrams). This implies for the corresponding counterterms that

$$\delta M_Z^2 = \text{Re } \Sigma_{ZZ}(M_Z^2), \quad \delta M_W^2 = \text{Re } \Sigma_{WW}(M_W^2). \tag{4.67}$$

Also the $A$-boson is renormalized on-shell,

$$\text{Re } \hat{\Sigma}_{AA}(M_A^2) = 0, \tag{4.68}$$

with $\hat{\Sigma}_{AA}$ being the renormalized $A$-boson self-energy (see Figure 6.1 for $A$-boson self-energy diagrams). This implies

$$\delta M_A^2 = \text{Re } \Sigma_{AA}(M_A^2). \tag{4.69}$$

Furthermore, one demands that tadpole diagrams should vanish to ensure that $v_{1,2}$ are still the true vacua if considering higher-order corrections to the Higgs potential. To achieve this the tadpole counterterms have to be chosen accordingly,

$$\delta T_h = -T_{h(1)}, \quad \delta T_H = -T_{H(1)}, \tag{4.70}$$

where $T_{h(1)}$ and $T_{H(1)}$ are the sum of one-loop $h/H$-boson tadpole diagrams depicted in Figure 6.3 (the same condition applies for higher-order tadpole corrections). In the on-shell scheme the field renormalization constants are normally chosen such that the residua of the propagators are equal zero. It is in principle possible to use this strategy here for the determination of the field renormalization of the $A$-boson (see e.g. [13]). Nevertheless, it was shown that this procedure yields numerical unstable results. A better working alternative is to renormalize the fields using $\overline{\text{DR}}$ renormalization conditions (for a discussion of this issue, see [52]). The $\overline{\text{DR}}$ renormalization conditions for the field renormalization constants read

$$\delta Z_{\mathcal{H}_1} = \delta Z_{\mathcal{H}_1}^{\overline{\text{DR}}} = - \left[ \text{Re } \Sigma'_{HH}(p^2)_{\alpha=0} \right]^{\text{div}}, \tag{4.71}$$

$$\delta Z_{\mathcal{H}_2} = \delta Z_{\mathcal{H}_2}^{\overline{\text{DR}}} = - \left[ \text{Re } \Sigma'_{hh}(p^2)_{\alpha=0} \right]^{\text{div}}, \tag{4.72}$$

$$\delta \tan\beta = \frac{1}{2}(\delta Z_{\mathcal{H}_1} - \delta Z_{\mathcal{H}_2}) = \delta \tan\beta^{\overline{\text{DR}}}. \tag{4.73}$$

where $\Sigma'_{hh}$ and $\Sigma'_{HH}$ are the derivatives of the $h$- and $H$-boson self-energies with respect to $p^2$ (see Figure 6.1 for the respective diagrams). By this procedure a renormalization scale $\mu^{\overline{\text{DR}}}$ is introduced. In principle, it can be fixed freely. In this thesis, the default value of `FeynHiggs` is adopted, which is $\mu^{\overline{\text{DR}}} = m_t$.

### 4.7.4 Renormalized $h$, $H$ self-energies

Using the counterterms derived above, the renormalized Higgs self-energies of the $h$- and $H$-bosons can be written in terms of the unrenormalized self-energies. The field renormalization counterterms are necessary to cancel momentum dependent divergences.

Using the terminology of Eq. (4.55), the renormalized self-energies for the CP-even part of the Higgs-sector read as follows,

$$\hat{\Sigma}_{hh}(p^2) = \Sigma_{hh}(p^2) + \delta Z_{hh}(p^2 - m_h^2) - \delta m_h^2, \tag{4.74a}$$

$$\hat{\Sigma}_{hH}(p^2) = \Sigma_{hH}(p^2) + \delta Z_{hH}\left(p^2 - (m_h^2 + m_H^2)/2\right) - \delta m_{hH}^2, \tag{4.74b}$$

$$\hat{\Sigma}_{HH}(p^2) = \Sigma_{HH}(p^2) + \delta Z_{HH}(p^2 - m_H^2) - \delta m_H^2, \tag{4.74c}$$

with the entries of Eqs. (4.60) and (4.65). $\hat{\Sigma}_{hH}$ is the mixed $h$, $H$ self-energy (one $h$-boson and one $H$-boson as external legs) leading to coupled propagators. This means that the two-point function $\hat{\Gamma}$ for the $h$, $H$ bosons has matrix form (see Eq. (5.1)). These renormalized self-energies can now be used to calculate corrections to the Higgs boson masses (see Section 5.1).

# Chapter 5

# Calculation of $M_h$ - methods

The most straightforward way to calculate loop corrections to the lightest Higgs-boson mass is the Feynman-diagrammatic (FD) approach (see Section 5.1). Basically, this means calculating the Higgs self-energies by evaluating the corresponding Feynman diagrams. Nevertheless, this method has some shortcomings. I.e. for heavy sparticles higher-order contributions, which are not feasible in the Feynman-diagrammatic approach, become important. This is explained in Section 5.1. The issue can be solved within an effective field theory (EFT) framework. Renormalization group equations allow to resum the potentially large higher-order corrections effectively (see Section 5.3). However, in this EFT framework certain aspects of the MSSM, like the influence of complex parameters and non-degenerate mass spectra, are difficult to handle especially for light SUSY spectra. So the best way seems to combine both approaches. The method how to achieve this is described in Section 5.4.

## 5.1 Feynman-diagrammatic approach

To obtain the physical, loop-corrected mass of the lightest CP-even Higgs $M_h$, the poles of the inverse Higgs propagator matrix have to be found. This matrix is given by

$$\hat{\Gamma}_{hH} = i \begin{pmatrix} p^2 - m_h^2 + \hat{\Sigma}_{hh}(p^2) & \hat{\Sigma}_{hH}(p^2) \\ \hat{\Sigma}_{hH}(p^2) & p^2 - m_H^2 + \hat{\Sigma}_{HH}(p^2) \end{pmatrix} \tag{5.1}$$

with the renormalized self-energies $\hat{\Sigma}_{hh}$, $\hat{\Sigma}_{hh}$ and $\hat{\Sigma}_{HH}$ given in Eq. (4.74a). In the complex MSSM, the matrix has to be enlarged to include A-boson contributions.

Finding the poles corresponds to solving the quadratic equation (for $p^2$)

$$\left(p^2 - m_h^2 + \hat{\Sigma}_{hh}(p^2)\right) \left(p^2 - m_H^2 + \hat{\Sigma}_{HH}(p^2)\right) - \left(\hat{\Sigma}_{hH}(p^2)\right)^2 = 0. \tag{5.2}$$

Solving this equation analytically is challenging, since the dependence of the self-energies on $p^2$ can be complex. In general, the loop-corrected lightest Higgs-boson mass can be expanded as

$$M_h^2 = m_{h,tree}^2 + \Delta M_{h,1L}^2 + \Delta M_{h,2L}^2 + \dots . \tag{5.3}$$

The self-energies incorporate only loop terms. In consequence plugging in the 1-loop corrected $M_h^2$ into the 1-loop self energies leads to two-loop terms. Therefore, it is sufficient to use the

(known) tree-level mass $m_h^2$ as input for the 1-loop self energies, if one is interested only in the one-loop correction,

$$\left(p^2 - m_h^2 + \hat{\Sigma}_{hh}(m_h^2)\right)\left(p^2 - m_H^2 + \hat{\Sigma}_{HH}(m_h^2)\right) - \left(\hat{\Sigma}_{hH}(m_h^2)\right)^2 + \mathcal{O}(k^2) = 0, \tag{5.4}$$

where $k \equiv 1/(16\pi^2)$ is used to keep track of the loop order. Using the approximation $p^2 = 0$ for the self-energies leads to an incomplete result, since in this way terms proportional to the weak gauge couplings ($\mathcal{O}(g^2, g'^2)$) are missed already at the one-loop level.

The solution to Eq. (5.4) is (the argument of the $\hat{\Sigma}$'s is omitted),

$$M_{h,H} = \frac{1}{2}\left(m_h^2 + m_H^2 - \hat{\Sigma}_{hh} - \hat{\Sigma}_{HH} \mp \sqrt{4\left(\hat{\Sigma}_{hH}\right)^2 + \left(m_h^2 - m_H^2 - \hat{\Sigma}_{hh} + \hat{\Sigma}_{HH}\right)^2}\right)$$
$$+ \mathcal{O}(k^2). \tag{5.5}$$

Considering that the self-energies $\hat{\Sigma}$ are formally at least of one-loop order, this result can be expanded in $\hat{\Sigma}$,

$$M_h^2 = m_h^2 - \hat{\Sigma}_{hh}(m_h^2) + \mathcal{O}(k^2), \tag{5.6}$$
$$M_H^2 = m_H^2 - \hat{\Sigma}_{HH}(m_H^2) + \mathcal{O}(k^2). \tag{5.7}$$

The issue arising within this approach can already be spotted in the dominant one-loop correction to the lightest Higgs-boson mass. At the one-loop level, contributions proportional to the strong gauge coupling are absent, since the Higgs boson neither couples directly to the gluon nor the gluino. In consequence the top-Yukawa coupling becomes dominant. A straightforward one-loop diagrammatic calculation restricted to diagrams involving the top-Yukawa coupling yields the following term (for vanishing stop-mixing)

$$M_h^2 = m_h^2 + \frac{3}{\pi}\alpha_t m_t^2 \ln\left(\frac{M_S^2}{m_t^2}\right), \tag{5.8}$$

where $M_S \equiv \sqrt{m_{\tilde{t}_1} m_{\tilde{t}_2}}$ is the mass scale of the stops.

The problematic piece in this term is the logarithm. For high stop masses it gets large potentially compensating the loop suppression. At higher-order similar logarithms are expected. In consequence higher-order contributions can be large in comparison to the tree-level value spoiling the convergence of the perturbative loop expansion.

## 5.2   Effective field theories

These issues arising due to largely separated scales can be addressed by the use of effective field theories (EFTs). The main idea of EFTs is that the physics at low energies only weakly depends on the physics at high energies. More formally, in an effective field theory the 'heavy' degrees of freedom are integrated out or decoupled leading to an effective Lagrangian containing only 'light' fields suitable to describe the low energy physics.

Consider e.g. the toy-model

$$\mathcal{L}_{\text{toy}} = \frac{1}{2}\partial_\mu\phi\partial^\mu\phi + \frac{1}{2}\partial_\mu\Phi\partial^\mu\Phi - m^2\phi^2 - M^2\Phi^2 - V(\phi,\Phi), \tag{5.9}$$

$$V(\phi,\Phi) = \frac{\lambda_1}{4!}\phi^4 + \frac{\lambda_2}{4}\phi^2\Phi^2 + \frac{\lambda_3}{4!}\Phi^4 \tag{5.10}$$

with $m \ll M$.

For energies $p^2 \ll M^2$ the heavy field $\Phi$ is decoupled and the effective Lagrangian can be obtained by writing down all allowed terms involving $\phi$,

$$\mathcal{L}_{\text{eff}} = \frac{1}{2}\partial_\mu\phi\partial^\mu\phi - m^2\phi^2 - \frac{g_{\text{eff}}}{3!}\phi^3 - \frac{\lambda_{\text{eff}}}{4!}\phi^4. \tag{5.11}$$

At this point, the question arises how it is ensured that the effective field theory gives the right result meaning the same result as in the full theory. This is achieved by matching the effective field theory to the full theory at the scale $Q = M$. Consider e.g. the four-point function of $\phi$.
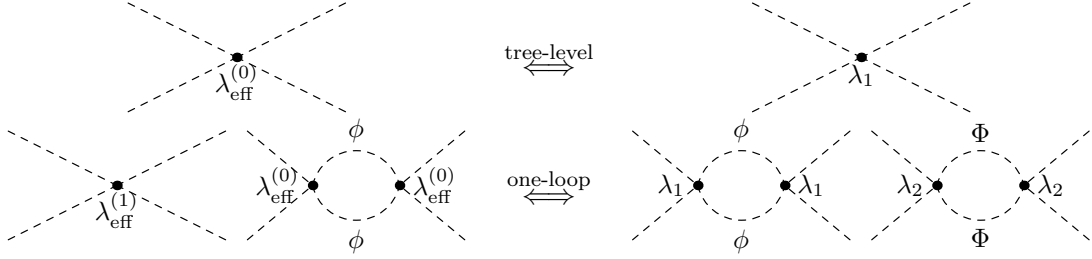


Figure 5.1: Matching the effective theory to the full theory at the tree-level and at the one-loop level.

At tree-level, this process corresponds to the upper left diagram in Figure 5.1 in the effective field theory, in the full theory to the upper right one. If the calculation of the four-point function in both, the effective and full field theory, are required to yield the same result, it follows immediately that

$$\lambda_{\text{eff}}^{(0)}(Q = M) \equiv \lambda_{\text{eff}}^{\text{tree-level}}(Q = M) = \lambda_1(Q = M). \tag{5.12}$$

If the result should be identical also at the one-loop level, the results have to be matched accordingly. This is depicted in the bottom row of Figure 5.1. The one-loop diagrams of the full theory contain loops involving not only the light $\phi$ but also the heavy field $\Phi$. The diagrams involving $\Phi$ have to be compensated by adjusting $\lambda_{\text{eff}}$ at the one-loop level,

$$\lambda_{\text{eff}}(Q = M) = \lambda_1(Q = M) + k\lambda_{\text{eff}}^{(1)}(Q = M). \tag{5.13}$$

This one-loop correction enters through the tree-level diagram (lower left diagram in Figure 5.1) and is normally called threshold correction. The procedure can easily be extended to higher loop-orders. Applying it to the three-point function of $\phi$ shows that

$$g_{\text{eff}} = 0. \tag{5.14}$$

So far $\Phi$ has only entered through loop corrections which are compensated by adjusting the effective coupling. But $\Phi$ can also be responsible that a certain process is allowed in the first place. Consider the same toy-model as above (Eq. (5.9)) but with the changed potential

$$V(\phi, \Phi) = g\phi^3\Phi. \tag{5.15}$$

Naively, one could think that the effective Lagrangian is again given by

$$\mathcal{L}_{\text{eff}} = \frac{1}{2}\partial_\mu\phi\partial^\mu\phi - m^2\phi^2 - \frac{g_{\text{eff}}}{3!}\phi^3 - \frac{\lambda_{\text{eff}}}{4!}\phi^4. \tag{5.16}$$

The decoupled field $\Phi$ however can also mediate interactions of six $\phi$ fields (see left diagram in Figure 5.2). To reproduce this effect in the EFT, higher-dimensional terms have to be included into the effective Lagrangian, i.e.

$$\mathcal{L}_{\text{eff}} = ... - \frac{\kappa_{\text{eff}}}{6!}\phi^6. \tag{5.17}$$

Clearly, $\kappa_{\text{eff}}$ must have mass dimension -2. Therefore, the coupling $\kappa_{\text{eff}}$ is not renormalizable. This is however no issues, because the EFT is replaced by the full renormalizable theory at $Q = M$. The observation that the internal propagator involved in the $\Phi$-exchange diagram behaves like

$$\frac{1}{p^2 - M^2} \stackrel{p^2 \ll M^2}{\longrightarrow} -\frac{1}{M^2} \tag{5.18}$$

in the limit $p^2 \ll M^2$ shows that

$$\kappa_{\text{eff}} \propto g^2/M^2. \tag{5.19}$$

In other words, the effects of high-energy physics are suppressed by the scale of these high-energy physics. In this thesis, all such suppressed operators are omitted. This is normally a good approximation. One should nevertheless keep in mind that such terms are needed to fully reproduce the results of a calculation using the underlying full theory.
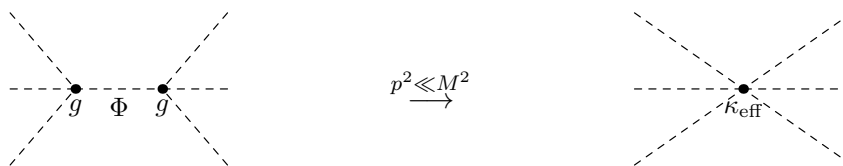


Figure 5.2: Matching the effective theory to the full theory, higher dimensional terms.

## 5.3 Resummation of logarithmic contributions

So far, it was discussed how to match the EFT to the full theory at the decoupling scale $Q = M$ obtaining $\lambda_{\text{eff}}(Q = M)$. If using an EFT however, one normally wants to calculate a process at an energy $Q_{\text{low}}^2 \sim m^2 \ll M^2$. The corresponding amplitude involves $\lambda_{\text{eff}}(Q \approx m)$. $\lambda_{\text{eff}}(m)$ and $\lambda_{\text{eff}}(Q = M)$ are related by renormalization group equations (RGEs), which have the structure

$$\frac{d\lambda_{\text{eff}}}{d\ln Q^2} = \text{polynomial of couplings involved in the theory.} \tag{5.20}$$

The right-hand side is called $\beta$-function of the coupling $\lambda_{\text{eff}}$. Exploiting the structure of the $\beta$-function allows to resum potentially large logarithms $\ln(M/m)$ involving both distinct scales.

This is exactly what is wanted in the case of the calculation of $M_h$ in the MSSM, as discussed below Eq. (5.8). Typically, the scale of the SUSY breaking parameters and thereby the scale of the sparticles is chosen as decoupling scale. For this reason, supersymmetry is broken in the EFT below the decoupling scale. In other words, all sparticles are decoupled such that the remaining EFT is the SM.

The mass of the lightest Higgs boson (or correspondingly the Higgs self coupling parameter $\lambda$) is the only free parameter of the EFT/SM. The matching of the EFT to the full MSSM however fixes $\lambda$ at the decoupling scale. Renormalization group equations can now be used to run $\lambda$ down to the scale $\mu$ at which the Higgs-boson mass

$$M_h^2 = 2\lambda(\mu)v^2 \tag{5.21}$$

should be evaluated. In this thesis, $\mu = m_t$ is chosen as in [39]. As discussed above, the running of $\lambda$ corresponds to logarithms entering the loop corrections to the Higgs-boson mass. The logarithms involve the high decoupling scale and the low $m_t$ scale and can therefore be identified as potentially large logarithms.

The question is now, if there are also other sources of such logarithms. Needless to say, the formula $M_h^2 = 2\lambda(m_t)v^2$ gets loop corrected too. The right-hand side is the $\overline{\text{MS}}$ Higgs-boson mass, which has to be converted to the on-shell Higgs-boson mass if comparing it with experimental results. Remarkably, this conversion now contains no potentially large logarithms, since all heavy sparticles are decoupled in the low energy EFT and therefore their masses do not appear in the calculation. The non-logarithmic terms due to this conversion are already included in the FD result implemented into `FeynHiggs`. Consequently, the running of $\lambda$ from the decoupling scale to $m_t$ is the only source of such logarithms and therefore must reproduce the logarithms found in the Feynman-diagrammatic calculation using the full theory.

In the simplest case all sparticles share a common mass scale, which is chosen to be $M_S \equiv \sqrt{m_{\tilde{t}_1} m_{\tilde{t}_2}}$. Since all sparticles are heavy and get decoupled at $Q = M_S$, the EFT below $M_S$ is the SM. The one-loop SM-RGE for $\lambda$ is given by (neglecting the weak gauge couplings, $h_t = m_t/v$)[1]

$$\frac{d\lambda}{dt} = 6k\left(\lambda^2 + \lambda h_t^2 - h_t^4\right), \tag{5.22}$$

where $t \equiv \ln Q^2$ and $k \equiv 1/(16\pi^2)$. $k$ is used to keep track of the loop order. This equation can be solved approximately by iteration (for details on the iteration procedure see App. B),

$$\lambda(m_t) \approx \lambda(M_S) + \int_{M_s}^{m_t} \frac{d\lambda}{dt} dt \approx \tag{5.23}$$

$$\approx \lambda(M_S) - 6k\left(\lambda^2(M_s) + \lambda(M_s)h_t^2(m_t) - h_t^4(m_t)\right)\ln\left(\frac{M_S^2}{m_t^2}\right) \approx \tag{5.24}$$

$$\approx \lambda_{tree} + 6kh_t^4(m_t)\ln\left(\frac{M_S^2}{m_t^2}\right). \tag{5.25}$$

$\lambda(M_S)$ is fixed by a matching condition as explained in Section 5.2. Here, $\lambda(M_S) = 0$ is assumed at the one-loop level in the third step, because $\lambda(M_S)$ is proportional to the weak gauge couplings

---

[1]Note that $t \equiv \ln Q^2$, if it appears as a single character. In contrast, if $t$ appears as a subscript, it denotes the quantity as top related (e.g. top mass, top-Yukawa coupling).

$(\lambda(M_S) = \frac{1}{4}(g^2 + g'^2)c_{2\beta}^2 + \mathcal{O}(k))$ and therefore neglected in this approximation. Multiplying the result with $2v^2$ to get the Higgs-boson mass reproduces, as expected, the most dominant correction term obtained in the Feynman-diagrammatic approach (see Eq. (5.8)).

Generally, a system of RGEs for couplings $g_i$ is of the structure

$$\frac{dg_i}{dt} = \beta_{g_i}(g_1, ..., g_n) = k\beta_{g_i}^{(1)}(g_1, ..., g_n) + k^2\beta_{g_i}^{(2)}(g_1, ..., g_n) + k^3 \cdot ... + ... \quad (5.26)$$

The functions $\beta_{g_i}^{(j)}$ are the beta-functions of loop order $j$ of the couplings $g_i$. They are polynomial in the couplings $g_i$. Solving the system iteratively shows that the 1-loop part of the RGEs $\propto k^1$ gives rise to $k^n L^n$ terms with $L$ being a shorthand for $\ln(M_S^2/m_t^2)$. These logarithms, whose loop order is identical to the exponent of the logarithm, are called leading logarithms. The 2-loop part of the RGEs $\propto k^2$ gives rise to $k^n L^{n-1}$ terms called subleading or next-to-leading (NLL) logarithms. Generally speaking, the m-loop part of the RGEs yields sub$^{m-1}$leading logarithms $k^n L^{n-m+1}$ (N$^{m-1}$LL).

Another aspect of the resummation is the influence of threshold corrections to the matching conditions (in general $\lambda(M_S) \neq \frac{1}{4}(g^2 + g'^2)c_{2\beta}^2$), which originate from the non-logarithmic terms in the FD calculation (see Section 5.2). Consider e.g. $\lambda(M_S)$ as it appears in the example given above (see Eqs. (5.22)-(5.25)). The tree-level value is modified by threshold corrections originating from the decoupling of heavy sparticles (see Section 5.2),

$$\lambda(M_S) = \lambda_{tree} + k\Delta_1\lambda_{threshold} + k^2\Delta_2\lambda_{threshold} + ... \quad (5.27)$$

The effect of these corrections can be seen by looking e.g. at the third term in Eq. (5.24),

$$-6k\lambda(M_S)h_t^2(m_t)L = -6k\lambda_{tree}h_t^2(m_t)L - 6k^2\Delta_1\lambda_{threshold}h_t^2(m_t)L + \mathcal{O}(k^3). \quad (5.28)$$

The one-loop threshold correction produces a subleading logarithm. Generalizing the statement, $n$-loop threshold corrections give rise to sub$^n$leading logarithms. In other words, a complete resummation of sub$^n$leading logarithms presupposes $n$-loop threshold corrections to the matching conditions involved.

In principle, using this iteration procedure logarithms of arbitrary loop order can be obtained. As an alternative method the RGEs can also be solved numerically. Since a numerically solution is 'exact', it corresponds to a resummation of logarithms up to all orders. This method offers some clear advantages over an iterative solution. It is easier to implement and yields more accurate results. The possibility of obtaining analytic expressions is lost on the other hand.

## 5.4 Combining both methods

Despite of the non ignorable advantages of an EFT approach implementing the running from $M_S$ down to $m_t$, there are several shortcomings. First off all, there might be missing terms. To exactly reproduce the results of an explicit diagrammatic calculation in the full theory, higher dimensional operators $(D > 4)$ have to be included into the EFT-Lagrangian. They are suppressed by the decoupling scale. So, it should be a good approximation to neglect them. Nevertheless, a precise result would require to include them, especially for light sparticles, significantly complicating the calculation. Second, it is at first glance unclear, how to implement the influence of complex phases into the resummation procedure. These issues can and have

been addressed successfully in the Feynman-diagrammatic approach [47]. Third, highly non-degenerate sparticle spectra are difficult to handle within the EFT approach. In principle, it would become necessary to define a new EFT every time a sparticle gets decoupled. This quickly becomes not feasible. In consequence, the best way seems to be to combine both approaches to profit from the advantages of both sides.

In `FeynHiggs` the full diagrammatic one-loop result as well as the leading two-loop contributions of order $\mathcal{O}(\alpha_s\alpha_t, \alpha_t^2)$ are already implemented. Needless to say, these results contain potentially large logarithms. So a first point of consideration, if combining both approaches, should be the avoidance of double-counting of large logarithms. This can be done in two ways. Either the RGEs can be solved iteratively to obtain the corresponding one- and two-loop logarithms or the logarithms can be extracted out of the full Feynmann diagrammatic result. In praxis, it is best to follow both paths, since a comparison between the logarithms obtained in the two approaches serves as a helpful check of the whole calculation.

A second issue concerns the definition of the input parameters. The Feynman-diagrammatic calculation is performed using an hybrid OS-$\overline{\text{DR}}$ scheme. In contrast, the RGEs are derived in the $\overline{\text{MS}}$-scheme. Consequently, the input parameters of the FD calculation are OS (or $\overline{\text{DR}}$) quantities, whereas the ones of the EFT calculation are $\overline{\text{MS}}$-quantities. The conversion between the two schemes can potentially involve logarithms, which would spoil the consistency of the calculation if not taken into account properly. In general the relations between the schemes involve also non-logarithmic terms. However, for a consistent combination of both approaches they have to be omitted. This can be understood as follows.

Quantities which have to be converted can enter the calculation in two ways, either trough threshold corrections or as arguments of the resummed logarithms ($t_\beta$ is an exception discussed in Chapter 8). If a quantity $A$ enters through threshold corrections, it will appear only as a prefactor of subleading logarithms in the final result (see Section 5.3), e.g. (other prefactors are suppressed),

$$\Delta M_h^2 \propto k^2 A^{\overline{\text{MS}}} \ln \frac{M_S^2}{m_t^2}. \tag{5.29}$$

Converting $A$ from the $\overline{\text{MS}}$-scheme to the OS-scheme using

$$A^{\overline{\text{MS}}} = A^{\text{OS}}(1 + k\delta_1 \ln(M_S^2/m_t^2) + k\delta_2), \tag{5.30}$$

where $\delta_1, \delta_2$ are numerical prefactors, yields

$$\Delta M_h^2 \propto k^2 A^{\overline{\text{MS}}} \ln \frac{M_S^2}{m_t^2} = k^2 A^{\text{OS}} \ln \frac{M_S^2}{m_t^2} + k^3 \delta_1 A^{\text{OS}} \ln^2 \frac{M_S^2}{m_t^2} + k^3 \delta_2 A^{\text{OS}} \ln \frac{M_S^2}{m_t^2}. \tag{5.31}$$

The logarithmic term in the conversion produces a 3-loop subleading logarithm. The non-logarithmic term instead leads to a 3-loop sub-subleading logarithm which is beyond the order of approximation employed in this thesis. Therefore the non-logarithmic terms in the conversion do not contribute in this approximation.

In the other case, the quantity, which has to be converted, enters as an argument of a resummed logarithm. Consider e.g. $M_S$ entering in the form (prefactors are suppressed)

$$\Delta M_h^2 \propto k \ln \frac{(M_S^2)^{\overline{\text{MS}}}}{m_t^2}. \tag{5.32}$$

Converting $M_S$ from the $\overline{\text{MS}}$-scheme to the OS-scheme using

$$M_S^{\overline{\text{MS}}} = M_S^{\text{OS}}(1 + k\delta_1 \ln((M_S^2)^{\text{OS}}/m_t^2) + k\delta_2) \tag{5.33}$$

yields

$$\Delta M_h^2 \propto k \ln \frac{(M_S^2)^{\text{OS}}(1 + k\delta_1 \ln(M_S^2/m_t^2) + k\delta_2)}{m_t^2} = \tag{5.34}$$

$$= k \ln \frac{(M_S^2)^{\text{OS}}}{m_t^2} + k^2\delta_1 \ln \frac{(M_S^2)^{\text{OS}}}{m_t^2} + k^2\delta_2 + \mathcal{O}(k^3). \tag{5.35}$$

Obviously, the logarithmic term in the conversion formula gives rise to a subleading logarithm. If the conversion is employed for a subleading logarithm, it gives rise to a sub-subleading logarithm, which neglected in the used approximation. The non-logarithmic in contrast leads to a non-logarithmic term which is possibly already included in the FD result. This would spoil the consistency of the combination of both approaches. Subtracting the non-logarithmic terms after the conversion is also not an option, since it is not possible to gain a corresponding subtraction expression in the case of numeric resummation. Therefore, the only option is to omit the non-logarithmic terms in the conversion formulas. This ensures that no uncontrollable non-logarithmic terms arise. The sub-subleading or even further suppressed logarithms, which are missed, can be neglected. This argument can easily be extended to higher powers of logarithms.

At this point, it should be noted that a complete resummation of all subleading logarithms would require that leading logarithms up to arbitrary order are included into the conversion formula (at least if all input parameters should be renormalized in the OS-scheme). In this thesis however, just the one-loop leading logarithms are considered.

The conversion of input parameters is not the only possible source of non-logarithmic terms in the EFT approach. In fact, the RGE running produces also non-logarithmic terms via the matching conditions. This can be seen explicitly in the simple example of Eqs. (5.23)-(5.25). $\lambda_{tree}$ is already included in the FD result. Thus $\lambda_{tree}$ has to be subtracted of the EFT result. The same consideration applies to threshold-corrections to the tree-level matching conditions. Naively, it seems like $\overline{\text{MS}}$-quantities should be used in this subtraction part, since it is part of the EFT calculation. The conversion from $\overline{\text{MS}}$ to OS can however involve logarithms. In this way, a non-logarithmic part involving $\overline{\text{MS}}$-parameters develops a logarithmic part after converting to the OS-scheme. Consequently, OS-quantities have to be used in the subtraction part. To clarify this statement, the one-loop stop-threshold correction to $\lambda(M_S)$ (neglecting the weak gauge couplings, see [53]) is taken as an example,

$$\Delta\lambda_{\text{threshold}} = 6kh_t^4 \hat{X}_{t,\overline{\text{MS}}}^2 \left(1 - \frac{1}{12}\hat{X}_{t,\overline{\text{MS}}}^2\right). \tag{5.36}$$

In the EFT calculation this threshold correction leads to the non-logarithmic term

$$\Delta M_{h,\text{EFT}}^2 = 12km_t^2 h_t^2 \hat{X}_{t,\overline{\text{MS}}}^2 \left(1 - \frac{1}{12}\hat{X}_{t,\overline{\text{MS}}}^2\right) = \tag{5.37}$$

$$= 12km_t^2 h_t^2 \hat{X}_{t,\text{OS}}^2 \left(1 - \frac{1}{12}\hat{X}_{t,\text{OS}}^2\right) + \text{logarithmic terms.} \tag{5.38}$$

In contrast, the corresponding appearing in the FD calculation reads

$$M_{h,\text{FD}}^2 = 12km_t^2 h_t^2 \hat{X}_{t,\text{OS}}^2 \left(1 - \frac{1}{12}\hat{X}_{t,\text{OS}}^2\right). \tag{5.39}$$

Now it becomes clear that, if $\overline{\text{MS}}$-quantities are used in the subtraction of non-logarithmic terms, the logarithmic terms at the right-hand side of Eq. (5.37) are subtracted as well. So these logarithms would be missed in the resummation procedure. Using OS-quantities as input for the subtraction of non-logarithmic terms cures this problem.

All these considerations can be cast into the equations

$$M_h^2 = (M_h^2)^{\text{FD}} + \Delta M_h^2, \tag{5.40}$$

$$\Delta M_h^2 = (\Delta M_h^2)^{\text{RGE}}(A_i^{\overline{\text{MS}}}) - (\Delta M_h^2)^{\text{RGE, non-log}}(A_i^{\text{OS}}) - (\Delta M_h^2)^{\text{FD,logs}}(A_i^{OS}). \tag{5.41}$$

The Higgs-boson mass calculated in the FD approach gets corrected by $\Delta M_h^2$ containing the resummed logarithms $(\Delta M_h^2)^{\text{RGE}}$. To avoid double-counting of logarithms already contained in the FD result, $(\Delta M_h^2)^{\text{FD,logs}}$ is subtracted. Respectively, to avoid double-counting of non-logarithmic terms contained in the RGE result, $(\Delta M_h^2)^{\text{RGE, non-log}}$ is subtracted. The input parameters $A_i$ enter defined in the OS-scheme ($A_i^{OS}$) for the FD calculation as well as for the subtraction part of the RGE calculation and in the $\overline{\text{MS}}$-scheme for the EFT calculation ($A_i^{\overline{\text{MS}}}$).

# Chapter 6

# Extraction of logarithms in the Feynman-diagrammatic approach

As discussed in Section 5.1 large logarithms, e.g. $\ln(M_S^2/m_t^2)$ with $M_S$ being the stop scale, appear in the Feynman-diagrammatic (FD) calculation of $M_h$. For the comparison and combination of the FD result with the RGE result, those logarithms have to be identified in the FD result. This Chapter explains which methods are used to achieve this.

The two-loop logarithms contained in the FD calculation of $M_h$ implemented into `FeynHiggs` are in principle already known. Nevertheless, it is quite hard to isolate them in the general result consisting out of complicated expressions. Therefore, the two-loop logarithms are identified using the RGE approach (see Chapter 7).

The one-loop logarithms (except the ones proportional to $\alpha_t m_t^2$) are not known in general so far. In [54] a result in the limit $\tan\beta \to \infty$ was presented. For arbitrary $\tan\beta$ a result for $M_\chi = M_{Susy}$ can be found in [32]. The extraction of logarithms for general $\tan\beta$ and $M_\chi$ is described below. Explicit analytic expressions are given.

For the one-loop correction to $M_h$ it is sufficient to calculate $\hat{\Sigma}_{hh}(m_h^2)$, as was shown in Section 5.1. Looking at Eqs. (4.74a) and the corresponding defintions of the counterterms in Sections 4.7.2 and 4.7.3 it becomes clear that the self-energies of the $h, H, A$-scalars (see Figure 6.1), the $Z$-self energy (see Figure 6.2) as well as the $h, H$-tadpole diagrams (see Figure 6.3) have to be evaluated to obtain the full diagrammatic result as a starting point of the calculation.

The amplitudes are generated using the Mathematica package `FeynArts` [53]. `FormCalc` [55] is used to process them further. The appearing loop functions are reduced to the scalar integrals $A_0$, $B_0$ as described in App. D. Finally, for $A_0$ and $B_0$ the analytic expressions, also given in App. D, are plugged in. The renormalization scale $\mu^{\overline{\text{DR}}}$ entering through the $\overline{\text{DR}}$-renormalization of the Higgs fields is set to $\mu^{\overline{\text{DR}}} = m_t$, which is the default value of `FeynHiggs`.

## 6.1 Approximations

Throughout the thesis all Yukawa couplings (except of the top-Yukawa coupling $h_t$) and therefore the masses of all SM fermions (except of the top quark) are set to zero. In addition, the simplifications discussed in Section 4.2 are employed. Conveniently, also $X_t = 0$ can be assumed, since logarithms proportional to $X_t$ do not enter at the one-loop level. This is due to the fact that in the RGE approach $X_t$ enters the calculation only through the one-loop threshold correction

41
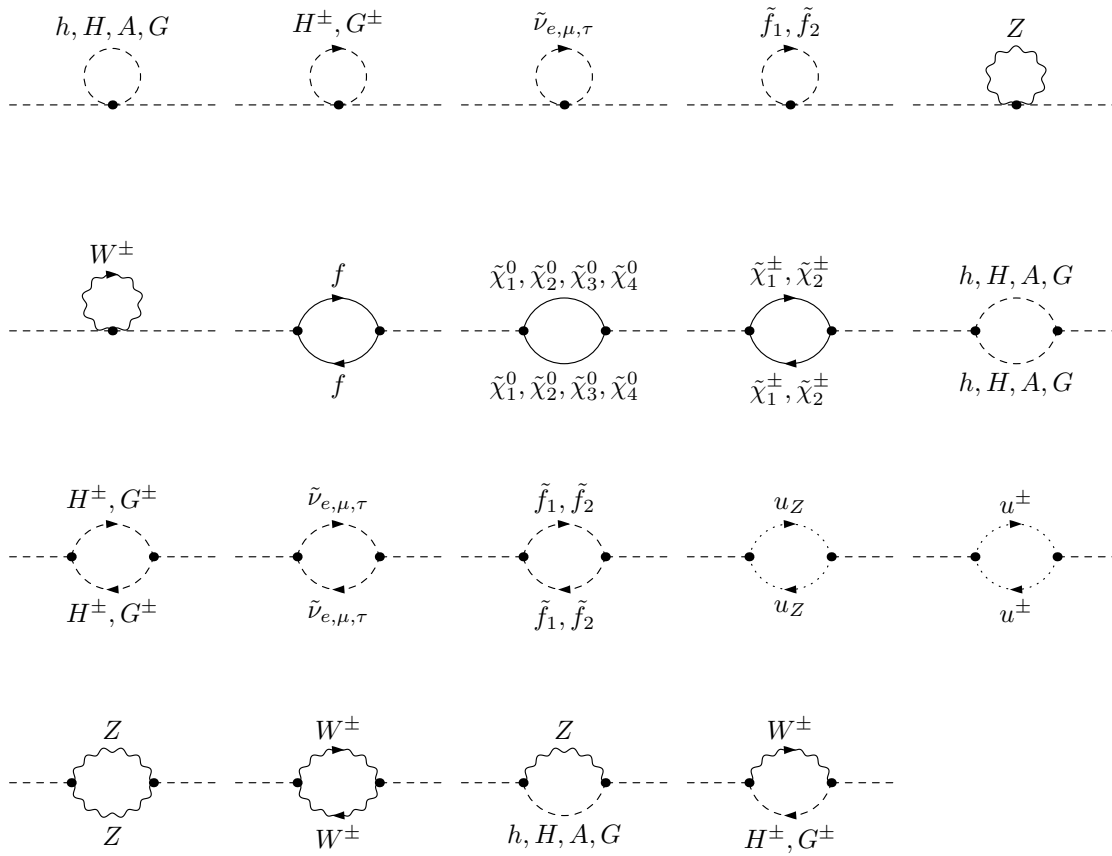
Figure 6.1: Generic Feynman diagrams for the $h, H, A, G$ self-energies ($f = e, \mu, \tau, u, d, c, s, t, b$).

$h, H, A, G$ $H^{\pm}, G^{\pm}$ $\tilde{\nu}_{e,\mu,\tau}$ $\tilde{f}_1, \tilde{f}_2$ $W$

$\nu_{e,\mu,\tau}$ $f_1, f_2$ $\tilde{\chi}_1^0, \tilde{\chi}_2^0, \tilde{\chi}_3^0, \tilde{\chi}_4^0$ $\tilde{\chi}_1^{\pm}, \tilde{\chi}_2^{\pm}$ $A, G$

$nu_{e,\mu,\tau}$ $f_1, f_2$ $\tilde{\chi}_1^0, \tilde{\chi}_2^0, \tilde{\chi}_3^0, \tilde{\chi}_4^0$ $\tilde{\chi}_1^{\pm}, \tilde{\chi}_2^{\pm}$ $h, H$

$\tilde{\nu}_{e,\mu,\tau}$ $\tilde{f}_1, \tilde{f}_2$ $u^{\pm}$ $W$ $Z$

$\tilde{\nu}_{e,\mu,\tau}$ $\tilde{f}_1, \tilde{f}_2$ $u^{\pm}$ $W$ $h, H$

$W^{\pm}$

$G^{\pm}$
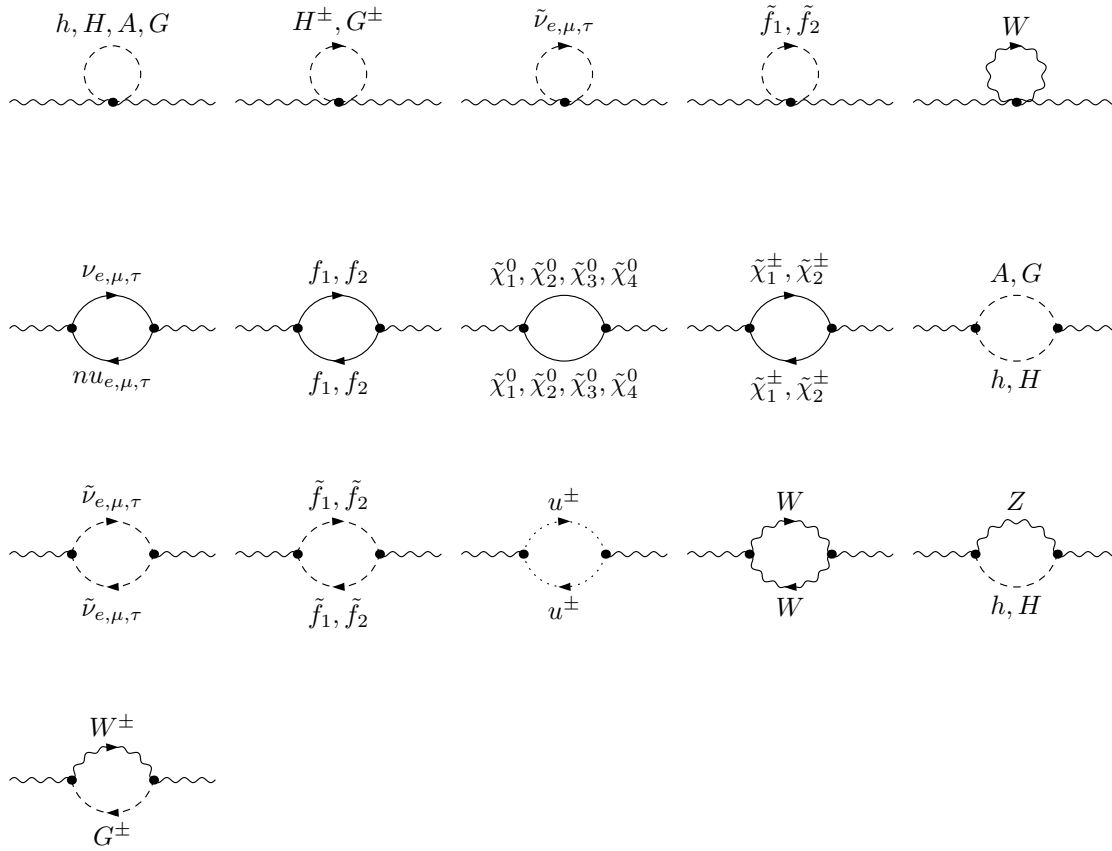
Figure 6.2: Generic Feynman diagrams for the $Z$ self-energy ($f = e, \mu, \tau, u, d, c, s, t, b$).

$h, H, A, G$ $H^{\pm}, G^{\pm}$ $\tilde{\nu}_{e,\mu,\tau}$ $\tilde{f}_1, \tilde{f}_2$ $f$

$\tilde{\chi}_1^0, \tilde{\chi}_2^0, \tilde{\chi}_3^0, \tilde{\chi}_4^0$ $\tilde{\chi}_1^{\pm}, \tilde{\chi}_2^{\pm}$ $u_Z, u^{\pm}$ $Z$ $W^{\pm}$
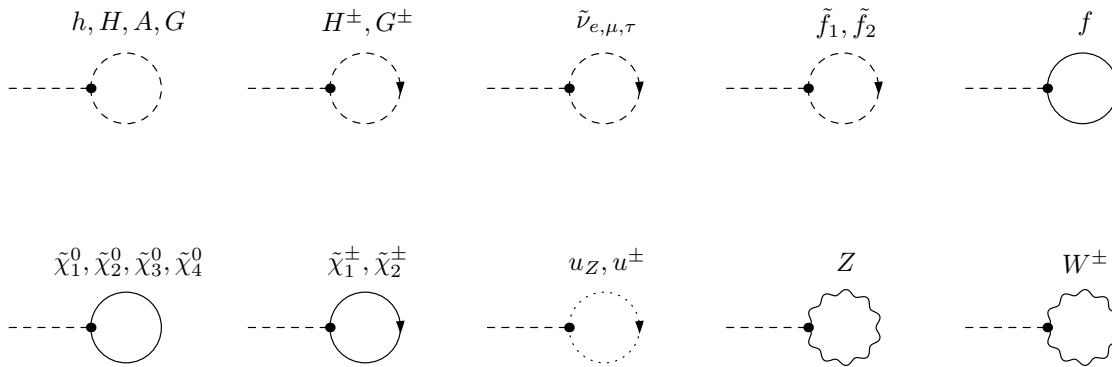
Figure 6.3: Generic Feynman diagrams for the $h, H$ tadpoles ($f = e, \mu, \tau, u, d, c, s, t, b$).

43

to $\lambda(M_S)$. This threshold correction gives rise to non-logarithmic terms at the one-loop level but logarithmic terms due to this threshold correction appear only from the two-loop level on (see Eq. (5.28)).

For the derivation of the needed self-energies the approximate expressions for masses and mixing matrices of charginos and neutralinos given in App. C are used. These expressions are power series in the variable $x_\chi \equiv M_Z/M_\chi$ (remember that $M_Z \ll M_\chi$ is assumed). To work consistently without mixing orders, the introduced expansion is employed to the whole expression for the $hh$ self-energy by replacing $M_\chi$ through $M_Z/x_\chi$. In this way, the $hh$ self-energy is consistently written as a power series in $x_\chi$. An explicit calculation yields that all terms proportional to a negative power of $x_\chi$ vanish in the final result. Terms of order $\mathcal{O}(x_\chi^1)$ or higher are suppressed and are therefore beyond the order of approximation considered here. In consequence only terms of order $\mathcal{O}(x_\chi^0)$ contribute to the final result.

Below this procedure is illustrated for an example term, which might appear in the self-energies,

$$\left(1 + x_\chi + x_\chi^2 + x_\chi^3\right) A_0(M_\chi) = \tag{6.1}$$

$$= M_\chi^2 \left(1 + x_\chi + x_\chi^2 + x_\chi^3\right) \left(\Delta + 1 - \ln\frac{M_\chi^2}{m_t^2}\right) = \tag{6.2}$$

$$= M_Z^2 \frac{1}{x_\chi^2} \left(1 + x_\chi + x_\chi^2 + x_\chi^3\right) \left(\Delta + 1 - \ln\frac{M_Z^2}{m_t^2} - \ln x_\chi^{-2}\right) = \tag{6.3}$$

$$= M_Z^2 \left(x_\chi^{-2} + x_\chi^{-1} + 1 + \mathcal{O}(x_\chi)\right) \left(\Delta + 1 - \ln\frac{M_Z^2}{m_t^2} - \ln x_\chi^{-2}\right). \tag{6.4}$$

The logarithm containing $M_Z$ and $m_t$ can be seen as a fixed number, since it does not involve a scale, which could get large. The second logarithms however does.

In a similar way, the tree level expression for the Higgs-boson masses as well as the relation between $\alpha$ and $\beta$ are expanded in the variable $x_A = M_Z/M_A$ (under the assumption that $M_A \gg M_Z$). $M_A$ is replaced by $M_Z/x_A$. All terms proportional to a negative power of $x_A$ again cancel in the final result. Terms of order $\mathcal{O}(x_A^1)$ or higher are omitted such that only terms of order $\mathcal{O}(x_A^0)$ contribute to the final expression. In this decoupling limit, the mixing angle $\alpha \to \beta - \pi/2$ (see Eqs. (4.47) and (4.48)). The relevant expansion formulas for quantities dependent on $M_A$ (like the tree-level Higgs-boson masses) are given in App. C.4.

In the obtained expression terms suppressed by $M_S$ are omitted, because they can not be reproduced in the EFT approach if no higher-dimensional operators are introduced.

## 6.2 Cancellation of divergences

Using the approximations described in Section 6.1, the UV finiteness of the renormalized $hh$ self-energy is checked analytically. As expected, all divergences up to the order $\mathcal{O}(x_Z^0)$, $\mathcal{O}(x_A^0)$ and $\mathcal{O}((M_Z/M_S)^0)$ cancel. For terms proportional to higher powers of $x_\chi$, $x_A$ and $M_Z/M_S$, the cancellation is not checked, since therefore higher-order expressions for e.g. the neutralino masses and mixing matrix would be needed.

It is interesting to note that

- all divergences (even $\propto g, g'$) cancel within the each (s)quark-sector, e.g. the (s)top-sector. Contributions from the related SU(2)-partner sector, here the (s)bottom-sector are not necessary to get a finite expression.

- for the finiteness of the $hh$ self-energy in the electroweak sector, all contributions from the neutralino, chargino, gauge, Higgs and ghost sector are necessary. This is due to the underlying $SU(2) \times U(1)$ symmetry connecting these sectors.

- all logarithms proportional to one of the large scales $M_S, M_\chi, M_A$ vanish.

## 6.3    Extraction of logarithms

To extract the logarithmic contributions in the $hh$ self-energy, analytic expressions for the occurring loop functions (see App. D) have to be plugged in. In the next step, only logarithms with arguments involving $m_t$ and one of the high scales, like $M_\chi^2/m_t^2$, are kept (see Section 5.3). To extract these logarithms out of all logarithmic contributions to the $hh$ self-energy the arguments of the logarithms are expanded for large scales (here for large $M_\chi$), e.g. ($x_\chi = M_Z/M_\chi$)

$$\ln \frac{M_\chi^2 + M_Z^2}{m_t^2} = \ln \frac{M_\chi^2}{m_t^2} + \ln\left(1 + \frac{M_Z^2}{M_\chi^2}\right) \approx \ln \frac{M_\chi^2}{m_t^2} + \mathcal{O}(x_\chi^2). \tag{6.5}$$

Terms involving positive powers of $x_\chi$ are omitted (as long as they are not multiplied by an inverse power of $x_\chi$), because they contain no logarithms and are suppressed for large $M_\chi$.

## 6.4    Analytic expressions

In the limit $M_S, M_{Susy}, M_A, M_\chi \gg M_Z$ the one-loop leading logarithmic contributions of the $hh$ self energy in the Feynman-diagrammatic approach can be given in a relatively compact form (using the abbreviations introduced in Eq. (4.15)),

$$\hat{\Sigma}_{hh}^{1L,LL}(p^2 = m_{h,tree}^2) =$$
$$= \frac{\alpha}{72\pi M_W^2 s_w^2} \cdot$$
$$\underbrace{\left\{ \frac{3}{8}\left(16 M_W^2 M_Z^2 - 40 M_W^4 - 29 M_Z^4 + 4\left(2 M_W^4 + 4 M_W^2 M_Z^2 + M_Z^4\right) c_{4\beta} + 9 M_Z^4 c_{8\beta}\right) \ln \frac{M_A^2}{m_t^2}\right.}_{\text{Higgs-sector}}$$
$$\underbrace{- \left(108 m_t^4 + 54 m_t^2 M_Z^2 c_{2\beta} + \left(32 M_W^4 - 40 M_W^2 M_Z^2 + 17 M_Z^4\right) c_{2\beta}^2\right) \ln \frac{M_S^2}{m_t^2}}_{\text{(s)top-sector}}$$
$$\underbrace{- \left(160 M_W^4 - 200 M_W^2 M_Z^2 + 103 M_Z^4\right) c_{2\beta}^2 \ln \frac{M_{Susy}^2}{m_t^2}}_{\text{(s)lepton-, rest of (s)quark-sector}}$$
$$\underbrace{+ 3\left(44 M_W^4 - 10 M_W^2 M_Z^2 + 11 M_Z^4 + \left(20 M_W^4 - 10 M_W^2 M_Z^2 - M_Z^4\right) c_{4\beta}\right) \ln \frac{M_\chi^2}{m_t^2}}_{\text{chargino-, neutralino-sector}} \left. \right\},$$

$$\tag{6.6}$$

where $\alpha = e^2/4\pi$ is the fine-structure constant ($e = g s_w = g' c_w$ is the elementary electric charge). In the limit of $\tan\beta \to \infty$, this agrees with the result of [54].

45

This result can further be simplified. First, $\ln(M_{Susy}^2/m_t^2)$ can be replaced by $\ln(M_S^2/m_t^2)$, since

$$\ln \frac{M_{Susy}^2}{m_t^2} = \ln \frac{M_S^2}{m_t^2} + \text{ terms suppressed by } M_S. \tag{6.7}$$

Moreover, in the RGE approach it is assumed that the heavy Higgses and the stops have a common mass scale, i.e. $M_A = M_S$. Applying both simplifications to Eq. (6.6) yields

$$\begin{aligned}
\hat{\Sigma}_{hh}^{1\text{L,LL}}(p^2 = m_{h,tree}^2) &= \\
&= -\frac{\alpha}{72\pi M_W^2 s_w^2} \cdot \\
&\quad \left\{ -\frac{3}{8} \left[ 288 m_t^4 + 144 m_t^2 M_Z^2 c_{2\beta} + 296 M_W^2 - 336 M_W^2 M_Z^2 + 189 M_Z^4 + \right.\right. \\
&\qquad \left. 4(62 M_W^4 - 84 M_W^2 M_Z^2 + 39 M_Z^4) c_{4\beta} - 9 M_Z^4 c_{8\beta} \right] \ln \frac{M_S^2}{m_t^2} \\
&\qquad \left. + 3 \left[ 44 M_W^4 - 10 M_W^2 M_Z^2 + 11 M_Z^4 + \left(20 M_W^4 - 10 M_W^2 M_Z^2 - M_Z^4\right) c_{4\beta} \right] \ln \frac{M_\chi^2}{m_t^2} \right\}.
\end{aligned} \tag{6.8}$$

Neglecting all terms $\propto M_W, M_Z$, the most dominant correction term is again recovered (see Eq. 5.8).

# Chapter 7

# Resummation of logarithms in the RGE approach

As outlined in Section 5.3, RGEs can be used to resum the potentially large logarithms appearing in a Feynman-diagrammatic calculation by solving the system of RGEs with corresponding boundary conditions numerically. This method has already been applied to improve the prediction for $M_h$ and implemented into `FeynHiggs` [39]. The electroweak gauge couplings were neglected ($g = g' = 0$), such that only logarithms $\propto \alpha_t, \alpha_s$ are resummed. In this Chapter three refinements are proposed. In a first step, electroweak contributions are taken fully into account ($g, g' \neq 0$), while assuming that all sparticles have a common mass scale ($M_\chi = M_{\tilde{g}} = M_S$). In a second step, the case of light charginos and neutralinos is considered ($M_\chi \leq M_S$). Thirdly, also the gluino is allowed to be light ($M_{\tilde{g}} \leq M_S$).

## 7.1 Electroweak contributions

In this first refinement, it is assumed that all sparticles have a common mass scale. Consequently, the EFT below $M_S$ is the SM. This scenario is shown in Figure 7.1.



Figure 7.1: All sparticles have the common mass scale $M_S$. The EFT below $M_S$ is the SM. $\lambda(m_t)$ is obtained by running $\lambda(M_S)$ down using SM-RGEs and taking $h_t(m_t), g_3(m_t), ...$ as input values.
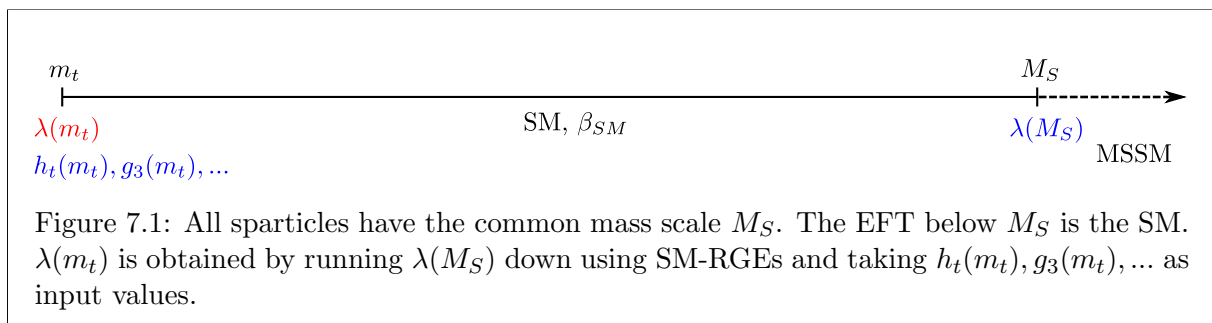
To resum also electroweak contributions, the full SM RGEs including $g$ and $g'$ have to be taken into account (see App. A.1). Futhermore, the simple threshold correction used in [39] ($\lambda(M_S) = 6kh_t^4\hat{X}_t^2(1 - 1/12\hat{X}_t^2)$) is not sufficient anymore. There are additional threshold contributions proportional to the weak gauge coupling from the stop sector as well as from other

sectors. These can be found e.g. in [35, 36],

$$
\begin{aligned}
\lambda(M_S) = \\
= \underbrace{\frac{1}{4}\cos^2(2\beta)\left(g^2 + g'^2\right)}_{\text{tree level}} \\
\underbrace{-k\left[\left(\frac{3}{4} - \frac{1}{6}c_{2\beta}^2\right)g^4 + \frac{1}{2}g^2 g'^2 + \frac{1}{4}g'^4\right]}_{\text{tree-level term } \overline{\text{DR}} \to \overline{\text{MS}}} \\
\underbrace{+6h_t^2 k\left\{\left[h_t^2 + \frac{1}{8}\left(g^2 + g'^2\right)c_{2\beta}\right]\left(\frac{X_t^2}{M_S^2}\right) - \frac{1}{12}h_t^2\left(\frac{X_t^4}{M_S^4}\right)\right\} - \frac{1}{4}kh_t^2\left(g^2 + g'^2\right)c_{2\beta}^2\left(\frac{X_t^2}{M_S^2}\right)}_{\text{stop-threshold corr.}} \\
\underbrace{-\frac{3}{16}k(g'^2 + g^2)^2 s_{4\beta}^2}_{\text{heavy Higgs threshold corr.}} \\
\underbrace{+\frac{1}{24}k(c_\beta + s_\beta)^2\left\{-51g^4 - 24g^2 g'^2 - 13g'^4 + (3g^2 + g'^2)\left[(g^2 + g'^2)c_{4\beta} + 2(g^2 - g'^2)s_{2\beta}\right]\right\}}_{\text{chargino/neutralino threshold corr.}}.
\end{aligned}
$$

$$(7.1)$$

All couplings at the right-hand side of Eq. (7.1) have to be evaluated at $Q = M_S$. This includes $\beta$. The input value of $\tan\beta$ is nevertheless given at $Q = m_t$ making it necessary to run $\tan\beta$ up to $Q = M_S$. The issues related to the running of $\tan\beta$ are discussed separately in Section 7.4. Below, it is taken as a convention that the right-hand side of an equation has to be evaluated at the same scale as the left-hand side, if not explicitly noted otherwise.

At this point, it should be noted that the threshold corrections found in [35, 36] contain additional contributions, which are zero for the assumptions made in this thesis (see Section 4.2). Furthermore, they are derived for a different renormalization of $\tan\beta$ as the one employed here (see Eq. 4.73). Therefore, most of the corrections have been recalculated using the method described in Section 5.2 (here, it is easier to match the results for $M_h$ directly instead of matching the quartic coupling $\lambda$). The calculation confirms the results of [35, 36] in spite of the different renormalization schemes.

The origin of the tree-level matching condition is the MSSM Higgs potential given in Eq. (4.28). The term in the second line of Eq. (7.1) is due to the fact that the tree-level term has to be converted from the $\overline{\text{DR}}$- to the $\overline{\text{MS}}$-scheme (a detailed explanation can be found in Chapter 8). All other threshold correction originate from the decoupling of heavy sparticles. In the gaugeless limit ($g = g' = 0$) this expression reduces to the threshold correction of [39].

Note that in [34] a factor $-c_{2\beta}$ is missing in the threshold correction of the stop-sector. The reason is that in the referenced articles [26, 32] the threshold correction was obtained in the limit $\tan\beta \to \infty$, in which $c_{2\beta} \to -1$. The last term in the stop-sector threshold correction proportional to $c_{2\beta}^2$ was completely missed. This has been already noted by the authors of [36].

Using one-loop RGEs (see App. A.1, the leading one-loop logarithms can be calculated,

$$(\Delta M_h^2)^{\text{1L,LL}} = kv^2 \left\{ 12h_t^4 + 3h_t^2(g^2 + g'^2)c_{2\beta} - \frac{1}{12}\left[ 18(c_{2\beta}^2 - 1)^2 g^2 g'^2 \right.\right.$$
$$\left.\left. + (9c_{2\beta}^4 - 8c_{2\beta}^2 + 27)g^4 + (9c_{2\beta}^4 - 50c_{2\beta}^2 + 9)g'^4 \right] \right\} \ln\frac{M_S^2}{m_t^2}. \quad (7.2)$$

All couplings have to be evaluated at $Q = m_t$. This agrees with the result of [32] and also reproduces the result of the FD calculation (see Eq. (6.8) with $M_\chi = M_S$).

Using 2-loop RGEs, the leading and subleading two-loop logarithms already contained in theFD result implemented into `FeynHiggs` ($\propto \alpha_s\alpha_t, \alpha_t^2$) can be derived,

$$(\Delta M_h^2)^{\text{2L,LL+NLL}} = 2k^2 v^2 h_t^4 \left\{ [9h_t^2 - 48g_3^2]\ln\frac{M_S^2}{m_t^2} + \frac{1}{2}\left[ 16g_3^2\left(4 - 12\hat{X}_{t,\text{OS}}^4 + \hat{X}_{t,\text{OS}}^8\right) \right.\right.$$
$$\left.\left. - 3h_t^2\left(20 - 12\hat{X}_{t,\text{OS}}^4 + \hat{X}_{t,\text{OS}}^8\right)\right] \right\} \ln\frac{M_S^2}{m_t^2}. \quad (7.3)$$

Again, all couplings have to be evaluated at $Q = m_t$.

To resum the logarithms up to all order, the full SM RGEs including $g$ and $g'$ (see App. A.1) have to be solved numerically with the boundary condition given in Eq. (7.1). The boundary conditions for $g$, $g'$, $g_3$ and $h_t$ are given in Eqs. (9.7)-(9.10).

## 7.2 Chargino/neutralino threshold

The assumption of a common sparticle mass scale is quite limiting. A realistic spectrum probably involves more than one mass scale. One possible extension is the introduction of a variable chargino/neutralino-threshold $M_\chi$ ($m_t \ll M_\chi \equiv M_1 = M_2 = \mu \leq M_S$). At this scale, the charginos and neutralinos are decoupled. Therefore, they still contribute to the RGE running between $M_\chi$ and $M_S$ (see App. A.2 for the corresponding set of RGEs). The EFT in this interval is called split-model and can be seen basically as the SM plus charginos and neutralinos (the overall scenario is depicted in Figure 7.2). The Lagrangian is given by

$$\mathcal{L}_{\text{split}} = \ldots + -\frac{1}{2}M_\chi\tilde{W}\tilde{W} - \frac{1}{2}M_\chi\tilde{B}\tilde{B} - M_\chi\tilde{\mathcal{H}}_2 \cdot \tilde{\mathcal{H}}_1 - \frac{1}{\sqrt{2}}H^\dagger\left(\tilde{g}_{2u}\sigma^a\tilde{W}^a + \tilde{g}_{1u}\tilde{B}\right)\tilde{\mathcal{H}}_2$$
$$- \frac{1}{\sqrt{2}}H \cdot \left(-\tilde{g}_{2d}\sigma^a\tilde{W}^a + \tilde{g}_{1d}\tilde{B}\right)\tilde{\mathcal{H}}_1 + h.c., \quad (7.4)$$

where $H$ is the SM-like Higgs doublet remaining below $Q = M_S$ and $\sigma^a$ are the Pauli matrices. Below $Q = M_\chi$ the SM is recovered. The notation of the Higgs-gaugino-gaugino couplings $\tilde{g}_{1u}, \tilde{g}_{2u}, \tilde{g}_{1d}, \tilde{g}_{2d}$ is adopted from [35,36]. In there, a different notation for the electroweak gauge couplings and the Higgs doublets is used. $g$ and $g'$ correspond to $g_2$ and $g_1$, $\mathcal{H}_1$ and $\mathcal{H}_2$ to $\mathcal{H}_d$ and $\mathcal{H}_u$. In consequence, the number in subscripts of $\tilde{g}_{1u}, \tilde{g}_{2u}, \tilde{g}_{1d}, \tilde{g}_{2d}$ specifies, which gauge symmetry causes the coupling ($U(1)$, if the number is 1, $SU(2)$, if the number is 2). The small letter expresses which Higgsino field is coupled to the SM like Higgs field $H$ ($\mathcal{H}_1$, if the letter is $d$, $\mathcal{H}_1$, if the letter is $u$).

Figure 7.2: All sparticles except of the charginos and neutralinos have the common mass scale $M_S$. The charginos and neutralinos have the common mass scale $M_\chi$. The EFT below $M_S$ is the SM plus charginos and neutralinos called split-model. Below $M_\chi$ the SM is recovered. $\lambda(m_t)$ is obtained by running $\lambda(M_S)$ down using split-model RGEs from $M_S$ to $M_\chi$ and SM-RGEs from $M_\chi$ to $m_t$. At $Q = M_\chi$ the SM is matched to the split-model. $h_t(m_t), g_3(m_t), ...$ are taken as input values.

Numerical values for the couplings $\tilde{g}_{1u}, \tilde{g}_{2u}, \tilde{g}_{1d}, \tilde{g}_{2d}$ are obtained by matching the split-model to the full MSSM at the scale $Q = M_S$ [35, 36],

$$\tilde{g}_{1u}(M_S) = g_\chi s_{\beta_\chi} \left\{ 1 + k \left[ \frac{3}{16} g_\chi^2 \left( -2 + 7c_{\beta_\chi}^2 \right) + \frac{1}{20} g_\chi'^2 \left( -44 + 7c_{\beta_\chi}^2 \right) + \frac{9}{4s_{\beta_\chi}^2} h_{t,\chi}^2 \right] \right\}, \quad (7.5a)$$

$$\tilde{g}_{1d}(M_S) = g_\chi c_{\beta_\chi} \left\{ 1 + k \left[ \frac{3}{16} g_\chi^2 \left( -2 + 7s_{\beta_\chi}^2 \right) + \frac{1}{20} g_\chi'^2 \left( -44 + 7s_{\beta_\chi}^2 \right) \right] \right\}, \quad (7.5b)$$

$$\tilde{g}_{2u}(M_S) = g_\chi' s_{\beta_\chi} \left\{ 1 + k \left[ -g_\chi^2 \left( \frac{2}{3} + \frac{11}{16} c_{\beta_\chi}^2 \right) + \frac{1}{20} g_\chi'^2 \left( -2 + 7c_{\beta_\chi}^2 \right) + \frac{9}{4s_{\beta_\chi}^2} h_{t,\chi}^2 \right] \right\}, \quad (7.5c)$$

$$\tilde{g}_{2u}(M_S) = g_\chi' c_{\beta_\chi} \left\{ 1 + k \left[ -g_\chi^2 \left( \frac{2}{3} + \frac{11}{16} s_{\beta_\chi}^2 \right) + \frac{1}{20} g_\chi'^2 \left( -2 + 7s_{\beta_\chi}^2 \right) \right] \right\}. \quad (7.5d)$$

Here all couplings have a subscript $\chi$ (e.g. $g_\chi$) to make clear that the couplings of the split-model and not of the SM are meant. The RGEs for the couplings $\tilde{g}_{1u}, \tilde{g}_{2u}, \tilde{g}_{1d}, \tilde{g}_{2d}$ can be found in App. A.2.

The chargino/neutralino contribution to the threshold condition for $\lambda(M_S)$ (see Eq. (7.1)) is now present at the scale $Q = M_\chi$ in the form [35, 36]

$$\begin{aligned}
\lambda_{\text{SM}}(M_\chi) =\, & \lambda_\chi(M_\chi) + k \left\{ -\frac{7}{12}(\tilde{g}_{1d}^4 + \tilde{g}_{1d}^4) - \frac{9}{4}(\tilde{g}_{2d}^4 + \tilde{g}_{1u}^4) - \frac{3}{2}\tilde{g}_{1d}^2 g_{1u}^2 - \frac{7}{2} g_{2d}^2 g_{2u}^2 \right. \\
& - \frac{8}{3}\tilde{g}_{1d}\tilde{g}_{1u}\tilde{g}_{2d}\tilde{g}_{2u} - \frac{7}{6}(\tilde{g}_{1d}^2\tilde{g}_{2d}^2 + \tilde{g}_{1u}^2\tilde{g}_{2u}^2) - \frac{1}{6}(\tilde{g}_{1d}^2\tilde{g}_{2u}^2 + \tilde{g}_{1u}^2\tilde{g}_{2d}^2) \\
& - \frac{4}{3}(\tilde{g}_{1d}\tilde{g}_{2u}^2 + \tilde{g}_{1u}\tilde{g}_{2d})(\tilde{g}_{1d}\tilde{g}_{2d} + \tilde{g}_{1u}\tilde{g}_{2u}) \\
& + \frac{2}{3}\tilde{g}_{1d}\tilde{g}_{1u}(\lambda_\chi - 2\tilde{g}_{1d}^2 - 2\tilde{g}_{1u}^2) + 2\tilde{g}_{2d}\tilde{g}_{2u}(\lambda_\chi - 2\tilde{g}_{2d}^2 - 2\tilde{g}_{2u}^2) \\
& \left. + \frac{1}{3}\lambda_\chi(\tilde{g}_{1d}^2 + \tilde{g}_{1u}^2) + \lambda_\chi(\tilde{g}_{2d}^2 + \tilde{g}_{2u}^2) \right\}.
\end{aligned} \quad (7.6)$$

The subscript SM identifies a coupling of the SM valid below $M_\chi$. For $M_\chi = M_S$ this expression reduces to the one of Eq. (7.1) by plugging in the following tree-level relations [35, 36]

$$\lambda_\chi(M_S) = \frac{1}{4}(g_{\mathrm{SM}}^2 + g_{\mathrm{SM}}'^2)c_{2\beta_{\mathrm{SM}}}^2, \tag{7.7a}$$

$$\tilde{g}_{1u}(M_S) = g_{\mathrm{SM}}' s_{\beta_{\mathrm{SM}}}, \tag{7.7b}$$

$$\tilde{g}_{1d}(M_S) = g_{\mathrm{SM}}' c_{\beta_{\mathrm{SM}}}, \tag{7.7c}$$

$$\tilde{g}_{2u}(M_S) = g_{\mathrm{SM}} s_{\beta_{\mathrm{SM}}}, \tag{7.7d}$$

$$\tilde{g}_{2d}(M_S) = g_{\mathrm{SM}} c_{\beta_{\mathrm{SM}}}. \tag{7.7e}$$

Not only $\lambda$ receives a threshold correction at $Q = M_\chi$ but also the top-Yukawa coupling $h_t$. Its explicit form is given in [35, 36],

$$h_{t,\chi}(M_\chi) = h_{t,\mathrm{SM}}(M_\chi) \left\{ 1 - k \left[ \frac{1}{6}\tilde{g}_{1u}\tilde{g}_{1d} + \frac{1}{12}(\tilde{g}_{1u}^2 + \tilde{g}_{1d}^2) \right.\right.$$
$$\left.\left. + \frac{1}{2}\tilde{g}_{2u}\tilde{g}_{2d} + \frac{1}{4}(\tilde{g}_{2u}^2 + \tilde{g}_{2d}^2) \right] \right\}. \tag{7.8}$$

The gauge-couplings remain unaffected at the one-loop level [35, 36],

$$g_\chi(M_\chi) = g_{\mathrm{SM}}(M_\chi), \tag{7.9a}$$

$$g_\chi'(M_\chi) = g_{\mathrm{SM}}'(M_\chi), \tag{7.9b}$$

$$g_{3,\chi}(M_\chi) = g_{3,\mathrm{SM}}(M_\chi). \tag{7.9c}$$

Their RGEs however are modified above $Q = M_\chi$ (see App. A.2).

## 7.3   Gluino threshold

A further extension of this framework is the introduction of a variable Gluino threshold $m_t \ll M_{\tilde{g}} \leq M_S$. Above $Q = M_{\tilde{g}}$ the gluino contributes to the RGE-running, below it gets decoupled. This scenario is shown in Figure 7.3.



Figure 7.3: The additional gluino threshold $M_{\tilde{g}}$ is allowed to vary between $m_t$ and $M_S$. Below $M_{\tilde{g}}$ the gluino gets decoupled.
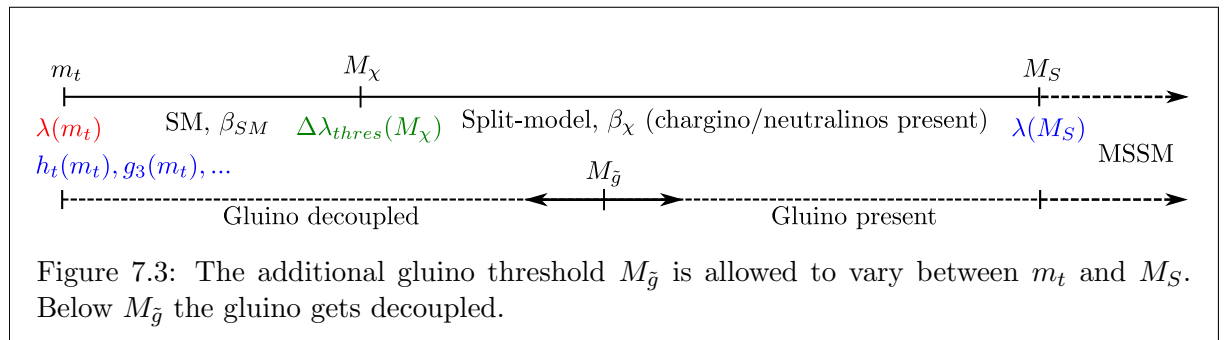
Conveniently, no new threshold corrections appear. For the Higgs self-coupling $\lambda$, this is immediately clear, since the gluino contributes only from the two-loop level on. The same argument applies for the threshold corrections for $g$, $g'$ and $h_t$ at the scale $Q = M_{\tilde{g}}$. In the case of $g_3$, however, this argument does not apply, since the gluon couples directly to gluinos.

51

Nevertheless, an explicit calculation shows that also $g_3$ does not receive a threshold correction at the scale $Q = M_{\tilde{g}}$ (see [35, 36]). Despite the fact that none of the couplings receives a threshold correction at the scale $Q = M_{\tilde{g}}$, the RGEs have to be modified above $Q = M_{\tilde{g}}$ (see App. A.1 and App. A.2), since above this scale gluinos contribute to the running of the couplings.

Looking at Eq. 5.40 it becomes clear that one should also take care of possible two-loop logarithms of the form $\ln(M_S/M_{\tilde{g}})$ or $\ln(M_{\tilde{g}}/m_t)$, which should be subtracted to avoid double-counting. At the two-loop level, however, no such logarithms arise. This can be seen by studying the RGEs given in App. A.1 and App. A.2.

Above the gluino threshold only three terms are modified, the one- and two-loop term in the RGE of $g_3$ and the two-loop term in the RGE of $h_t$. The effects of this modification get apparent by solving the RGEs iteratively (see App. B). In the first iteration step, none of the modifications enters the expression for $\lambda(m_t)$, since the couplings evaluated at $Q = m_t$ are inserted into the beta-function of $\lambda$,

$$\lambda^{(1)}(m_t) = \lambda(M_S) + \int_{M_S}^{m_t} d\ln Q^2 \left[ k\beta_\lambda^{(1)}\left(h_t(m_t), ...\right) + k^2\beta_\lambda^{(2)}\left(g_3(m_t), h_t(m_t), ...\right) \right], \quad (7.10)$$

where $\beta_\lambda^{(1)}$ and $\beta_\lambda^{(2)}$ are defined in Eq. (5.26). Note that $\beta_\lambda^{(1)}$ is independent of $g_3$ (see App. A.1 and App. A.2).

In the second iteration step, the expressions for $h_t, g_3$ after the first iteration are used as an input for the beta-functions,

$$\begin{aligned}
\lambda^{(2)}(m_t) = &\lambda(M_S) \\
&+ \int_{M_S}^{m_t} d\ln Q^2 \left[ k\beta_\lambda^{(1)}\left(h_t(m_t) + k\beta_{h_t}^{(1)}\ln\left(\frac{Q^2}{m_t^2}\right) + k^2\beta_{h_t}^{(2)}\ln\left(\frac{Q^2}{m_t^2}\right), ...\right) \right. \\
&+ \left. k^2\beta_\lambda^{(2)}\left(g_3(m_t) + k\beta_{g_3}^{(1)}\cdot ... + ..., ...\right) \right].
\end{aligned} \quad (7.11)$$

$\beta_{h_t}^{(2)}$ entering in the argument of $\beta_\lambda^{(1)}$ is multiplied by a factor of $k^2$. $\beta_\lambda^{(1)}$ itself has per definition a prefactor $k$. In consequence, $\beta_{h_t}^{(2)}$ contributes to $\lambda(m_t)$ from the three-loop level on (factor $k^3$). In other words, a modification of $\beta_{h_t}^{(2)}$ leads to a modification of the final result for $M_h$ at the three-loop level. The same argumentation shows that $\beta_{g_3}^{(1)}$ contributes to $\lambda(m_t)$ not before the three-loop level. Consequently, also the modification of $\beta_{g_3}^{(1)}$ is a three-loop effect. The modification of $\beta_{g_3}^{(2)}$ implies an effect of even higher-order. In conclusion, no logarithms of the form $\ln(M_S/M_{\tilde{g}})$ or $\ln(M_{\tilde{g}}/m_t)$ are induced at the two-loop level. Therefore, no additional logarithms have to be subtracted if introducing a gluino threshold.

One might argue against this statement by referring to the diagrammatic $\mathcal{O}(\alpha_s\alpha_t)$ results derived in [16] which in fact contain logarithms involving $M_{\tilde{g}}$. In the limit $M_{\tilde{g}} \ll M_S$, which is intrinsically assumed if introducing a gluino threshold below $Q = M_S$, these logarithms are however suppressed by $M_S$.

## 7.4 Running of $\tan\beta$

In the FD calculation implemented into `FeynHiggs`, $\tan\beta$ is an input parameter renormalized in the $\overline{\text{DR}}$-scheme at the scale $Q = m_t$ (see Eq. (4.73)). In the EFT calculation $\tan\beta$ enters as a

parameter defined in the $\overline{\text{MS}}$-scheme at the scale $Q = M_S$. In consequence, $\tan \beta$ has clearly to be seen as a running parameter (the conversion between $\overline{\text{DR}}$ and $\overline{\text{MS}}$ is discussed in Chapter 8). The issue however is the question how $\tan \beta$ should be defined below $Q = M_A \approx M_S$. In the MSSM $\tan \beta$ is defined as the ratio of the vacuum expectation values of the two Higgs doublets. If following an EFT approach, one of the Higgs doublets is integrated out below $Q = M_A$ such that it is not clear anymore how to define $\tan \beta$ for $Q < M_A$.

This problem has been already noted in [32]. There it was suggested to use alternative definitions of $\tan \beta$ in terms of physical observables, which do not suffer from this problem, and showed that their results (one-loop corrections to $M_h$) are independent of the chosen definition. Another point of view is to see $\tan \beta$ as a high-energy parameter whose value is studied at low energies.

In this case, its running is governed by the anomalous dimensions of the two Higgs doublets. At the one-loop level they read [32]

$$\gamma_1 = \frac{d}{dt} \ln Z_{\mathcal{H}_1}^2 = \frac{k}{4} \left( 9g^2 + 3g'^2 \right), \tag{7.12}$$

$$\gamma_2 = \frac{d}{dt} \ln Z_{\mathcal{H}_2}^2 = \frac{k}{4} \left( 9g^2 + 3g'^2 - 12\tilde{h}_t^2 \right), \tag{7.13}$$

where $Z_{\mathcal{H}_1}$ and $Z_{\mathcal{H}_2}$ are the field renormalization constants of the two Higgs doublets $\mathcal{H}_1, \mathcal{H}_2$ ($Z_{\mathcal{H}_{1,2}} = 1 + \delta Z_{\mathcal{H}_{1,2}}$, see Eqs. (4.61) and (4.62)). $\tilde{h}_t$ is the SUSY top-Yukawa coupling, related to the SM top-Yukawa coupling $h_t$ at tree-level via

$$\tilde{h}_t = \frac{gm_t}{\sqrt{2}m_W s_\beta} \Rightarrow \tilde{h}_t^2 = \frac{h_t^2}{s_\beta^2}. \tag{7.14}$$

The resulting equation for the running of $\tan \beta$ reads

$$\frac{1}{1 + \tan^2 \beta} \frac{d \tan^2 \beta}{dt} = -3kh_t^2. \tag{7.15}$$

According to [32], all of the terms originate from SM fields. In consequence, the equation has not to be modified for $Q < M_S$, even if passing a intermediary sparticle threshold.

In principle, for the resummation of the subleading logarithms the anomalous dimensions have to be known at the two-loop level. For the MSSM they can be found in [56, 57]. It is however unknown which parts of the two-loop beta function are due to sparticles. It could well be that below e.g. $Q = M_\chi$ the beta function has to be modified to account for integrating out the charginos and neutralinos. In addition, also potential one-loop threshold corrections are unknown.

Consequently, four different options are basically available to proceed further,

1. ignore the running of $\tan \beta$ and identify $t_\beta(m_t)$ with $t_\beta(M_S)$

2. use a one-loop fixed-order expression to relate $t_\beta(m_t)$ to $t_\beta(M_S)$ (derived using the one-loop RGE given in Eq. (7.15))

3. use the one-loop RGE of $\tan \beta$ to relate $t_\beta(m_t)$ to $t_\beta(M_S)$

4. use the two-loop RGE of $\tan \beta$ to relate $t_\beta(m_t)$ to $t_\beta(M_S)$ neglecting possible threshold corrections

The first option is not acceptable. The expression in Eq. (7.3) is derived assuming that $\tan\beta$ runs. The found correspondence to the Feynman-diagrammatic result 6.8 is not reproduced assuming that $\tan\beta$ does not run. Following the second option, the EFT calculation does reproduce the one-loop logarithms given in Eq. (6.8). It is however not clear, why only a one-loop fixed-order expression should be used for $\tan\beta$, if full all-order running is applied for all other couplings. Therefore, option three seems to be favorable.

As mentioned before, for a consistent resummation of subleading logarithms it would be necessary to employ a two-loop running for $\tan\beta$. Deriving the necessary one-loop threshold corrections and checking the origin of the terms in the two-loop running is however beyond the scope of this thesis. In consequence, option four can only be used to estimate the error induced by additional subleading logarithms originating from the running of $\tan\beta$ at the two-loop level (two-loop RGE). Therefore, the third option seems to be the best choice and is used throughout this thesis.

A further discussion including numerical comparisons can be found in App. E.

# Chapter 8

# Conversion of input parameters

In the renormalization group approach, all quantities are renormalized in the $\overline{\text{MS}}$-scheme. In contrast in the Feynman-diagrammatic approach, all quantities (except of the field renormalization constants, which are renormalized using the $\overline{\text{DR}}$ scheme) are renormalized in the OS-scheme. Therefore, to properly combine the result obtained using the different approaches, relations connecting the OS- and $\overline{\text{MS}}$-values of appearing quantities have to be derived (as noted in Section 5.4, see [34] for an extensive discussion).

A bare parameter $p$ appearing in a Lagrangian is related to its corresponding on-shell/$\overline{\text{MS}}$-definition via

$$p = p^{OS} + \delta p^{OS} = p^{\overline{\text{MS}}} + \delta p^{\overline{\text{MS}}}. \tag{8.1}$$

At tree level all definitions correspond to each other ($p = p^{OS} = p^{\overline{\text{MS}}}$). At higher-orders the counterterms do not vanish. Therefore the relation between the OS- and the $\overline{\text{MS}}$-definition of a quantity is

$$p^{\overline{\text{MS}}} = p^{OS} + \delta p^{OS} - \delta p^{\overline{\text{MS}}} = p^{OS} + \delta p^{OS}|_{\Delta \text{ subtr.}}. \tag{8.2}$$

The $\overline{\text{MS}}$-counterterm cancels the part of $\delta p^{OS}$ proportional to $\Delta = 1/\epsilon - \gamma_E + \log 4\pi$ and therefore renders the results UV-finite. As noted in Section 5.4, for the present analysis only logarithmic terms in the conversion between the schemes need to be known.

In addition to the conversion of the input parameters, the conversion of the tree-level matching condition between the $\overline{\text{DR}}$- and the $\overline{\text{MS}}$-scheme is discussed in the last part of this Chapter.

**Conversion of the stop-mixing parameter $X_t$**

The relation between $X_t^{\text{OS}}$ and $X_t^{\overline{\text{MS}}}$ has been already studied in e.g. [22, 29, 34, 58] (in the limit $g = g' = 0$). This relation can be obtained by using the definition of the counterterm for $\delta X_t$ given in [59],

$$\delta X_t = \frac{1}{m_t} \left[ (\delta m_{\tilde{t}_1}^2 - \delta m_{\tilde{t}_2}^2) \mathbf{U}_{\tilde{t},11} \mathbf{U}_{\tilde{t},12} + \delta m_{\tilde{t}_1 \tilde{t}_2}^2 (\mathbf{U}_{\tilde{t},21} \mathbf{U}_{\tilde{t},12} + \mathbf{U}_{\tilde{t},11} \mathbf{U}_{\tilde{t},22}) - X_t \delta m_t^2 \right], \tag{8.3}$$

where $\delta m_t^2$ is the top mass counterterm (see Figure 8.2 for the corresponding diagrams) and $\mathbf{U}_{\tilde{t}}$ is the stop mixing matrix as defined in Section 4.3. The appearing stop mass counterterms are defined in the OS scheme as follows,

$$\delta m_{\tilde{t}_1}^2 = \text{Re}\Sigma_{\tilde{t}_1\tilde{t}_1}(m_{\tilde{t}_1}^2), \tag{8.4}$$

$$\delta m_{\tilde{t}_1}^2 = \text{Re}\Sigma_{\tilde{t}_2\tilde{t}_2}(m_{\tilde{t}_2}^2), \tag{8.5}$$

$$\delta m_{\tilde{t}_1\tilde{t}_2}^2 = \frac{1}{2}\text{Re}\left\{\Sigma_{\tilde{t}_1\tilde{t}_2}(m_{\tilde{t}_1}^2) + \Sigma_{\tilde{t}_1\tilde{t}_2}(m_{\tilde{t}_2}^2)\right\}, \tag{8.6}$$

where $\Sigma_{\tilde{t}_1\tilde{t}_1}$, $\Sigma_{\tilde{t}_1\tilde{t}_2}$ and $\Sigma_{\tilde{t}_2\tilde{t}_2}$ are stop self-energies (see Figure 8.1 for corresponding diagrams). In the $\overline{\text{MS}}$-scheme, the counterterms are equal to the parts of the self-energies proportional to $\Delta$. The appearing renormalization scale has to be chosen to be $Q = M_S$, since at this scale $X_t$ appears in the RGE-approach (see Eq. (7.1)). An explicit calculation in the limit $\mathcal{O}(M_Z) \ll M_{Susy}, M_\chi, M_{\tilde{g}}$ yields (see Figure 8.1 and 8.2 for the involved Feynman diagrams and Chapter 6 for the used calculation techniques)

$$X_t^{\overline{\text{MS}}} = X_t^{\text{OS}}\left[1 + \left(\underbrace{\frac{\alpha_s}{\pi}}_{\text{Gluon/Gluino sector}} \underbrace{-\frac{3\alpha_t}{16\pi}(1-\hat{X}_t^2)}_{\text{Higgs sector}} \underbrace{-\frac{\alpha}{96\pi}(1-26c_w^2)}_{\text{Massive vector boson sector}}\right)\log\frac{M_S^2}{m_t^2}\right]. \tag{8.7}$$

with $\hat{X}_t \equiv X_t/M_S$ and $\alpha$ being the fine-structure constant. In the one-loop part of the formula above it is not specified if $\hat{X}_t$ is OS- or $\overline{\text{MS}}$-renormalized, since distinguishing between OS and $\overline{\text{MS}}$ at the one-loop level is formally an effect of two-loop order. So at one-loop accuracy, one is free to use either $X_t^{\text{OS}}$ or $X_t^{\overline{\text{MS}}}$.

The result agrees with the result of [29] if setting $g = g' = 0$. Note that the term proportional to $\hat{X}_t^2$ is missing in [39]. It originates from the stop self-energy diagrams involving one virtual stop/sbottom and a Goldstone boson (see Figure 8.1). Particle sectors not mentioned in Eq. (8.7) do not contribute logarithmically.

### Conversion of the stop-mass scale $M_S$

The stop mass scale $M_S$ is defined by

$$M_S \equiv \sqrt{m_{\tilde{t}_1}m_{\tilde{t}_2}}. \tag{8.8}$$

Its counterterm can be derived by a counterterm expansion yielding

$$\delta M_S^2 = \frac{1}{2}\left(\frac{m_{\tilde{t}_2}}{m_{\tilde{t}_1}}\delta m_{\tilde{t}_1}^2 + \frac{m_{\tilde{t}_1}}{m_{\tilde{t}_2}}\delta m_{\tilde{t}_2}^2\right). \tag{8.9}$$

Again the appearing scale has to be chosen to be $Q = M_S$ since at this scale also $M_S$ appears in the RGE approach (see Eq. (7.1)). An explicit calculation shows that in the limit $\mathcal{O}(M_Z) \ll M_S$ there are no logarithms present in the corresponding conversion relation (see Figure 8.1 for the involved Feynman diagrams).

### Residual parameters

In addition to $M_S$ and $X_t$, there are some other quantities appearing in the RGE approach, which have to be converted, namely $M_\chi$, $M_{\tilde{g}}$, $m_t$ and $t_\beta(m_t)$. The chargino/neutralino mass
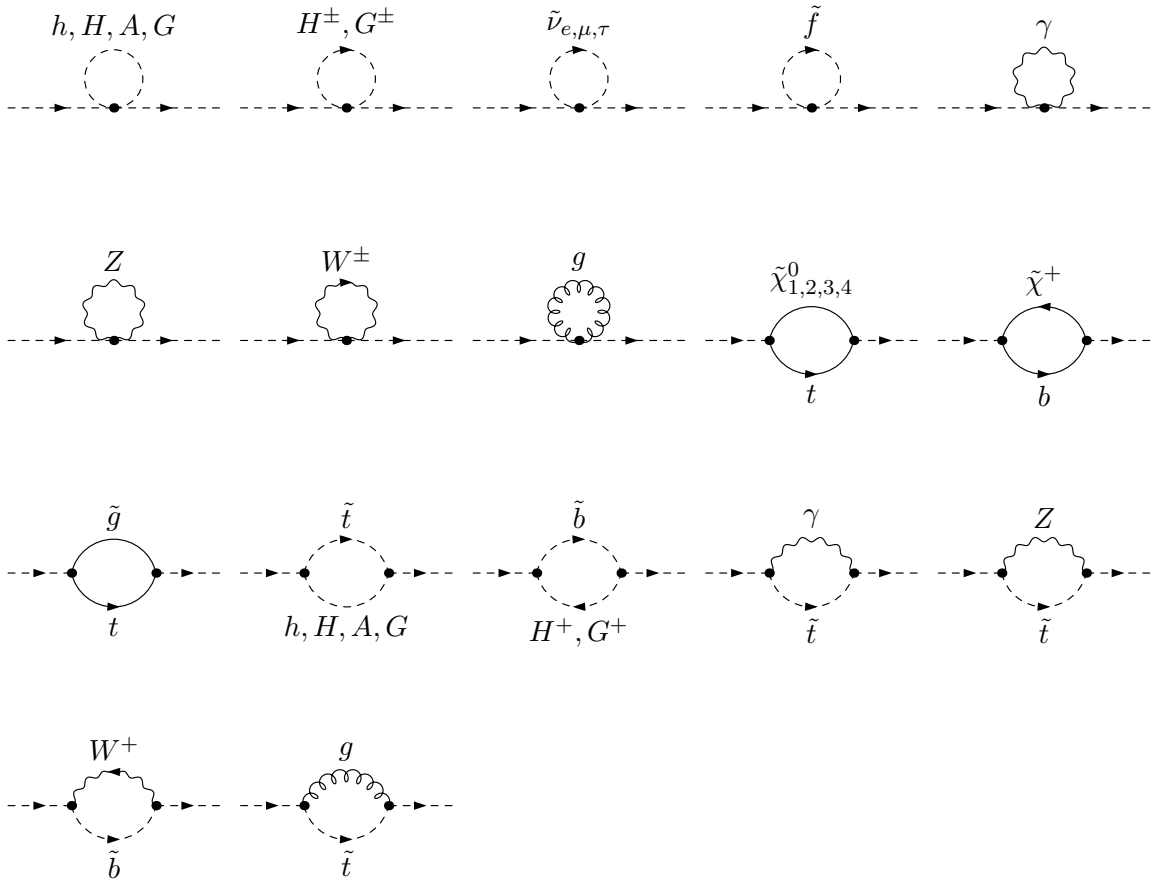
Figure 8.1: Generic Feynman diagrams for the stop self-energies.
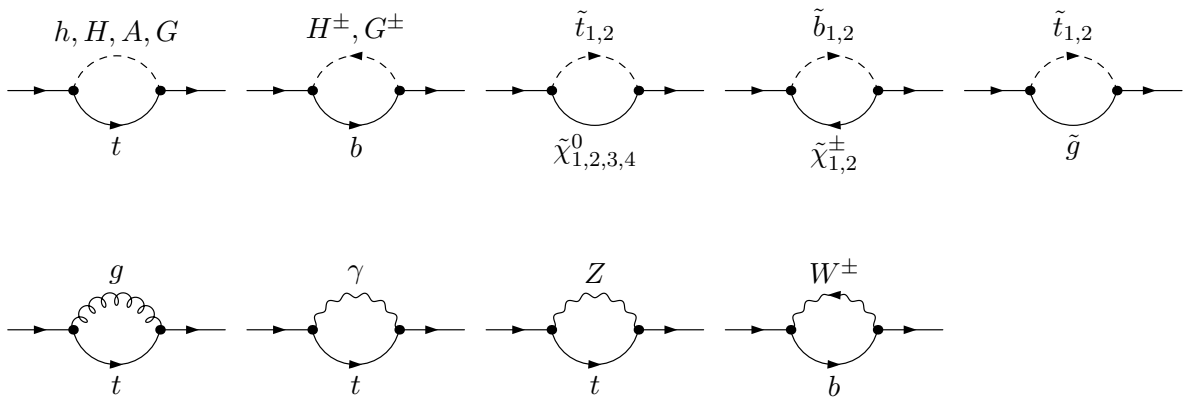


Figure 8.2: Generic Feynman diagrams for the top-quark self-energy.

57
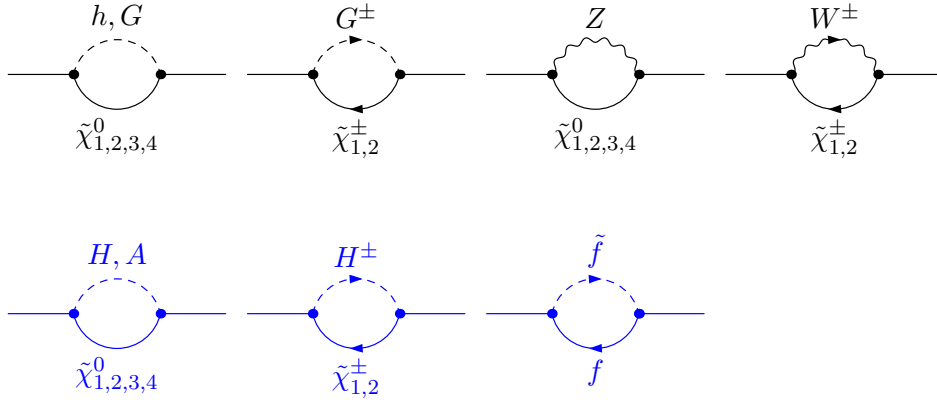
Figure 8.3: Generic Feynman diagrams for the $\tilde{\chi}_2^0$ self-energy ($f = e, \mu, \tau, u, d, c, s, t, b$). Diagrams painted in blue are not present for $M_\chi \ll M_S$ in the effective field theory approach.
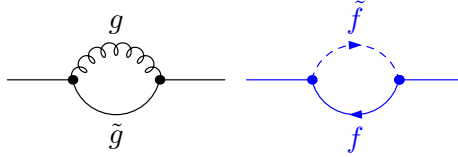


Figure 8.4: Generic Feynman diagrams for the gluino self-energy ($f = e, \mu, \tau, u, d, c, s, t, b$). Diagrams painted in blue are not present for $M_{\tilde{g}} \ll M_S$ in the effective field theory approach.

scale $M_\chi$ has to be converted at the scale $Q = M_\chi$. Note that the mass of $\tilde{\chi}_2^0$ is exactly $M_\chi$ at tree-level (see Eq. C.6). By defining $M_\chi \equiv M_{\tilde{\chi}_2^0}$ the corresponding mass-counterterm can be used to convert $M_\chi$ (see Figure 8.3 for the corresponding Feynman diagrams). No logarithmic terms are found.

The choice of the counterterm is a bit arbitrary. Nevertheless intuitively, the counterterm of $M_\chi$ should be associated with one or a combination of the mass counterterms of the charginos/neutralinos. Since the couplings of the charginos/neutralinos are all similar, also a different choice for the renormalization of $M_\chi$ should not induce any logarithm.

$M_{\tilde{g}}$ is the mass of the gluino. Therefore, the mass counterterm of the gluino has to be used (see Figure 8.4 for the corresponding Feynman diagrams). Again no logarithmic terms are found.

Concerning $m_t$, no extra effort has to be made, since it is advantageous to use the $\overline{\text{MS}}$-running top mass $\overline{m}_t(m_t)$ as input for the FD calculation. Using $\overline{m}_t(m_t)$ absorbs higher-order QCD effects. In consequence, the same scheme is used in both approaches making a conversion unnecessary.

The ratio of the vacuum expectation values of the two Higgs doublets $t_\beta(m_t)$ is renormalized in the $\overline{\text{DR}}$-scheme in the FD calculation. In the RGE approach, it enters renormalized in the $\overline{\text{MS}}$-scheme. The conversion between $\overline{\text{DR}}$ and $\overline{\text{MS}}$ yields no logarithmic terms, since at the scale $Q = m_t$ no heavy sparticles are present. In principle, also non-logarithmic terms should be included, since $t_\beta(m_t)$ enters in the prefactors of leading logarithms. These contributions are however neglected in this thesis.

**Conversion of the tree-level matching condition of $\lambda$**

At tree-level $\lambda(M_S)$ is given by

$$\lambda(M_S) = \frac{1}{4}(g^2 + g'^2)c_{2\beta}^2. \tag{8.10}$$

As discussed in Section 7.1, this relations originates from the MSSM Higgs potential given in Eq. (4.28). The MSSM, as a supersymmetric theory, is renormalized using DRED as noted in Section 4.7.1. Therefore, also the quantities appearing in tree-level matching condition for $\lambda(M_S)$ ($g$, $g'$ and $t_\beta$) are $\overline{\text{DR}}$-renormalized. However, the EFT below $Q = M_S$ is renormalized in the $\overline{\text{MS}}$-scheme, i.e. $g$, $g'$ and $t_\beta$. Consequently, the tree-level matching condition has to be converted from the $\overline{\text{DR}}$-scheme to the $\overline{\text{MS}}$-scheme. This conversion results in an additional one-loop threshold correction (see Eq. (7.1)).

# Chapter 9

# Numerical results

In this Chapter the numerical results of the `FeynHiggs` extensions described above are presented. The logarithms are resummed by solving the system of RGEs with corresponding matching conditions numerically. This numerical resummation is implemented into a separate `Fortran` program (a `Mathematica` version is also available). The program calculates $\Delta M_h^2$ as defined in Eq. (5.40). Afterwards, the result is combined with the numeric result of `FeynHiggs` $(M_h^2)^{\text{FD}}$ by simply adding both results (see Eq. (5.40)).

For the SM parameters appearing in the Feynman-diagrammatic calculation the `FeynHiggs` default values are used,

$$M_Z = 91.1876 \text{ GeV}, \tag{9.1}$$

$$M_W = 80.385 \text{ GeV}, \tag{9.2}$$

$$m_b^{\text{OS}} = 4.2 \text{ GeV}, \tag{9.3}$$

$$m_t^{\text{OS}} = 173.2 \text{ GeV}, \tag{9.4}$$

$$G_F = 1/(2\sqrt{2}v^2) = 1.16639 \cdot 10^{-5} \text{ GeV}^{-2}, \tag{9.5}$$

$$\alpha_s(M_Z) = 0.118. \tag{9.6}$$

The numerical values for the running $\overline{\text{MS}}$ gauge and Yukawa couplings evaluated at the scale $Q = m_t$ are adapted from [60], in which the measured SM parameters listed above are used to derive these couplings,

$$g'_{\text{SM}}(m_t) = 0.3576, \tag{9.7}$$

$$g_{\text{SM}}(m_t) = 0.6482, \tag{9.8}$$

$$g_{3,\text{SM}}(m_t) = 1.1666, \tag{9.9}$$

$$h_{t,\text{SM}}(m_t) = 0.9356. \tag{9.10}$$

These values found in [60] are of three-loop order (NNLO) or even four-loop QCD order (NNNLO) in the case of $h_t$. Formally it would also be correct to use the one-loop (NLO) values, because only one-loop threshold corrections are needed. Using the NNNLO value for $h_t$ gives however rise to large corrections as noted by [38, 61]. Therefore, using the NNNLO value for $h_t$ and the NNLO values for the other couplings seems to be favourable.

In this Chapter, $X_t^{\text{OS}}$ is meant, if the stop-mixing parameter $X_t$ appears without a superscript. Furthermore, the shorthand $t_\beta$ is used for $t_\beta(m_t)$. The often occurring statement that

the electroweak gauge couplings are neglected (i.e. $g = g' = 0$) applies only to the resummation of logarithms, i.e. $g, g' \neq 0$ in the Feynman-diagrammatic calculation.

## 9.1   Electroweak contributions

In this part of the analysis it is assumed that all sparticles share a common mass scale (see Section 7.1), i.e.

$$M_\chi = M_{\tilde{g}} = M_S. \tag{9.11}$$

First, the dependence of $M_h$ on $M_S$ is investigated. In a second step, the influence of $X_t$ is scrutinized. The dependence on $\tan\beta$ is discussed in the third part. Last, the importance of the resummation is studied using iteratively obtained fixed-order expression.

### Dependence on stop mass scale $M_S$

The impact of resumming also electroweak contributions is depicted in Figure 9.1. $M_h$ is shown in dependence of $M_S$ for vanishing stop-mixing. $M_h$ is calculated in different ways using the

- fixed-order `FeynHiggs` result.

- fixed-order `FeynHiggs` result + resummation of LL logarithms $\propto \alpha_t, \alpha_s$.

- fixed-order `FeynHiggs` result + resummation of LL+NLL $\propto \alpha_t, \alpha_s$.

- fixed-order `FeynHiggs` result + resummation of LL logarithms $\propto \alpha_t, \alpha_s, g, g'$.

- fixed-order `FeynHiggs` result + resummation of LL+NLL $\propto \alpha_t, \alpha_s, g, g'$.

Here LL is an abbreviation for leading logarithm, NLL for next-to-leading or subleading logarithm.

Figure 9.1 shows clearly the importance of resumming logarithmic contributions for $M_S \gtrsim 1$ TeV. The fixed-order result is significantly below the results including resummation. For $M_S \gtrsim 15$ TeV the discrepancy can be higher than 20 GeV. It can also be observed that the greatest part of this shift is due to logarithms $\propto \alpha_s, \alpha_t$. The electroweak contributions in the resummation amount to only 2-3 GeV for $M_S \sim 20$ TeV showing the dominance of the logarithms $\propto \alpha_s, \alpha_t$. To gain a precise result, it is nevertheless mandatory to include them, since already for moderate $M_S$ ($\sim 2.5$ TeV) they shift $M_h$ upwards by $\sim 1$ GeV. Figure 9.1 also illustrates the impact of subleading (NLL) logarithms. Resumming them decreases $M_h$ in comparison with resumming only leading logarithms by $2 - 2.5$ GeV for $M_S \sim 20$ TeV showing their significance. Figure 9.2 shows that this shift is mainly due to subleading logarithms $\propto \alpha_t, \alpha_s$. Subleading logarithms proportional to the electroweak gauge couplings only have minor effects.
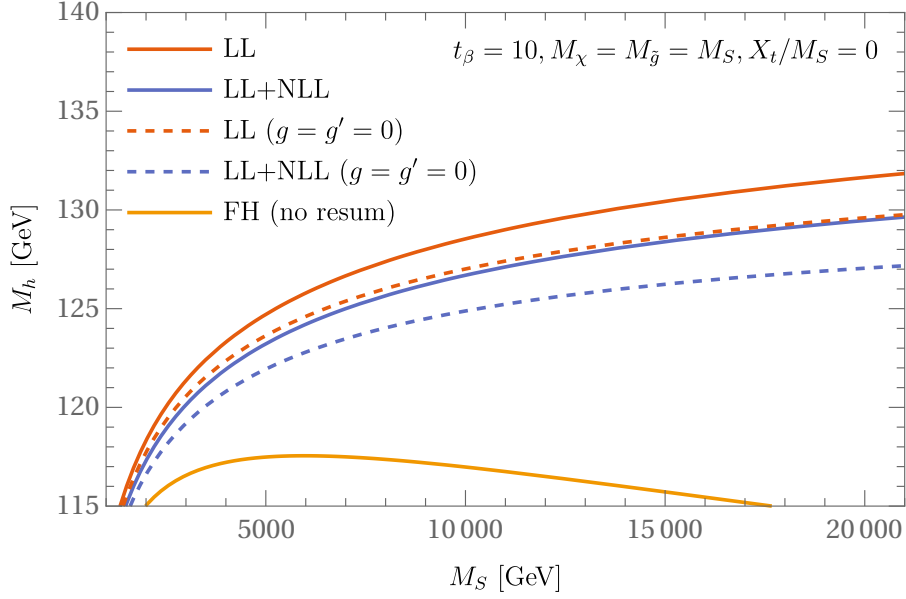
Figure 9.1: $M_h$ as a function of $M_S$ for $X_t/M_S = 0$. The fixed-order `FeynHiggs` result (FH, orange) is compared with results containing the resummation of leading (red) and next-to-leading (blue) logarithms neglecting the weak gauge couplings (dashed) and including the weak gauge couplings (solid).
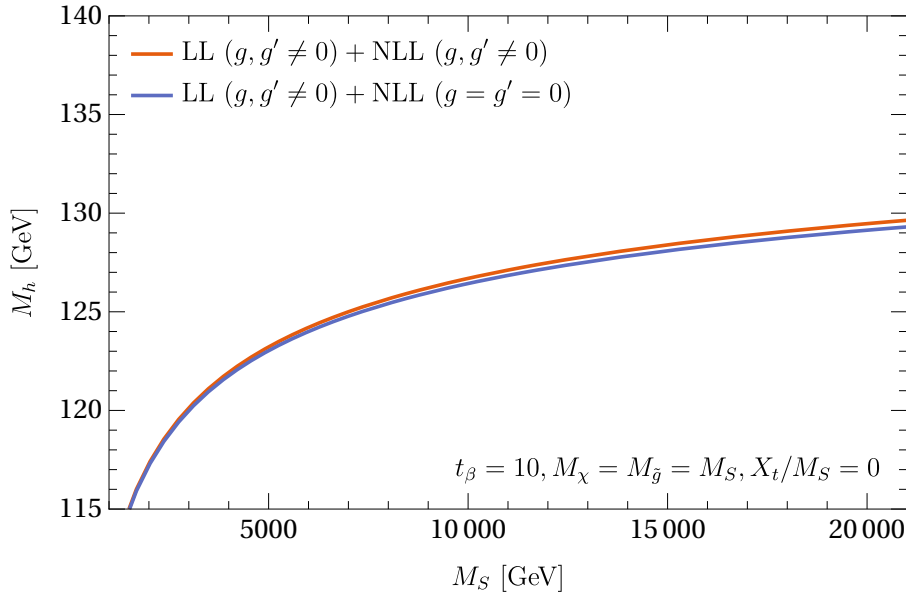


Figure 9.2: $M_h$ as a function of $M_S$ for $X_t/M_S = 0$. The results containing the resummation of leading and next-to-leading logarithms neglecting the weak gauge couplings at the next-to-leading logarithm level (blue) and including the weak gauge couplings at the next-to-leading logarithm level (red) are compared.
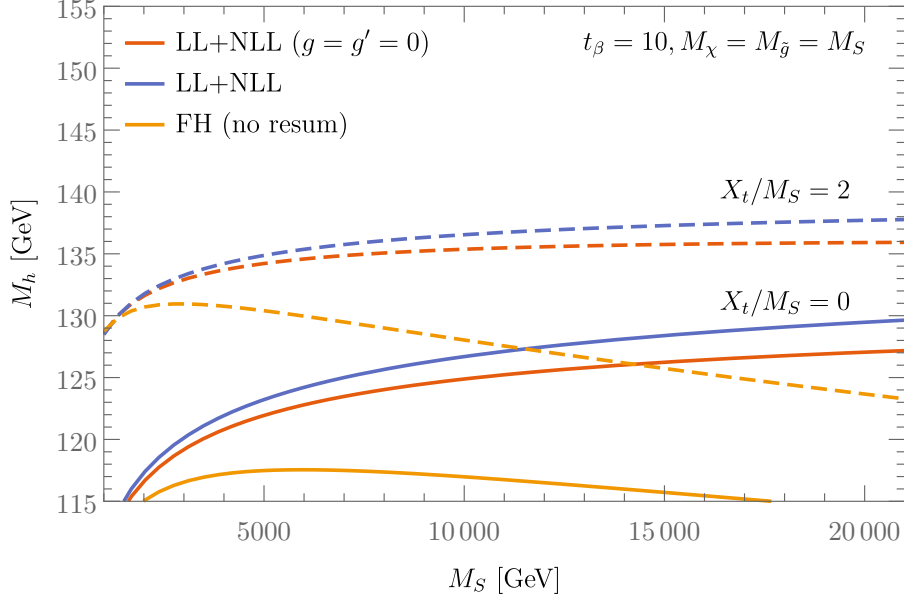
Figure 9.3: $M_h$ as a function of $M_S$ for $X_t/M_S = 0$ (solid) and $X_t/M_S = 2$ (dashed). The fixed-order `FeynHiggs` result (FH, orange) is compared with results containing the resummation of leading and subleading logarithms neglecting the weak gauge couplings (red) and including the weak gauge couplings (blue)

## Dependence on stop-mixing parameter $X_t$

The influence of stop-mixing is illustrated in Figure 9.3. It again shows $M_h$ in dependence of $M_S$ for the three cases:

- fixed-order `FeynHiggs` result

- fixed-order `FeynHiggs` result + resummation of LL+NLL $\propto \alpha_t, \alpha_s$.

- fixed-order `FeynHiggs` result + resummation of LL+NLL $\propto \alpha_t, \alpha_s, g, g'$.

But now, the results are not only shown for vanishing stop mixing but also for $X_t/M_S = 2$ (nearly maximal stop mixing).

Choosing $X_t/M_S = 2$ increases $M_h$ significantly by $\sim 10$ GeV in comparison to the case of $X_t/M_S = 0$ in all three cases. Interestingly, the curves including resummation are shallower in the cases of $X_t/M_S$ such that the difference between vanishing and nearly maximal stop mixing decreases with rising $M_S$.

As seen before in Figure 9.1, including the weak gauge couplings into the resummation procedure amounts to an upward shift of $M_h$ for $X_t/M_S = 0$. For nearly maximal mixing $X_t/M_S = 2$, the Higgs-boson mass $M_h$ is also shifted upwards. However, the shift is smaller ($\sim 2$ GeV for $M_S = 21$ TeV).

Similar observation can be made in Figure 9.4. It shows $M_h$ in dependence of $X_t/M_S$ for $M_S = 10$ TeV in the five cases

- fixed-order `FeynHiggs` result

- fixed-order `FeynHiggs` result + resummation of LL $\propto \alpha_t, \alpha_s$.

- fixed-order `FeynHiggs` result + resummation of LL+NLL $\propto \alpha_t, \alpha_s$.

- fixed-order `FeynHiggs` result + resummation of LL $\propto \alpha_t, \alpha_s, g, g'$.

- fixed-order `FeynHiggs` result + resummation of LL+NLL $\propto \alpha_t, \alpha_s, g, g'$.

The inclusion of the weak gauge couplings into the resummation procedure raises $M_h$. As observed before, the shift gets smaller for rising $|X_t/M_S|$. The sift induced by subleading logarithms is bigger for higher $|X_t/M_S|$. For $|X_t/M_S| = 0$ this Higgs-boson mass is lowered by $\sim 2$ GeV, whereas the shift is $\gtrsim 10$ GeV for $|X_t/M_S| \gtrsim 2.5$. Figure 9.4 illustrates also another noteworthy point. Resumming large logarithms does not necessarily amount to an upward shift of $M_h$. In fact, $M_h$ is shifted even below the fixed-order result for $|X_t/M_S| \gtrsim 2.7$ by the subleading logarithms (note that $X_t$ does not appear as a prefactor of leading logarithms).
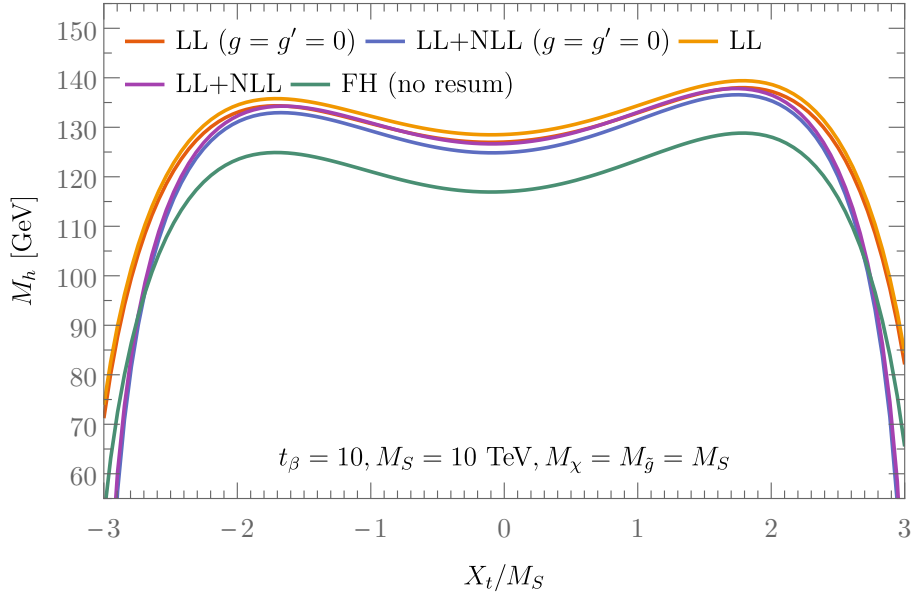


Figure 9.4: $M_h$ as a function of $X_t/M_S$ for $M_S = 10$ [TeV]. The fixed-order `FeynHiggs` result (FH, green) is compared with results containing the resummation of logarithms $\propto \alpha_s, \alpha_t$ (red for leading logarithms and blue for leading and subleading logartihms) and logarithms $\propto \alpha_s, \alpha_t, g, g'$ (orange for leading logartihms and purple for leading and subleading logarithms).

## Dependence on tan$\beta$

The impact of $\tan\beta$ on the Higgs-boson mass can be visualized by plotting $M_h$ contours in $M_S$-$\tan\beta$ planes (see Figure 9.5 and 9.6). The solid contour line marks the values of $M_S, \tan\beta$ for which $M_h = 125.09$ GeV (see Eq. (1.1)). In addition, the experimental $2\sigma$-values of $M_h$ are shown. Note that the theoretical errors are far bigger [31]. For vanishing stop mixing, the two bands (for the two cases of neglecting and including weak contributions) do not overlap. This clearly shows the importance of the weak contributions if constraining the parameter space. E.g., for high $M_S$ ($\gtrsim 10$ TeV) the measured Higgs-boson mass favors $\tan\beta \sim 5 - 6$ if including the weak gauge coupling. Neglecting them instead yields a prediction of $\tan\beta \sim 7 - 8$. Generally, including the weak gauge couplings in the resummation allows for smaller values of $M_S$ and $\tan\beta$.
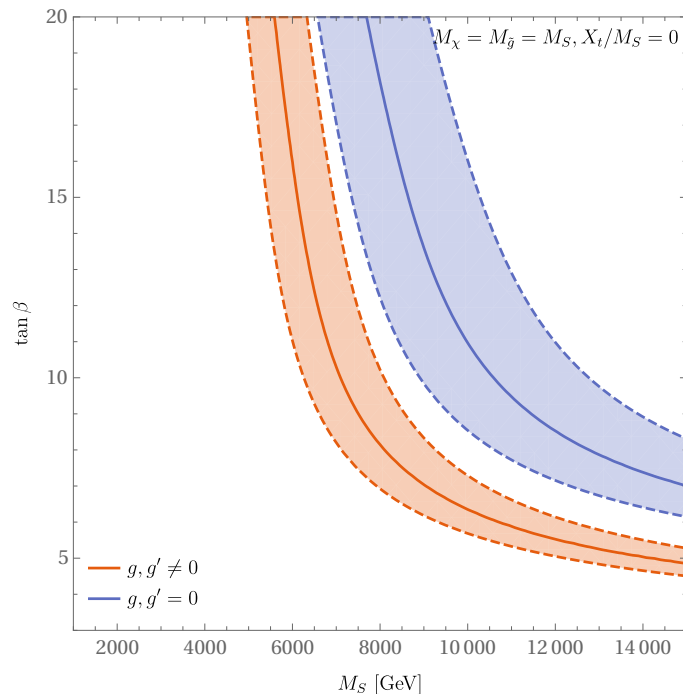


Figure 9.5: Plots of central (solid) and $2\sigma$ (dashed) contour lines of $M_h$ in the $\tan\beta$-$M_S$ plane for $X_t/M_S = 0$. The contour lines if neglecting weak gauge couplings in the resummation (blue) are compared with the full resummation including weak contributions (red).

In the case of nearly maximal stop mixing ($X_t/M_S = 2$), the weak contributions are not so important. Both bands overlap broadly showing that for maximal stop mixing neglecting the weak gauge coupling in the resummation is a better approximation as in the case of vanishing stop mixing (at least in the part of parameter space which allows for $M_h \sim 125$ GeV). The main reason is the fact that maximal stop mixing raises the Higgs-boson mass substantially requiring $M_S \sim 1$ TeV to reach the measured value of $M_h$. In consequence, the potentially large logarithms $\ln(M_S^2/m_t^2)$, which are resummed, are in fact relatively small such that also the numerical impact of the logarithms proportional to the electroweak gauge couplings is small.
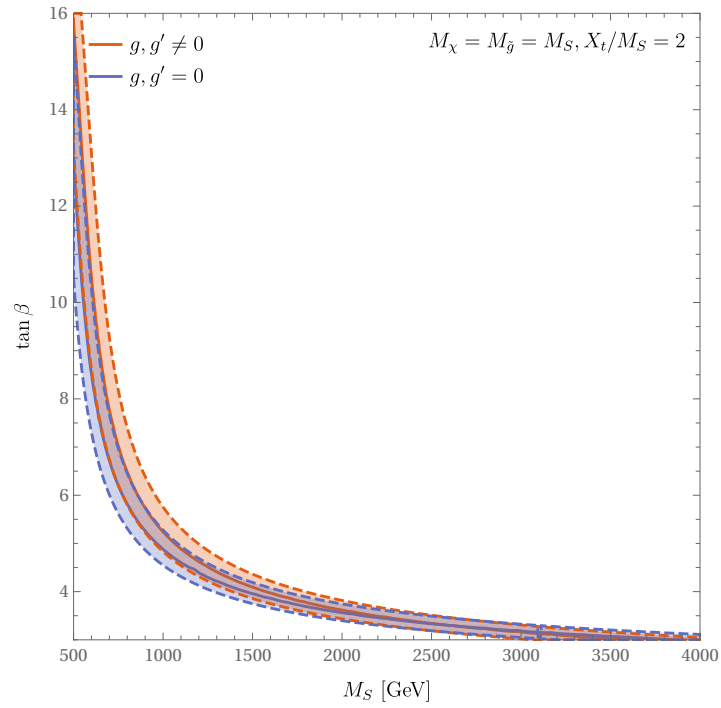
Figure 9.6: Plots of central (solid) and $2\sigma$ (dashed) contour lines of $M_h$ in the $\tan\beta$-$M_S$ plane for $X_t/M_S = 2$. The contour lines if neglecting weak gauge couplings in the resummation (blue) are compared with the full resummation including weak contributions (red).

## Iterative solution

The set of RGEs can not only be solved numerically corresponding to a resummation of logartihms up to all orders, but also iteratively as shown in App. B. It is interesting to investigate, at which loop-level $n$ a $n$-loop fixed-order result obtained by iteration is comparable to the numerical result. If the discrepancies are small, the gained analytic expression of the respective loop-level can be used as an approximate expression.

In Figure 9.7 fixed-order results up to the 7-loop level (for 7-loop subleading logarithms $\propto g, g'$ the computation is too time consuming) are compared to the numerical resummation for various cases,

- resumming LL.

- resumming LL+NLL.

- resumming only NLL.

All cases are considered for vanishing and non-vanishing weak gauge couplings in the resummation procedure, $t_\beta = 10$ and vanishing stop mixing.

Consider first the case of resumming only leading logarithms (first row of Figure 9.7). Obviously, also higher-order ($> 3$-loop) leading logarithms have huge effects on the Higgs-boson mass for moderate to high $M_S$ ($\gtrsim$ few TeV) showing that even a fixed-order two-loop calculation enhanced with leading three-loop logarithms is not a good approximation. For high $M_S$ ($\gtrsim 20$ TeV) even 7-loop leading logarithms correct the Higgs-boson mass by $\sim 1$ GeV.

Besides, it is noteworthy that the iterative results converge to the numerical results as expected. A alternating convergence behavior is visible meaning that if a $n$-loop results is above (below) the numerical results, the $n+1$-loop results will be below (above) the numerical result. The convergence is slightly worse in the case of non-vanishing weak gauge couplings.

Consider next the case of resumming leading as well as subleading logarithms (second row of Figure 9.7). Interestingly, the convergence against the numerical result is far better compared to the resummation of only leading logarithms. For small $M_S$ ($\lesssim 10$ TeV) already the 5-loop fixed-order result is a quite good approximation of the full numerical result. In this case however, the convergence is better in the case of non-vanishing weak gauge couplings.

A natural question is, why the convergence is better if leading and subleading logarithms are resummed. The reason is illustrated in the third row of Figure 9.7 showing the resummation of only subleading logarithm (obtained by subtracting the LL result from the LL+NLL results). The subleading logarithms feature the same alternating convergence behaviour as the leading logarithms. In contrast to the leading logarithms however, the convergence behaviour is reversed. Whereas the 3-loop fixed-order result is below the numerical result in the case of resumming leading logarithms, it is above the numerical result in the case of resumming leading and subleading logarithms. In other words, the deviation of the fixed-order NLL results has the opposite sign of the fixed-order LL results effectively reducing the error of the combined result.

Remarkably, the errors of the LL and NLL result are bigger in the case of non-vanishing weak gauge couplings. However, they coincide better leading to a smaller error of the combined LL+NLL result in comparison with the case of vanishing weak gauge couplings.
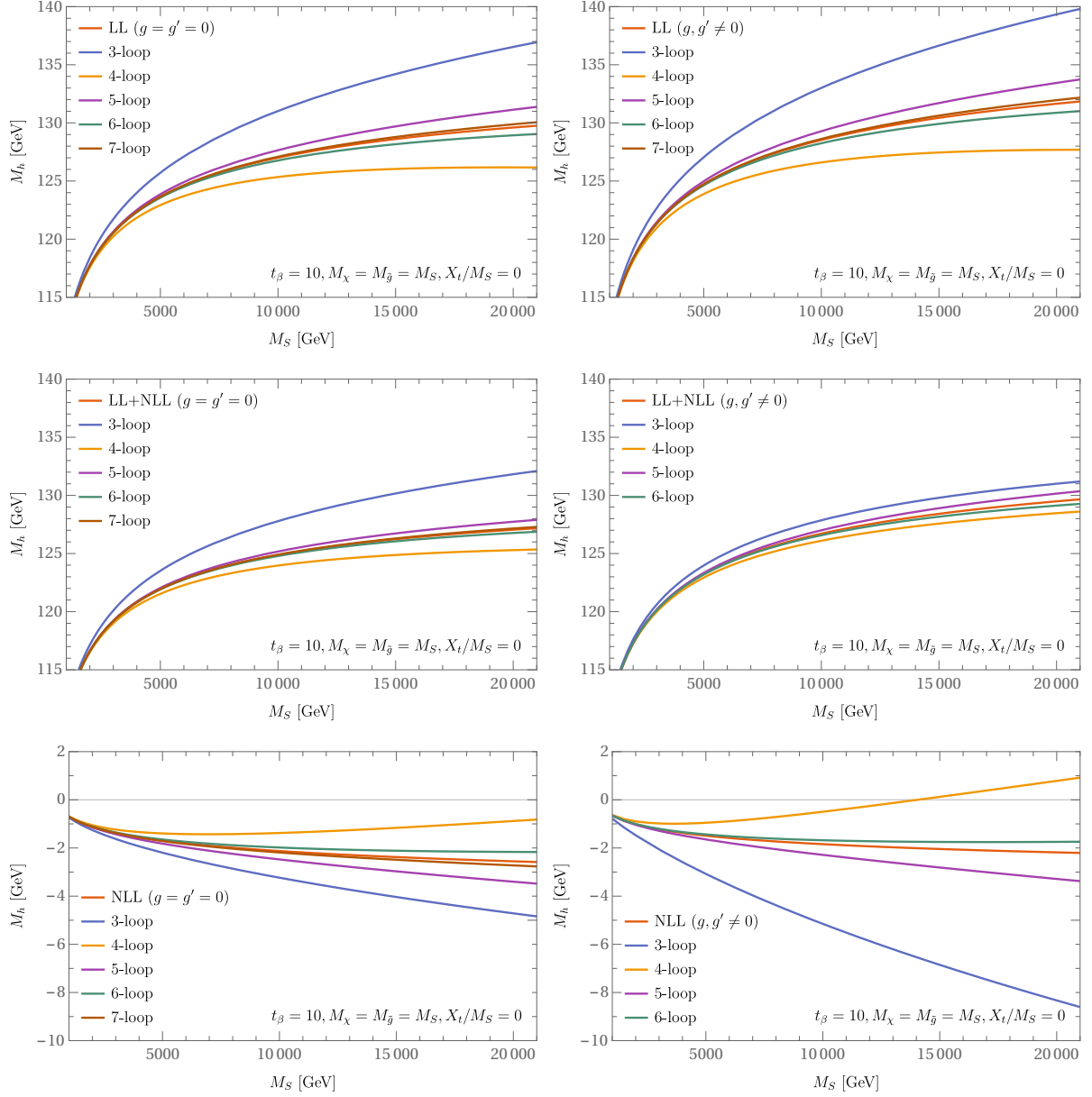
Figure 9.7: $M_h$ as a function of $M_S$ for $X_t/M_S = 0$. The result of numeric resummation of logarithms up to all orders (red) is compared to fixed-order iteratively derived $n$-loop expressions. The weak gauge couplings are neglected in the resummation in the left column and included in the right column. In the first row the resummation of leading logarithms (LL) is considered, in the second row the resummation of leading and subleading logarithms (LL+NLL) and in the third row the resummation of only subleading logarithms (NLL).

The question how non-vanishing stop mixing affects the convergence behavior of the fixed-order results is addressed in Figure 9.8. It shows $M_h$ in dependence of $M_S$ for $X_t/M_S = 0$ and $X_t/M_S = 2$ comparing the full numeric result to fixed-order expressions for vanishing and non-vanishing weak gauge couplings. It is clearly visible that choosing $X_t/M_S = 2$ improves the

convergence behavior (especially in the case of non-vanishing weak gauge couplings).
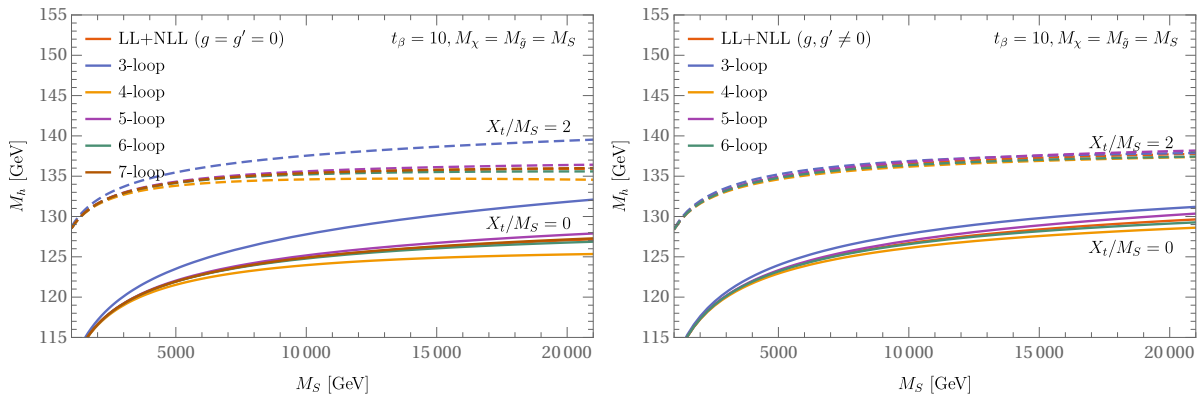


Figure 9.8: $M_h$ as a function of $M_S$ for $X_t/M_S = 0$ (solid) and $X_t/M_S = 2$ (dashed). The electroweak gauge couplings are neglected in the left plot and included in the right plot. The numerical resummation up to all orders (red) is compared to iteratively obtained fixed-order formulas up to the 7-loop level.

## 9.2 Neutralino/chargino threshold

Introducing a neutralino/chargino threshold allows to relax the assumption that all sparticles share a common mass scale,

$$M_\chi \leq M_S = M_{\tilde{q}} = M_{\tilde{g}}. \tag{9.12}$$

The following part of this Subsection explores how $M_h$ is affected by choosing $M_\chi < M_S$ for vanishing stop mixing and $\tan\beta = 10$. The scenario of nearly maximal stop mixing is investigated in the second part. The question how choosing $M_\chi < M_S$ affects the dependence of $M_h$ on $\tan\beta$ is examined in the last part.

**Dependence on chargino/neutralino mass scale $M_\chi$**

Figure 9.9 shows $M_h$ in dependence of $M_S$ for $X_t/M_S = 0$ and $t_\beta$ in the following cases:

- $M_\chi = 1$ TeV resumming LL+NLL

- $M_\chi = M_S$ resumming LL+NLL

- $M_\chi = M_S$ resumming LL+NLL (neglecting weak gauge couplings, i.e. $g = g' = 0$)

- fixed-order `FeynHiggs` result without resummation for $M_\chi = 1$ TeV

- fixed-order `FeynHiggs` result without resummation for $M_\chi = M_S$

Some of theses cases have been already discussed in Figure 9.1. There are shown here again for comparison with the cases of $M_\chi = 1$ TeV. As discussed before, including a resummation of logarithms $\propto \alpha_s, \alpha_t$ shifts the Higgs-boson mass up by $\sim 20$ GeV for $M_S \sim 20$ TeV. Furthermore including electroweak contribution into the resummation amounts to an additional

upwards shift of $\sim 2.5$ GeV (keeping $M_\chi = M_S \sim 20$ GeV). Lowering the mass scale of the charginos/neutralinos $M_\chi$ to 1 TeV raises the Higgs-boson mass by further $\sim 2$ GeV for $M_S \sim 20$ TeV. Even for $M_S \sim 4$ TeV the shift is $\sim 1$ GeV. This shows the importance of introducing an effective split model if $M_\chi \ll M_S$ to resum logarithms of the type $\ln(M_S^2/M_\chi^2)$ and $\ln(M_\chi^2/m_t^2)$ properly.
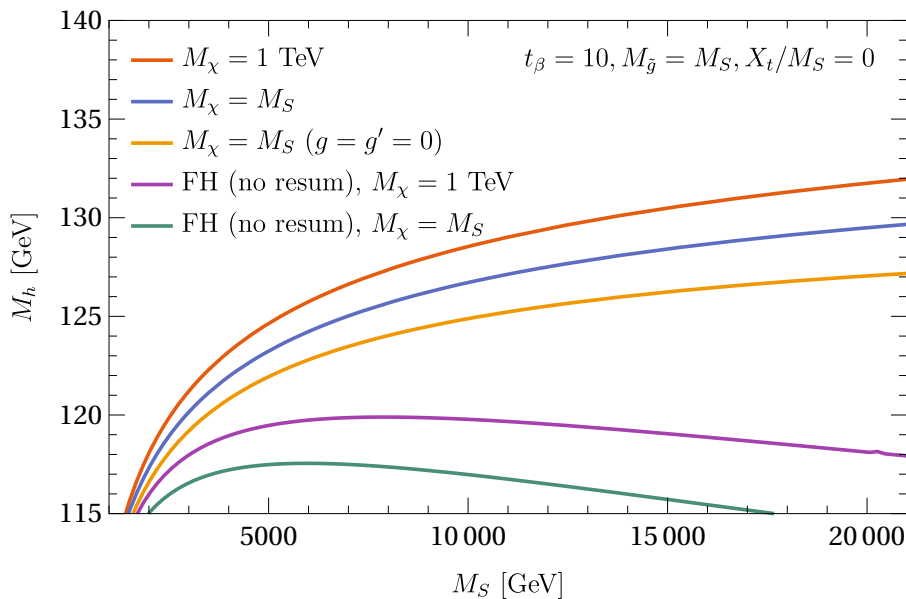


Figure 9.9: $M_h$ as a function of $M_S$ for $X_t/M_S = 0$. The case of $M_\chi = 1$ TeV (red) is compared to the case of $M_\chi = M_S$ (blue). The results obtained neglecting weak gauge coupling in the resummation (orange) and using 2-loop fixed-order formulas (purple) are also shown.

The impact of having light charginos/neutralinos is further investigated in Figure 9.10 showing contour lines for different values of $M_h$ in the $M_S$-$M_\chi$-plane for vanishing stop mixing ($M_\chi$ and $M_S$ are restricted to be $\geq 1$ TeV). The contour lines are only shown in the area for which $M_\chi \leq M_S$, since $M_\chi > M_S$ would correspond to an EFT of the MSSM without charginos and neutralinos which is not considered here. The first thing notable in Figure 9.10 is the already discussed feature that raising $M_S$ increases $M_h$. $M_h$ is also increased by lowering $M_\chi$, as noted before in the discussion of Figure 9.9. The effect is stronger for higher $M_S$. This is expected since choosing a higher $M_S$ enhances the logarithms of the type $\ln(M_S^2/M_\chi^2)$.
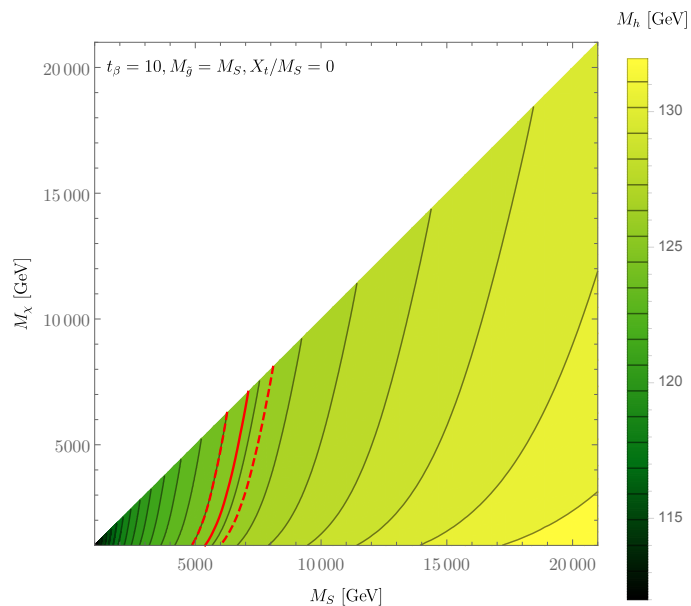
Figure 9.10: Contour plot of $M_h$ in the $M_\chi$-$M_S$ plane for $X_t/M_S = 0$. Contours for the measured Higgs-boson mass central value (red, solid) and corresponding $2\sigma$ values (red, dashed) are also shown.

The red solid line shows the measured central value of $M_h$ (see Eq. (1.1)). The dashed red lines mark the corresponding $2\sigma$ interval. If $M_\chi = M_S$, $M_S \sim 6.5$ TeV has to be chosen to reach the measured value of $M_h$. If in contrast $M_\chi = 1$ TeV is chosen, $M_S$ has to be $\sim 5.5$ TeV. In other words, having a light chargino/neutralino spectrum also lowers the mass of the stops, if $M_h$ should be equal to its measured value. The $2\sigma$ contour lines set limits on $M_S$ to be in the range of $5.5 - 6.5$ TeV for $M_\chi = M_S$ and $5 - 6$ TeV for $M_\chi = 1$ TeV. Including theoretical errors would of course substantially change this picture. The $2\sigma$ contour lines indicate however that the reached experimental precision would be high enough to strongly constrain the $M_S, M_\chi$-parameter space, if the theoretical error was below the experimental one.

## Dependence on stop-mixing parameter $X_t$

So far only the case of vanishing stop mixing was discussed for $M_\chi < M_S$. Figure 9.11 shows $M_h$ in dependence of $M_S$ for $M_\chi = 1$ TeV and $M_\chi = M_S$ comparing $X_t/M_S = 0$ and $X_t/M_S = 2$ . It can be observed that $M_h$ is shifted upwards for $X_t/M_S = 0$ and $X_t/M_S = 2$ if lowering $M_\chi$. In the case of $X_t/M_S = 2$ however the shift is smaller. It amounts to $\sim 1.5$ GeV for $M_S \sim 20$ TeV, whereas $M_h$ is shifted upwards by $\sim 2$ GeV for vanishing stop-mixing.

Figure 9.12 confirms this observation. It shows $M_h$ in dependence of $X_t/M_S$ for $M_S = 10$ TeV in the case of $M_\chi = 1$ TeV and $M_\chi = M_S$. $M_h$ is shifted upwards over the whole considered range of $X_t/M_S$ ($-3 < X_t/M_s < 3$). For low $|X_t/M_S|$ ($\lesssim 1$) the shift is bigger than for high $|X_t/M_S|$.
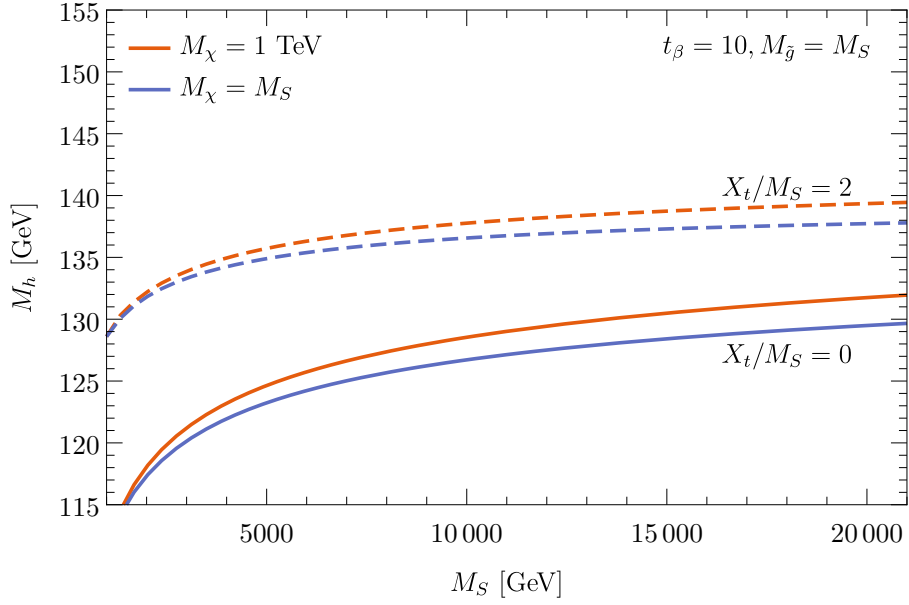
Figure 9.11: $M_h$ as a function of $M_S$ for $X_t/M_S = 0$ (solid) and $X_t/M_S = 2$ (dashed). The result obtained for $M_\chi = 1$ TeV (red) is compared to the result obtained for $M_\chi = M_S$ (blue).
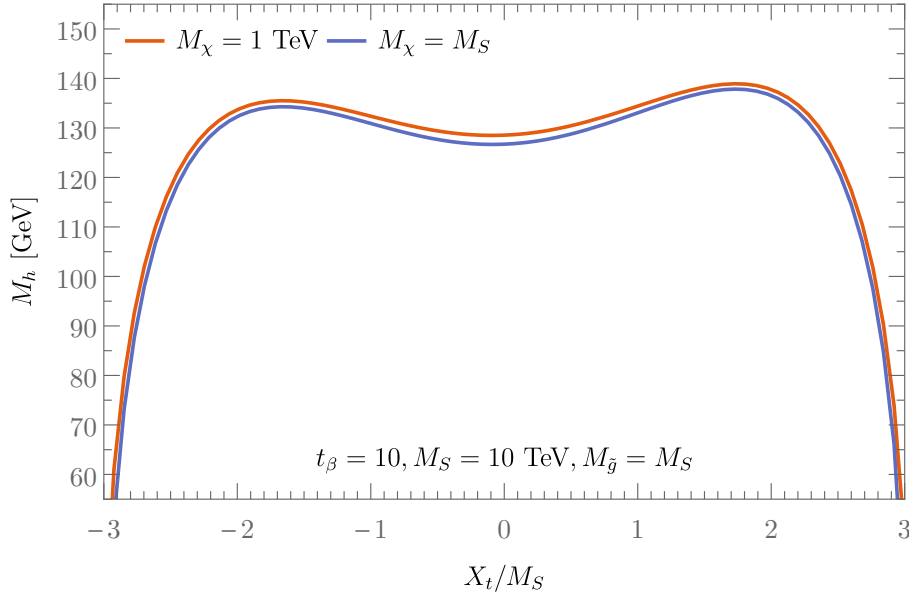


Figure 9.12: $M_h$ as a function of $X_t/M_S$ for $M_S = 10$ TeV. The result obtained for $M_\chi = 1$ TeV (red) is compared to the result obtained for $M_\chi = M_S$ (blue).

## Dependence on tan$\beta$

Figure 9.13 investigates the dependence of $M_h$ on $\tan\beta$ for $M_\chi = 1$ TeV and $M_\chi = M_S$. The solid contour lines mark the measured central value of $M_h$ in a $M_S$-$\tan\beta$ plane. The dashed lines indicate the experimental $2\sigma$-interval. Vanishing stop-mixing is assumed. As noted before, having light charginos and neutralinos raises $M_h$. This allows to have lower $M_S$, respectively lower $\tan\beta$. E.g. choosing $\tan\beta \sim 15 - 20$ requires $M_S \sim 6$ TeV for $M_\chi = M_S$, but only $M_S \sim 5$ TeV for $M_\chi = 1$ TeV. Fixing instead $M_S = 14$ TeV requires $\tan\beta \sim 5$ for $M_\chi = M_S$ and $\tan\beta \sim 4$ for $M_\chi = 1$ TeV.

The error bands are mainly separated, even if the separation is small. For high $\tan\beta$ ($\gtrsim 15$) they overlap. This indicates that for an effective discrimination of the two scenarios a higher experimental precision would be required, even if the theoretical errors were negligible.
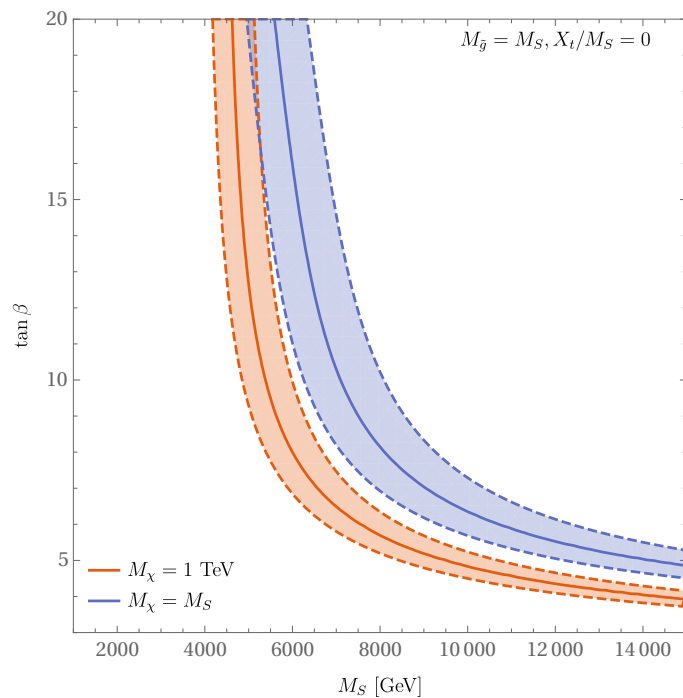


Figure 9.13: Plots of central (solid) and $2\sigma$ (dashed) contour lines of $M_h$ in the $\tan\beta$-$M_S$ plane for $M_\chi = 1$ TeV (red) and $M_\chi = M_S$ (blue).

## 9.3 Gluino threshold

Additionally introducing an independent gluino threshold allows to vary the gluino mass $M_{\tilde{g}}$ as a free parameter, as long as the hierarchy

$$M_\chi, M_{\tilde{g}} \leq M_S \tag{9.13}$$

is respected. The impact of having $M_{\tilde{g}} \leq M_S$ is investigated below.

### Dependence on gluino mass $M_{\tilde{g}}$

Figure 9.14 investigates the dependence of $M_h$ on $M_{\tilde{g}}$. $M_h$ is plotted against $M_S$ for $M_\chi = M_S$ and $X_t/M_S = 0, 2$. The two cases of $M_{\tilde{g}} = 1$ TeV and $M_{\tilde{g}} = M_S$ are compared. For $X_t/M_S = 0$, the numerical difference between both is only marginal (up to $\sim 0.3$ GeV) showing that the dependence of $M_h$ on $M_{\tilde{g}}$ is small. For $X_t/M_S = 2$ instead, $M_h$ is shifted downwards by up to 2 GeV for $M_S \sim 20$ TeV by choosing $M_{\tilde{g}} = 1$ TeV. A closer investigation reveals that this shift is mainly due to the Feynman-diagrammatic part $(M_h^2)^{\mathrm{FD}}$ (see Eq. (5.40)).
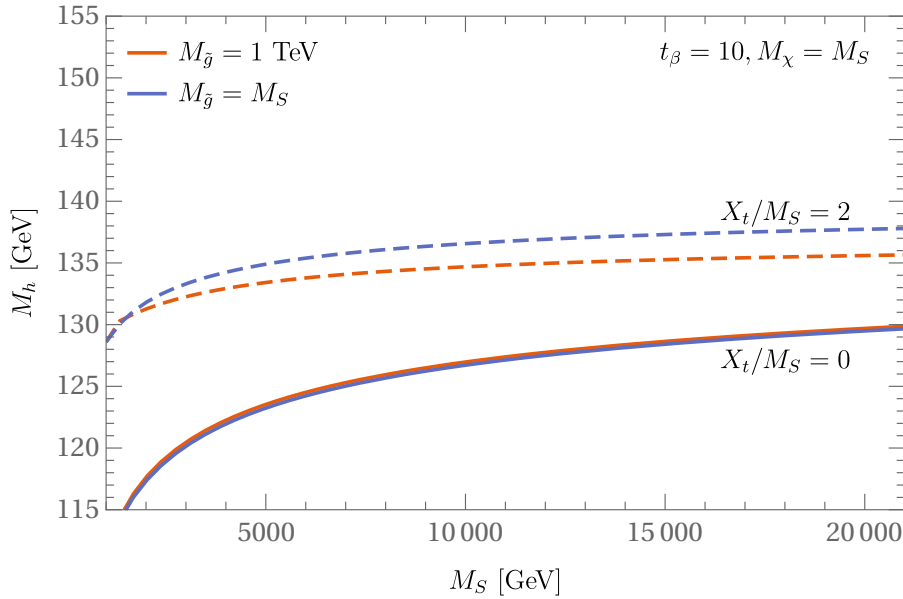


Figure 9.14: $M_h$ as a function of $M_S$ for $X_t/M_S = 0$ (solid) and $X_t/M_S = 2$ (dashed). The case of $M_{\tilde{g}} = 1$ TeV (red) is compared to the case of $M_{\tilde{g}} = M_S$ (blue).

The dependence on $M_{\tilde{g}}$ is more closely depicted in Figure 9.15 and 9.16 showing a contour plot of $M_h$ in the $M_{\tilde{g}}$-$M_S$ plane (with the restriction of $M_{\tilde{g}} \leq M_S$). The depicted area (1 TeV $\leq M_S, M_{\tilde{g}} \leq 10$ TeV) is chosen to clearly illustrate the effect of changing $M_{\tilde{g}}$, even if this range does not allow for $M_h \sim 125$ GeV in the case $X_t/M_S = 2$. For $X_t/M_S = 0$, the contour lines are nearly parallel to the $M_{\tilde{g}}$-axis. So, $M_h$ is indeed only marginally influenced by $M_{\tilde{g}}$ over the whole considered range 1 TeV $\leq M_S \leq 10$TeV. For $X_t/M_S = 2$ in contrast, the lines are not parallel to the $M_{\tilde{g}}$-axis. $M_h$ is maximal for $M_{\tilde{g}} \sim 0.85 M_S$ falling of by up to 2 GeV for smaller $M_{\tilde{g}}$ values and by up to 0.2 GeV for higher $M_{\tilde{g}}$ values.
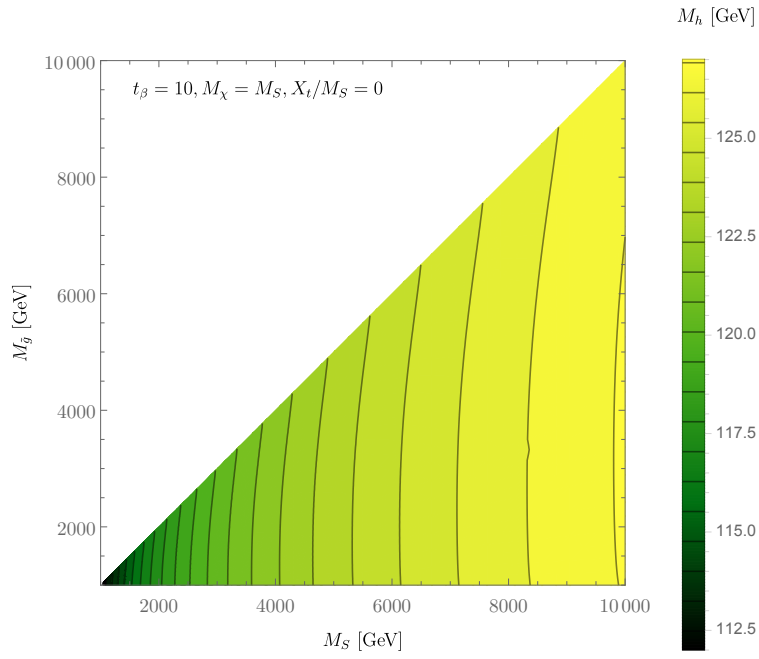
Figure 9.15: Contour plot of $M_h$ in the $M_{\tilde{g}}$-$M_S$ plane for $X_t/M_S = 0$.
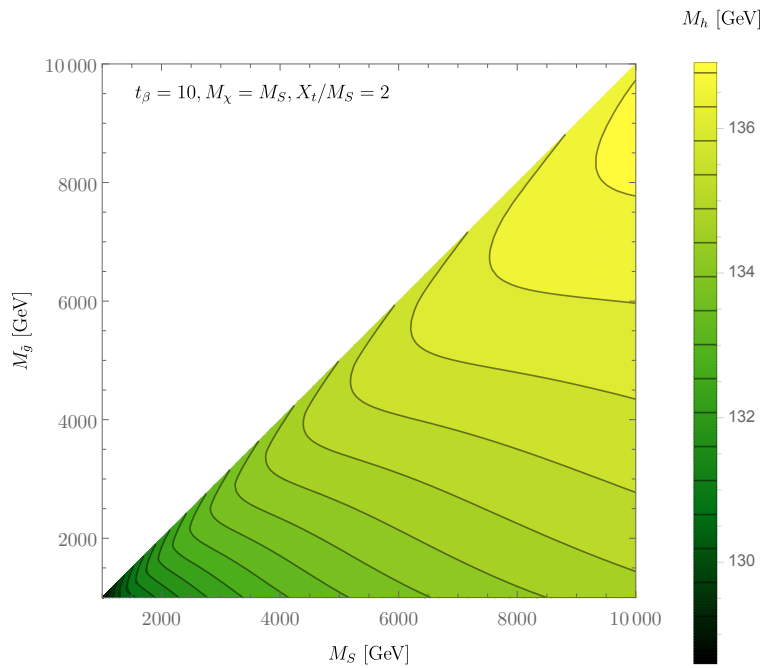


Figure 9.16: Contour plot of $M_h$ in the $M_{\tilde{g}}$-$M_S$ plane for $X_t/M_S = 2$.

## Dependence on stop-mixing parameter $X_t$

The dependence on $X_t$ is more closely examined in Figure 9.17 depicting $M_h$ as a function of $X_t/M_S$ for $M_{\tilde{g}} = 1$ TeV and $M_{\tilde{g}} = M_S$ for fixed $M_S = 10$ TeV. As noted before, for $X_t/M_S \sim 0$, no significant shift is observed. For $X_t/M_S = 2$, $M_h$ is decreased significantly. If $X_t/M_S$ is increased further, $M_h$ falls off faster for $M_{\tilde{g}} = M_S$ compared to $M_{\tilde{g}} = 1$ TeV such that for $X_t/M_S \sim 2.5$ both curves cross. For negative $X_t/M_S$ instead, $M_h$ is shifted upwards. The shift is especially large ($\sim 2$ GeV) for $X_t/M_S \lesssim -2$. This observed asymmetry confirms that the observed shifts are mainly due to the Feynman-diagrammatic part of the calculation $(M_h^2)^{\mathrm{FD}}$, since $X_t$ enters only quadratically in the EFT part $\Delta M_h^2$ (see Eq. (5.40)).
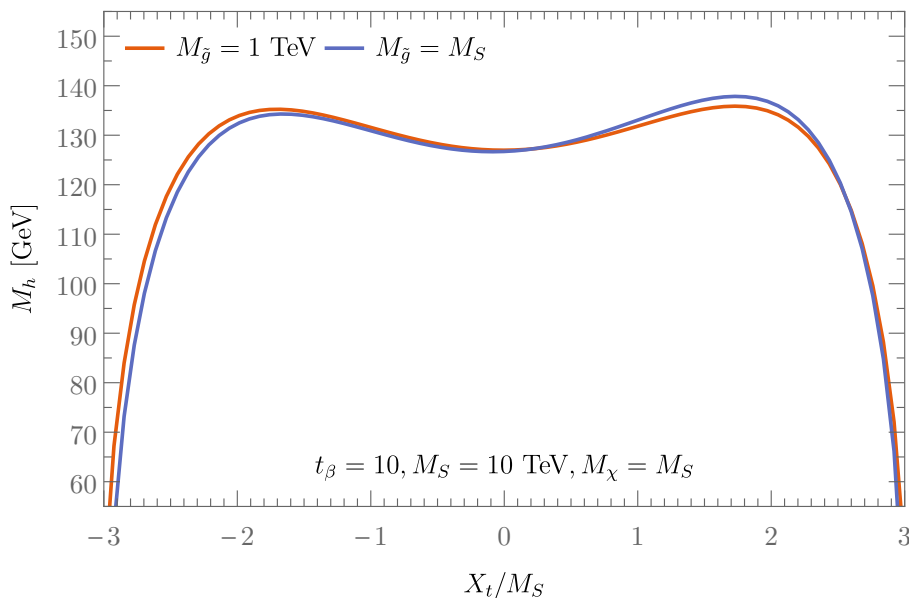


Figure 9.17: $M_h$ as a function of $X_t/M_S$ for $M_S = 10$ TeV. The result obtained for $M_{\tilde{g}} = 1$ TeV (red) is compared to the result obtained for $M_{\tilde{g}} = M_S$ (blue).

## Dependence on $\tan\beta$

Figure 9.18 shows the central value of the measured Higgs-boson mass and the corresponding $2\sigma$-intervals in the $M_S$-$\tan\beta$ plane for $M_{\tilde{g}} = 1$ TeV and $M_{\tilde{g}} = M_S$ in the case of $X_t/M_S = 2$ (for $X_t/M_S = 0$, the numerical differences are too small). Both bands overlap in most of the parameter space. In the region of $M_S < 0.9$ TeV and $M_S > 1.5$ TeV, choosing $M_{\tilde{g}} = M_S$ allows for smaller $M_S$ or $\tan\beta$. For $0.9$ TeV $< M_S < 1.5$ TeV, a higher $\tan\beta$ or $M_S$ has to be chosen to reach the measured $M_h$. The difference between $M_{\tilde{g}} = 1$ TeV and $M_{\tilde{g}} = M_S$ is however quite small such that it is hard to distinguish both cases within the errors.
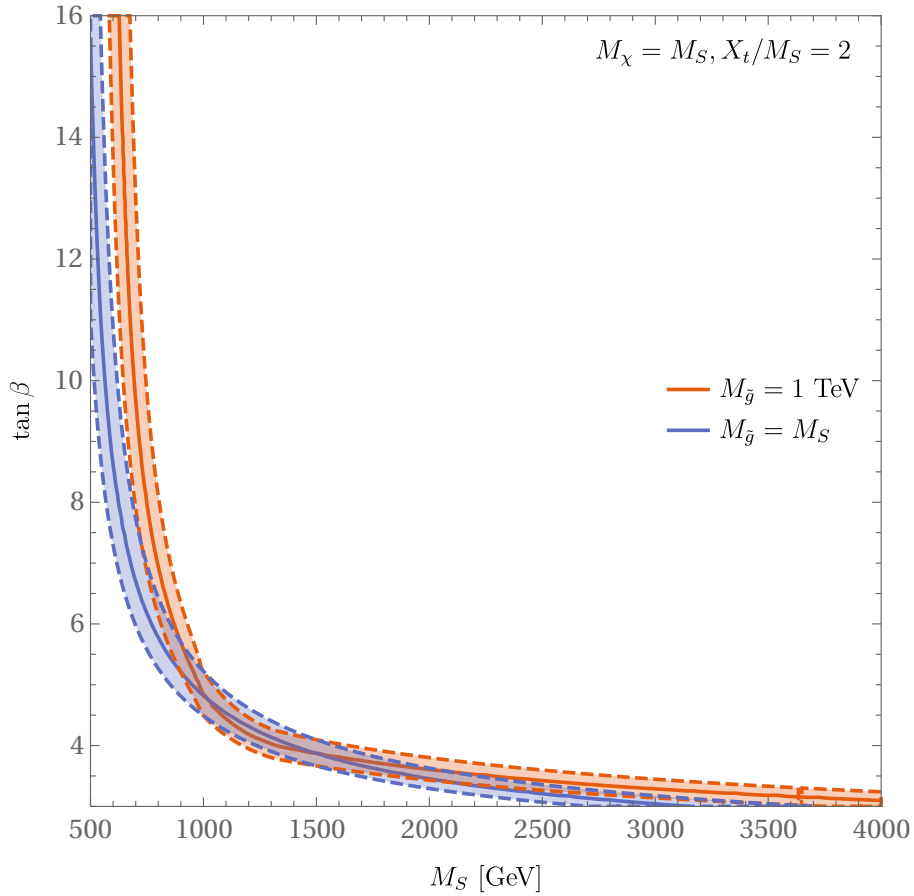
Figure 9.18: Plots of central (solid) and $2\sigma$ (dashed) contour lines of $M_h$ in the $\tan\beta$-$M_S$ plane for $M_\chi = 1$ TeV (red) and $M_\chi = M_S$ (blue).

## Varying chargino/neutralino mass scale $M_\chi$ and gluino mass $M_{\tilde{g}}$

Figure 9.19 and 9.20 illustrates how $M_h$ is changed if $M_{\tilde{g}}$ and $M_\chi$ are independently varied (from 1 TeV to 10 TeV). This parameter space not allowing for $M_h \sim 125$ GeV is chosen, since in it the numerical effects of varying $M_\chi$ and $M_{\tilde{g}}$ independently are nicely visible. The two figures show contour plots of $M_h$ in the $M_\chi$-$M_{\tilde{g}}$ plane leaving $M_S = 10$ TeV fixed for $X_t/M_S = 0$ and $X_t/M_S = 2$.

For $X_t/M_S$ the observed contours can be basically explained by the two previously mentioned effects. Lowering $M_\chi$ increases $M_h$. Varying $M_{\tilde{g}}$ has no significant impact (lowering $M_{\tilde{g}}$ slightly raises $M_h$). The transition between $M_{\tilde{g}} < M_\chi$ to $M_{\tilde{g}} < M_\chi$ corresponding to a transition between different EFTs, has no apparent impact on $M_h$.

For $X_t/M_S = 2$ basically the same effects can be observed. The main difference is however that the impact of varying $M_{\tilde{g}}$ is far bigger (note the different scales for the left and right plot). $M_h$ is maximized for $M_{\tilde{g}} \sim 9$ TeV and $M_\chi = 1$ TeV. Raising $M_\chi$ or lowering $M_{\tilde{g}}$ decreases $M_h$. Again, no transition effects are visible.
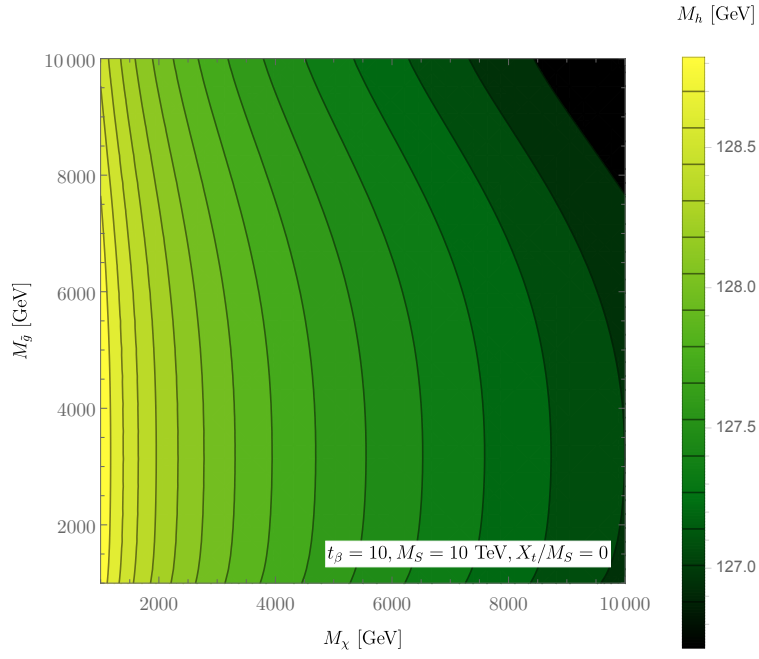
Figure 9.19: Contour plot of $M_h$ in the $M_{\tilde{g}}$-$M_\chi$ plane for $X_t/M_S = 0$ with fixed $M_S = 10$ TeV.
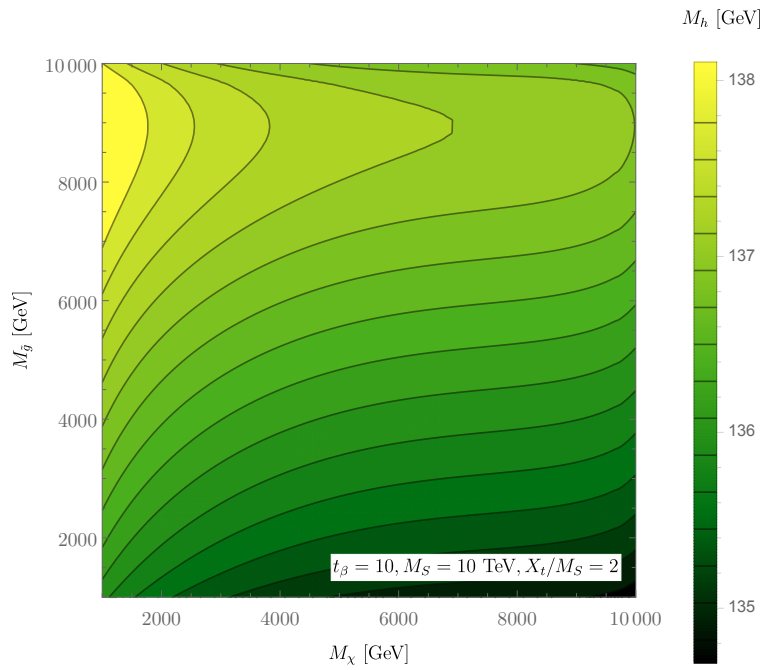


Figure 9.20: Contour plot of $M_h$ in the $M_{\tilde{g}}$-$M_\chi$ plane for $X_t/M_S = 2$ with fixed $M_S = 10$ TeV.

79

# Chapter 10

# Conclusion and outlook

The Minimal Supersymmetric Standard Model is one of the most promising candidates for physics beyond the Standard Model . It allows to calculate the mass of the lightest Higgs boson in dependence of the model parameters. The calculation can be addressed straightforwardly using explicit Feynman-diagrammatic calculations. For heavy super-particles, this approach suffers, however, from large logarithms (e.g. $\ln(M_S^2/m_t^2)$ with $M_S$ being the stop mass scale and $m_t$ being the top mass), which spoil the convergence of the perturbative expansion. This issue is addressed in an effective field theory approach resumming logarithmic contributions using renormalization group equations. To profit also from the advantages of a Feynman-diagrammatic calculation both approaches have to be combined consistently taking care of the different employed renormalization schemes.

The work presented in this thesis builds up on this method to resum leading and subleading logarithms extending the existing resummation of logarithms out of the (s)top sector implemented into `FeynHiggs` [39] in various ways,

- inclusion of electroweak contributions out of all MSSM sectors.

- introduction of a variable threshold for charginos and neutralinos.

- introduction of a variable threshold for the gluino.

For the consistent combination with the Feynman-diagrammatic result implemented in `FeynHiggs`, the one-loop leading logarithms have been isolated and subtracted from the full diagrammatic result and one-loop conversion formulas including electroweak contributions have been derived for all relevant input parameters.

The numerical impact can be summarized as follows. The mass of the lightest Higgs boson is shifted

- upwards by up to $\sim 2.5$ GeV for $M_S \sim 20$ TeV and $\sim 1$ GeV for $M_S \sim$ few TeV if including electroweak contributions.

- upwards by up to $\sim 2.5$ GeV for $M_S \sim 20$ TeV and $\sim 1$ GeV for $M_S \sim$ few TeV if having light charginos/neutralinos ($M_\chi \sim 1$ TeV).

- only marginally if having a light gluino ($M_{\tilde{g}} \sim 1$ TeV) for vanishing stop mixing.

- downwards by up to $\sim 2$ GeV for $M_S \sim 20$ TeV and $\sim 1$ GeV for $M_S \sim$ few TeV if having a light gluino ($M_{\tilde{g}} \sim 1$ TeV) for nearly maximal stop mixing ($X_t/M_S = 2$).

In conclusion, resumming logarithmic contributions not only of the stop-sector is mandatory to achieve a precise prediction for the mass of the lightest Higgs boson, especially for heavy stops ($M_S \gtrsim$ few TeV). Taking into account additional thresholds can also yield significant shifts in the Higgs-boson mass.

Further refinements of the resummation of logarithmic contributions are of course possible. First, sub-subleading logarithms, at least from the (s)top sector, could be resummed using three-loop RGEs as well as two-loop threshold corrections. Furthermore, the resummation could be extended to include (s)bottom contributions. Additional thresholds, especially a variable heavy Higgs threshold at $Q = M_A$, would also improve the calculation significantly. Certainly, it is also interesting to apply the procedure to models beyond the MSSM, like the next-to-minimal supersymmetric Standard Model.

# Acknowledgements

# Appendix A

# Renormalization group equations

## A.1  Standard Model

The SM RGEs are taken from [60,62], their modifications for $Q > M_{\tilde{g}}$ from [35] (see explanation in App. A.2). The following notations are used,

$$t \equiv \ln(Q^2), \tag{A.1}$$

$$k \equiv \frac{1}{16\pi^2}. \tag{A.2}$$

$k$ is used to keep track of the loop order. For the convention used for the normalization of $\lambda$ and $v$, see Eq. (2.4)-(2.5). All RGEs are given at the two-loop order in the form

$$\frac{dg_i}{dt} = \beta_{g_i} = k\beta_{g_i}^{(1)} + k^2\beta_{g_i}^{(2)}, \tag{A.3}$$

with $g_i$ being a generic coupling (see also Eq. (5.26)). The modified two-loop order SM RGEs are given by

$$\frac{dg'}{dt} = g'^3 k \left[ \frac{41}{12} + \frac{5}{6}k \left( \frac{44}{5}g_3^2 + \frac{27}{10}g^2 + \frac{199}{30}g'^2 - \frac{17}{10}h_t^2 \right) \right], \tag{A.4a}$$

$$\frac{dg}{dt} = g^3 k \left[ -\frac{19}{12} + \frac{1}{2}k \left( 12g_3^2 + \frac{35}{6}g^2 + \frac{3}{2}g'^2 - \frac{3}{2}h_t^2 \right) \right], \tag{A.4b}$$

$$\frac{dg_3}{dt} = \frac{1}{2}g_3^3 k \left[ -\langle 7; 5\rangle + k \left( \langle -26; +22\rangle g_3^2 - 2h_t^2 + \frac{9}{2}g^2 + \frac{11}{6}g'^2 \right) \right], \tag{A.4c}$$

$$\frac{dh_t}{dt} = \frac{1}{2}h_t k \left\{ \frac{9}{2}h_t^2 - 8g_3^2 - \frac{9}{4}g^2 - \frac{17}{12}g'^2 \right.$$

$$+ k \left[ h_t^2 \left( -12h_t^2 - 6\lambda + 36g_3^2 + \frac{225}{16}g^2 + \frac{131}{16}g'^2 \right) + \frac{3}{2}\lambda^2 - \langle 108; \frac{284}{3}\rangle g_3^4 \right.$$

$$\left. \left. - \frac{23}{4}g^4 + \frac{1187}{216}g'^4 + 9g_3^2 g^2 + \frac{19}{9}g_3^2 g'^2 - \frac{3}{4}g^2 g'^2 \right] \right\}, \tag{A.4d}$$

$$\frac{d\lambda}{dt} = k \left\{ 6\left( \lambda^2 + \lambda h_t^2 - h_t^4 \right) - \lambda \left( \frac{9}{2}g^2 + \frac{3}{2}g'^2 \right) + \frac{9}{8}g^4 + \frac{3}{8}g'^4 + \frac{3}{4}g^2 g'^2 \right.$$

83

$$+ k^2 \left[ \frac{1}{2} \lambda^2 \left( -\frac{156}{2} \lambda - 72 h_t^2 + 54 g^2 + \frac{54}{3} g'^2 \right) \right.$$

$$+ \lambda h_t^2 \left( -\frac{3}{2} h_t^2 + 40 g_3^2 + \frac{45}{4} g^2 + \frac{85}{12} g'^2 \right) + \lambda \left( -\frac{73}{16} g^4 + \frac{629}{48} g'^4 + \frac{39}{8} g^2 g'^2 \right)$$

$$+ 2 h_t^4 \left( 15 h_t^2 - 16 g_3^2 - \frac{4}{3} g'^2 \right) + 2 h_t^2 \left( -\frac{9}{8} g^4 - \frac{19}{8} g'^4 + \frac{21}{4} g^2 g'^2 \right)$$

$$\left. + \frac{305}{16} g^6 - \frac{379}{48} g'^6 - \frac{289}{48} g^4 g'^2 - \frac{559}{48} g^2 g'^4 \right] \Bigg\} . \tag{A.4e}$$

The notation $\langle a; b \rangle$ indicates that $a$ is used for $Q < M_{\tilde{g}}$ and $b$ for $Q > M_{\tilde{g}}$.

## A.2 Split model

The $\beta$-functions for the split model are mainly taken from [35]. The model considered in there (Split-SUSY) does not quite match the model considered in this thesis. It is more restricted in the sense that the gluino mass $M_{\tilde{g}}$ is set equal to $M_\chi$ and is therefore not allowed to be varied freely as assumed in this thesis.

It is nevertheless possible to use the $\beta$-functions derived in [35] by considering that the couplings of the gluino to other particles are proportional to $g_3$. Therefore the Split-SUSY $\beta$-functions can be used with the modification that for $Q < M_{\tilde{g}}$ (the scale, at which the gluino is integrated out) $g_3$-dependent terms are replaced by their corresponding expression within the SM $\beta$-functions.

In the case of terms proportional to one of the weak coupling $g, g'$ and $g_3$ this procedure seems not to be applicable since the Split-SUSY $\beta$-functions of $g, g'$ are different from the ones of the SM. A second issue concerns the effective coupling $\tilde{g}_{1u,1d,2u,2d}$ of the split model. The $\beta$-functions of the Split-SUSY model considered in [35] contain terms proportional to $g_3$ at the two-loop level. Since there are no SM $\beta$-functions to compare these terms with, it is at first glance not clear if their $\beta$-functions are altered when integrating out the gluino.

Both issues can be resolved by considering the possible couplings of the gluino. The gluino can couple in two ways. Either it couples to a gluon and a second gluino or to a quark/squark pair. Looking at the diagrams needed to derive the RGEs for $g, g'$ and $\tilde{g}_{1u,1d,2u,2d}$, it becomes clear that no gluino-gluon-gluon coupling is involved at the one- or two-loop level. This is due to the fact that the gluon only couples directly to quark and squarks. The respective diagrams, however, do not involve quarks or squarks as external legs. Consequently, quarks and squarks first appear as internal lines at the one-loop level such that gluon contributions appear first at the two-loop level. If gluons appear first at the two-loop level, the gluino-gluon-gluon coupling can first contribute at the three-loop level. Two-loop diagrams involving an one-loop tadpole subdiagram are an exception, since the tadpole subdiagram can involve the gluino-gluon-gluon coupling. Nevertheless, these diagrams are removed by renormalization.

The gluino-quark-squark coupling in contrast can already appear at the two-loop level. Nevertheless, none of the diagrams involving this coupling contribute, since in the effective field theory below $M_S$ the squarks and therefore the gluino-quark-squark coupling are integrated out. In conclusion, the gluino enters the calculation of the split-RGEs for $g, g'$ and $\tilde{g}_{1u,1d,2u,2d}$ first at the three-loop level. This shows that the corresponding RGEs given in [35] can also be

applied for $Q < M_{\tilde{g}}$. Modifying the RGEs given in [35] as described above yields

$$\frac{dg'}{dt} = \frac{15}{4}kg'^3 1 + \frac{5}{6}k^2 g'^3 \left[ -\frac{3}{20}(\tilde{g}_{1d}^2 + \tilde{g}_{1u}^2) + \frac{18}{5}g^2 - \frac{9}{20}(\tilde{g}_{2d}^2 + \tilde{g}_{2u}^2) \right.$$
$$\left. + \frac{44}{5}g_3^2 + \frac{104}{15}g'^2 - \frac{17}{10}h_t^2 \right], \tag{A.5a}$$

$$\frac{dg}{dt} = -\frac{7}{12}kg^3 + \frac{1}{2}k^2 g^3 \left[ -\frac{1}{4}(\tilde{g}_{1d}^2 + \tilde{g}_{1u}^2) + \frac{106}{3}g^2 - \frac{11}{4}(\tilde{g}_{2d}^2 + \tilde{g}_{2u}^2) \right.$$
$$\left. + 12g_3^2 + 2g'^2 - \frac{3}{2}h_t^2 \right], \tag{A.5b}$$

$$\frac{dg_3}{dt} = -\langle \frac{7}{2}; \frac{5}{2} \rangle kg_3^3 + \frac{1}{2}k^2 g_3^3 \left[ \frac{9}{2}g^2 - \langle 26; -22 \rangle g_3^2 + \frac{11}{6}g'^2 - 2h_t^2 \right], \tag{A.5c}$$

$$\frac{dh_t}{dt} = \frac{1}{2}kh_t \left[ -\frac{9}{4}g^2 - 8g_3^2 - \frac{17}{12}g'^2 + \frac{9}{2}h_t^2 + \frac{1}{2}(\tilde{g}_{1d}^2 + \tilde{g}_{1u}^2 + 3\tilde{g}_{2d}^2 + 3\tilde{g}_{2u}^2) \right]$$
$$+ \frac{1}{2}k^2 h_t \left\{ -12h_t^4 - \frac{9}{16}\tilde{g}_{1d}^4 - \frac{5}{4}\tilde{g}_{1d}^2\tilde{g}_{1u}^2 - \frac{9}{16}\tilde{g}_{1u}^4 - \frac{17}{4}g^4 - \frac{9}{8}\tilde{g}_{1d}^2\tilde{g}_{2d}^2 - \frac{45}{16}\tilde{g}_{2d}^4 \right.$$
$$- 3\tilde{g}_{1d}\tilde{g}_{1u}\tilde{g}_{2d}\tilde{g}_{2u} - \frac{9}{8}\tilde{g}_{1u}^2\tilde{g}_{2u}^2 - \frac{3}{4}\tilde{g}_{2d}^2\tilde{g}_{2u}^2 - \frac{45}{16}\tilde{g}_{2u}^4 - \langle 108; \frac{284}{3} \rangle g_3^4$$
$$+ g^2 \left( \frac{15}{16}\tilde{g}_{1d}^2 + \frac{15}{16}\tilde{g}_{1u}^2 + \frac{165}{16}\tilde{g}_{2d}^2 + \frac{165}{16}\tilde{g}_{2u}^2 + 9g_3^2 \right)$$
$$+ \frac{5}{3}g'^2 \left( \frac{3}{16}\tilde{g}_{1d}^2 + \frac{3}{16}\tilde{g}_{1u}^2 - \frac{9}{20}g^2 + \frac{9}{16}\tilde{g}_{2d}^2 + \frac{9}{16}\tilde{g}_{2u}^2 + \frac{19}{15}g_3^2 \right) + \frac{1303}{216}g'^4 + \frac{3}{2}\lambda^2$$
$$\left. + h_t^2 \left( -\frac{9}{8}(\tilde{g}_{1d}^2 + \tilde{g}_{1u}^2) + \frac{225}{16}g^2 - \frac{27}{8}(\tilde{g}_{2d}^2 + \tilde{g}_{2u}^2) + 36g_3^2 + \frac{131}{16}g'^2 - 6\lambda \right) \right\}, \tag{A.5d}$$

$$\frac{d\lambda}{dt} = \frac{1}{2}k \left[ -\tilde{g}_{1d}^4 - \tilde{g}_{1u}^4 + \frac{9}{4}g^4 - 5\tilde{g}_{2d}^4 - 4\tilde{g}_{1d}\tilde{g}_{1u}\tilde{g}_{2d}\tilde{g}_{2u} - 5\tilde{g}_{2u}^4 - 2(\tilde{g}_{1u}^2 + \tilde{g}_{2d}^2)(\tilde{g}_{1d}^2 + \tilde{g}_{2u}^2) \right.$$
$$+ \frac{3}{2}g^2 g'^2 + \frac{3}{4}g'^4 - 12h_t^4 + 2(\tilde{g}_{1d}^2 + \tilde{g}_{1u}^2 + 3\tilde{g}_{2d}^2 + 3\tilde{g}_{2u}^2)\lambda$$
$$\left. - 9 \left( g^2 + \frac{1}{3}g'^2 \right) \lambda + 12h_t^2\lambda + 12\lambda^2 \right]$$
$$+ \frac{1}{2}k^2 \left\{ \frac{209}{8}g^6 + \frac{1}{2} \left[ 5(\tilde{g}_{1d}^6 + \tilde{g}_{1u}^6) + 21(\tilde{g}_{1d}^2 + \tilde{g}_{1u}^2)\tilde{g}_{2d}^2\tilde{g}_{2u}^2 + 19\tilde{g}_{1d}^2\tilde{g}_{1u}^2(\tilde{g}_{2d}^2 + \tilde{g}_{2u}^2) \right. \right.$$
$$+ 7\tilde{g}_{2d}^2\tilde{g}_{2u}^2(\tilde{g}_{2d}^2 + \tilde{g}_{2u}^2) + 17(\tilde{g}_{1d}^4\tilde{g}_{1u}^2 + \tilde{g}_{1d}^2\tilde{g}_{1u}^4 + \tilde{g}_{1d}^4\tilde{g}_{2d}^2 + \tilde{g}_{1u}^4\tilde{g}_{2u}^2)$$
$$+ 11(\tilde{g}_{1d}^2\tilde{g}_{2d}^4 + \tilde{g}_{1u}^2\tilde{g}_{2d}^4) + 47(\tilde{g}_{2d}^6 + \tilde{g}_{2u}^6)$$
$$\left. + \tilde{g}_{1d}\tilde{g}_{1u}\tilde{g}_{2d}\tilde{g}_{2u}(42(\tilde{g}_{1d}^2 + \tilde{g}_{1u}^2) + 38(\tilde{g}_{2d}^2 + \tilde{g}_{2u}^2)) \right]$$
$$- \frac{137}{8}g'^6 - 64g_3^2 h_t^4 - \frac{16}{3}g'^2 h_t^4 + 60h_t^6$$
$$+ g^4 \left[ -\frac{3}{4}(\tilde{g}_{1d}^2 + \tilde{g}_{1u}^2 + 51\tilde{g}_{2d}^2 + 51\tilde{g}_{2u}^2) - \frac{385}{24}g'^2 - \frac{9}{2}h_t^2 \right]$$
$$+ \frac{25}{9}g'^4 \left[ -\frac{9}{100}(\tilde{g}_{1d}^2 + \tilde{g}_{1u}^2 + 3\tilde{g}_{2d}^2 + 3\tilde{g}_{2u}^2) - \frac{171}{50}h_t^2 \right]$$

$$+g^2\left[-\frac{197}{8}g'^4 - 4(\tilde{g}_{1d}^2\tilde{g}_{2d}^2 + 5\tilde{g}_{2d}^4 + 2\tilde{g}_{1d}\tilde{g}_{1u}\tilde{g}_{2d}\tilde{g}_{2u} + \tilde{g}_{1u}^2\tilde{g}_{2u}^2 + 2\tilde{g}_{2d}^2\tilde{g}_{2u}^2 + 5\tilde{g}_{2u}^4)\right.$$

$$\left.+\frac{5}{3}g'^2\left(-\frac{3}{10}(\tilde{g}_{1d}^2 + \tilde{g}_{1u}^2 - 21\tilde{g}_{2d}^2 - 21\tilde{g}_{2u}^2) + \frac{63}{5}h_t^2\right)\right]$$

$$+\lambda\left[\frac{47}{8}g^4 + \frac{223}{8}g'^4 + 80g_3^2h_t^2 - 3h_t^4\right.$$

$$-\frac{1}{4}(\tilde{g}_{1d}^4 + \tilde{g}_{1u}^4 + 5\tilde{g}_{2d}^4 + 2\tilde{g}_{1d}^2(\tilde{g}_{2d}^2 - 6\tilde{g}_{1u}^2)$$

$$-80\tilde{g}_{1d}\tilde{g}_{1u}\tilde{g}_{2d}\tilde{g}_{2u} + 2\tilde{g}_{1u}^2\tilde{g}_{2u}^2 + 44\tilde{g}_{2d}^2\tilde{g}_{2u}^2 + 5\tilde{g}_{2u}^4)$$

$$+\frac{5}{3}g'^2\left(\frac{3}{4}(\tilde{g}_{1d}^2 + \tilde{g}_{1u}^2 + 3\tilde{g}_{2d}^2 + 3\tilde{g}_{2u}^2) + \frac{17}{2}h_t^2\right)$$

$$\left.+g^2\left(\frac{15}{4}(\tilde{g}_{1d}^2 + \tilde{g}_{1u}^2 + 11\tilde{g}_{2d}^2 + 11\tilde{g}_{2u}^2) + \frac{39}{4}g'^2 + \frac{45}{2}h_t^2\right)\right]$$

$$+\lambda^2\left[54g^2 - 12(\tilde{g}_{1d}^2 + \tilde{g}_{1u}^2 + 3\tilde{g}_{2d}^2 + 3\tilde{g}_{2u}^2) + 18g'^2 - 72h_t^2\right] - 78\lambda^3\Big\}, \tag{A.5e}$$

$$\frac{d\tilde{g}_{1u}}{dt} = \frac{1}{2}k\left[3\tilde{g}_{1d}\tilde{g}_{2d}\tilde{g}_{2u} + \tilde{g}_{1u}\left(\frac{5}{4}\tilde{g}_{1u}^2 + 2\tilde{g}_{1d}^2 + \frac{9}{4}\tilde{g}_{2u}^2 + \frac{3}{2}\tilde{g}_{2d}^2 - \frac{9}{4}g^2 - \frac{3}{4}g'^2 + 3h_t^2\right)\right]$$

$$+\frac{1}{2}k^2\left\{-\frac{3}{4}\tilde{g}_{1u}^5 - \frac{9}{4}\tilde{g}_{1d}^3\tilde{g}_{2d}\tilde{g}_{2u} - 6\tilde{g}_{1d}\tilde{g}_{1u}^2\tilde{g}_{2d}\tilde{g}_{2u} + \frac{51}{4}\tilde{g}_{1d}\tilde{g}_{2d}\tilde{g}_{2u}g^2 - \frac{33}{4}\tilde{g}_{1d}\tilde{g}_{2d}^3\tilde{g}_{2u}\right.$$

$$-\frac{9}{2}\tilde{g}_{1d}\tilde{g}_{2d}\tilde{g}_{2u}^3 + \frac{3}{4}\tilde{g}_{1d}\tilde{g}_{2d}\tilde{g}_{2u}g'^2 - 9\tilde{g}_{1d}\tilde{g}_{2d}\tilde{g}_{2u}h_t^2 - 3\tilde{g}_{1d}\tilde{g}_{2d}\tilde{g}_{2u}\lambda$$

$$+\tilde{g}_{1u}^3\left(-\frac{15}{4}\tilde{g}_{1d}^2 + \frac{165}{32}g^2 - \frac{27}{16}\tilde{g}_{1d}^2 - \frac{9}{16}\tilde{g}_{2u}^2 + \frac{103}{32}g'^2 - \frac{27}{8}h_t^2 - 3\lambda\right)$$

$$+\tilde{g}_{1u}\left[-\frac{9}{4}\tilde{g}_{1d}^4 - \frac{17}{4}g^2 - \frac{75}{16}\tilde{g}_{1d}^2\tilde{g}_{2d}^2 - \frac{45}{16}\tilde{g}_{2d}^4 - \frac{75}{16}\tilde{g}_{1d}^2\tilde{g}_{2u}^2 - \frac{21}{8}\tilde{g}_{2d}^2\tilde{g}_{2u}^2 - \frac{99}{16}\tilde{g}_{2u}^4\right.$$

$$+g^2\left(\frac{39}{8}\tilde{g}_{1d}^2 + \frac{165}{16}\tilde{g}_{2d}^2 + \frac{549}{32}\tilde{g}_{2u}^2\right) + \frac{5}{3}g'^2\left(\frac{3}{40}\tilde{g}_{1d}^2 - \frac{27}{20}g^2 + \frac{9}{16}\tilde{g}_{2d}^2 + \frac{189}{160}\tilde{g}_{2u}^2\right)$$

$$+\frac{13}{8}g'^4 + h_t^2\left(-\frac{21}{4}\tilde{g}_{1d}^2 + \frac{45}{8}g^2 - \frac{27}{8}\tilde{g}_{2u}^2 + 20g_3^2 + \frac{85}{24}g'^2\right)$$

$$\left.\left.-\frac{27}{4}h_t^4 - 3\lambda(\tilde{g}_{1d}^2 + \tilde{g}_{2u}^2) + \frac{3}{2}\lambda^2\right]\right\}, \tag{A.5f}$$

$$\frac{d\tilde{g}_{1d}}{dt} = \frac{1}{2}k\left[3\tilde{g}_{1u}\tilde{g}_{2d}\tilde{g}_{2u} + \tilde{g}_{1d}\left(\frac{5}{4}\tilde{g}_{1d}^2 + 2\tilde{g}_{1u}^2 + \frac{9}{4}\tilde{g}_{2d}^2 + \frac{3}{2}\tilde{g}_{2u}^2 - \frac{9}{4}g^2 - \frac{3}{4}g'^2 + 3h_t^2\right)\right]$$

$$+\frac{1}{2}k^2\left\{-\frac{3}{4}\tilde{g}_{1d}^5 - 6\tilde{g}_{1d}^2\tilde{g}_{1u}\tilde{g}_{2d}\tilde{g}_{2u} - \frac{9}{4}\tilde{g}_{1u}^3\tilde{g}_{2d}\tilde{g}_{2u} + \frac{51}{4}g^2\tilde{g}_{1u}\tilde{g}_{2d}\tilde{g}_{2u} - \frac{9}{2}\tilde{g}_{1u}\tilde{g}_{2d}^3\tilde{g}_{2u}\right.$$

$$-\frac{33}{4}\tilde{g}_{1u}\tilde{g}_{2d}\tilde{g}_{2u}^3 + \frac{3}{4}g'^2\tilde{g}_{1u}\tilde{g}_{2d}\tilde{g}_{2u} - 9\tilde{g}_{1u}\tilde{g}_{2d}\tilde{g}_{2u}h_t^2 - 3\tilde{g}_{1u}\tilde{g}_{2d}\tilde{g}_{2u}\lambda$$

$$+\tilde{g}_{1d}^3\left(-\frac{15}{4}\tilde{g}_{1u}^2 + \frac{165}{32}g^2 - \frac{9}{16}\tilde{g}_{2d}^2 - \frac{27}{16}\tilde{g}_{2u}^2 + \frac{103}{32}g'^2 - \frac{27}{8}h_t^2 - 3\lambda\right)$$

$$+\tilde{g}_{1d}\left[-\frac{9}{4}\tilde{g}_{1u}^4 - \frac{17}{4}g^2 - \frac{75}{16}\tilde{g}_{1u}^2\tilde{g}_{2d}^2 - \frac{99}{16}\tilde{g}_{2d}^4 - \frac{75}{16}\tilde{g}_{1u}^2\tilde{g}_{2u}^2 - \frac{21}{8}\tilde{g}_{2d}^2\tilde{g}_{2u}^2 - \frac{45}{16}\tilde{g}_{2u}^4\right.$$

$$+g^2\left(\frac{39}{8}\tilde{g}_{1u}^2 + \frac{549}{32}\tilde{g}_{2d}^2 + \frac{165}{16}\tilde{g}_{2u}^2\right) + \frac{13}{8}g'^4 - \frac{27}{4}h_t^4$$

$$
+\frac{5}{3}g'^2\left(\frac{3}{40}\tilde{g}_{1u}^2-\frac{27}{20}g^2+\frac{189}{160}\tilde{g}_{2d}^2+\frac{9}{16}\tilde{g}_{2u}^2\right)-3(\tilde{g}_{1u}^2+\tilde{g}_{2d}^2)\lambda+\frac{3}{2}\lambda^2
$$
$$
+h_t^2\left(-\frac{21}{4}\tilde{g}_{1u}^2+\frac{45}{8}g^2-\frac{27}{8}\tilde{g}_{2d}^2+20g_3^2+\frac{85}{24}g'^2\right)\Big]\Big\}, \tag{A.5g}
$$

$$
\frac{d\tilde{g}_{2u}}{dt}=\frac{1}{2}k\left[\tilde{g}_{1d}\tilde{g}_{1u}\tilde{g}_{2d}+\tilde{g}_{2u}\left(\frac{1}{2}\tilde{g}_{1d}^2+\frac{3}{4}\tilde{g}_{1u}^2+\tilde{g}_{2d}^2+\frac{11}{4}\tilde{g}_{2u}^2-\frac{33}{4}g^2-\frac{3}{4}g'^2+3h_t^2\right)\right]
$$
$$
+\frac{1}{2}k^2\left\{-\frac{5}{4}\tilde{g}_{1d}^3\tilde{g}_{1u}\tilde{g}_{2d}-\frac{3}{2}\tilde{g}_{1d}\tilde{g}_{1u}^3\tilde{g}_{2d}+\frac{9}{4}\tilde{g}_{1d}\tilde{g}_{1u}\tilde{g}_{2d}g^2-\frac{9}{4}\tilde{g}_{1d}\tilde{g}_{1u}\tilde{g}_{2d}^3\right.
$$
$$
-\frac{7}{2}\tilde{g}_{2u}^5+\frac{1}{4}\tilde{g}_{1d}\tilde{g}_{1u}\tilde{g}_{2d}g'^2-3\tilde{g}_{1d}\tilde{g}_{1u}\tilde{g}_{2d}h_t^2-\tilde{g}_{1d}\tilde{g}_{1u}\tilde{g}_{2d}\lambda-4\tilde{g}_{1d}\tilde{g}_{1u}\tilde{g}_{2d}\tilde{g}_{2u}^2
$$
$$
+\tilde{g}_{2u}^3\left(-\frac{15}{16}\tilde{g}_{1d}^2-\frac{59}{16}\tilde{g}_{1u}^2+\frac{875}{32}g^2-\frac{27}{8}\tilde{g}_{2d}^2+\frac{145}{32}g'^2-\frac{45}{8}h_t^2-5\lambda\right)
$$
$$
+\tilde{g}_{2u}\left[-\frac{9}{16}\tilde{g}_{1d}^4-\frac{3}{2}\tilde{g}_{1d}^2\tilde{g}_{1u}^2-\frac{5}{16}\tilde{g}_{1u}^4-\frac{409}{12}g^4-\frac{13}{16}\tilde{g}_{1d}^2\tilde{g}_{2d}^2-\frac{31}{16}\tilde{g}_{1u}^2\tilde{g}_{2d}^2-\frac{11}{8}\tilde{g}_{2d}^4\right.
$$
$$
+g^2\left(\frac{15}{16}\tilde{g}_{1d}^2+\frac{111}{31}\tilde{g}_{1u}^2+\frac{17}{4}\tilde{g}_{2d}^2\right)+\frac{5}{3}g'^2\left(\frac{3}{16}\tilde{g}_{1d}^2+\frac{63}{160}\tilde{g}_{1u}^2+\frac{9}{20}g^2+\frac{3}{20}\tilde{g}_{2d}^2\right)
$$
$$
+\frac{13}{8}g'^4+h_t^2\left(-\frac{9}{8}\tilde{g}_{1u}^2+\frac{45}{8}g^2+\frac{3}{4}\tilde{g}_{2d}^2+20g_3^2+\frac{85}{24}g'^2\right)-\frac{27}{4}h_t^4
$$
$$
\left.-\lambda(\tilde{g}_{1u}^2+\tilde{g}_{2d}^2)+\frac{3}{2}\lambda^2\right]\Big\}, \tag{A.5h}
$$

$$
\frac{d\tilde{g}_{2d}}{dt}=\frac{1}{2}k\left[\tilde{g}_{1d}\tilde{g}_{1u}\tilde{g}_{2u}+\tilde{g}_{2d}\left(\frac{1}{2}\tilde{g}_{1u}^2+\frac{3}{4}\tilde{g}_{1d}^2+\tilde{g}_{2u}^2+\frac{11}{4}\tilde{g}_{2d}^2-\frac{33}{4}g^2-\frac{3}{4}g'^2+3h_t^2\right)\right]
$$
$$
\frac{1}{2}k^2\left\{-\frac{7}{2}\tilde{g}_{2d}^5-\frac{3}{2}\tilde{g}_{1d}^3\tilde{g}_{1u}\tilde{g}_{2u}-\frac{5}{4}\tilde{g}_{1d}\tilde{g}_{1u}^3\tilde{g}_{2u}+\frac{9}{4}\tilde{g}_{1d}\tilde{g}_{1u}\tilde{g}_{2u}g^2-4\tilde{g}_{1d}\tilde{g}_{1u}\tilde{g}_{2d}^2\tilde{g}_{2u}\right.
$$
$$
-\frac{9}{4}\tilde{g}_{1d}\tilde{g}_{1u}\tilde{g}_{2u}^3+\frac{1}{4}\tilde{g}_{1d}\tilde{g}_{1u}\tilde{g}_{2u}g'^2-3\tilde{g}_{1d}\tilde{g}_{1u}\tilde{g}_{2u}h_t^2-\tilde{g}_{1d}\tilde{g}_{1u}\tilde{g}_{2u}\lambda
$$
$$
+\tilde{g}_{2d}^3\left(-\frac{59}{16}\tilde{g}_{1d}^2-\frac{15}{16}\tilde{g}_{1u}^2+\frac{875}{32}g^2-\frac{27}{8}\tilde{g}_{2u}^2+\frac{145}{32}g'^2-\frac{45}{8}h_t^2-5\lambda\right)
$$
$$
+\tilde{g}_{2d}\left[-\frac{5}{16}\tilde{g}_{1d}^4-\frac{3}{2}\tilde{g}_{1d}^2\tilde{g}_{1u}^2-\frac{9}{16}\tilde{g}_{1u}^4-\frac{409}{12}g^4-\frac{31}{16}\tilde{g}_{1d}^2\tilde{g}_{2u}^2-\frac{13}{16}\tilde{g}_{1u}^2\tilde{g}_{2u}^2-\frac{11}{8}\tilde{g}_{2u}^4\right.
$$
$$
+g^2\left(\frac{111}{32}\tilde{g}_{1d}^2+\frac{15}{16}\tilde{g}_{1u}^2+\frac{17}{4}\tilde{g}_{2u}^2\right)+\frac{5}{3}g'^2\left(\frac{63}{160}\tilde{g}_{1d}^2+\frac{3}{16}\tilde{g}_{1u}^2+\frac{9}{20}g^2+\frac{3}{20}\tilde{g}_{2u}^2\right)
$$
$$
+\frac{13}{8}g'^4+h_t^2\left(-\frac{9}{8}\tilde{g}_{1d}^2+\frac{45}{8}g^2+\frac{3}{4}\tilde{g}_{2u}^2+20g_3^2+\frac{85}{24}g'^2\right)
$$
$$
\left.-\frac{27}{4}h_t^4-\lambda(\tilde{g}_{1u}^2+\tilde{g}_{2d}^2)+\frac{3}{2}\lambda^2\right]\Big\}. \tag{A.5i}
$$

The issue concerning the RGE and the running of $\tan\beta$ is discussed in Section 7.4.

# Appendix B

# Iteration procedure

Consider a first-order differential equation of the form

$$\frac{df}{dx} = F(x, f(x)) \tag{B.1}$$

with f(a) given. Under certain conditions (Lipschitz condition for $F$) an unique solution exists and can be obtained in an iterative way. The first step in the iteration procedure is to guess a solution called $f^{(0)}(x)$. Usually, a single valued function is chosen. Typically, $f^{(0)}(x) = f(a)$ is chosen, since this choice automatically fulfills the boundary condition. Then the differential equation is used to gain a better solution $f^{(1)}(x)$. This is done by integrating the equation using $f^{(0)}(x)$ on the right-hand side,

$$\int_a^x \frac{df^{(1)}}{dx'} dx' = \int_a^x F(x', f^{(0)}(x')) dx'. \tag{B.2}$$

Demanding that $f^{(1)}(x)$ again fulfills the boundary condition, the left-hand side can be rewritten,

$$f^{(1)}(x) - f(a) = \int_a^x F(x', f^{(0)}(x')) dx'. \tag{B.3}$$

These steps can be repeated, yielding

$$f^{(n+1)}(x) = f(a) + \int_a^x F(x', f^{(n)}(x')) dx'. \tag{B.4}$$

The gained function series $f^{(n)}$ will converge to the solution $f(x)$ of Eq. (B.1) with the boundary condition $f(a)$.

This procedure can easily generalized to a system of coupled first-order differential equations, e.g. for a system of two coupled differential equations

$$f^{(n+1)}(x) = f(a) + \int_a^x F(x', f^{(n)}(x'), g^{(n)}(x')) dx', \tag{B.5}$$

$$g^{(n+1)}(x) = g(b) + \int_b^x G(x', f^{(n)}(x'), g^{(n)}(x')) dx'. \tag{B.6}$$

The method will fail to produce exact solutions, if the initial conditions are coupled too as in the considered system of renormalization group equations, i.e. the boundary condition of

$\lambda(M_S)$ depends on $h_t(M_S)$ which again depends on $\lambda(M_S)$. One method to come around this is using a symbolic boundary condition during the iteration procedure. Precisely, e.g. $\lambda(M_S)$ is regarded as a symbol and left unevaluated during the iteration procedure. In the end, the actual boundary condition for $\lambda(M_S)$ is applied. The resulting equation is then solved for $\lambda(M_S)$. The obtained expression for $\lambda(M_S)$, which does not involve $\lambda(M_S)$ any more, is then plugged into the functions solving the differential equation system.

# Appendix C

# Expansions of masses and mixing matrices

The explicit expressions for masses and mixing matrices appearing in the MSSM are often quite complicated. Therefore, it is convenient to expand these expressions for large SUSY mass scales. The derived expressions are used in calculations described in Chapter 6 and Chapter 8.

All of the expressions presented below have been checked numerically using the Mathematica package `Diag` [63] as well as the program `FeynHiggs` [30] (`FeynHiggs` implements the routines of `Diag`).

## C.1 Stop sector

Expanding the masses and mixing-matrices of the stop sector (see Section 4.3) in the limit $M_Z \ll X_t$ yields (defining that $m_{\tilde{t}_1} < m_{\tilde{t}_2}$)

$$m_{\tilde{t}_1}^2 = M_{Susy}^2 \mp m_t X_t + m_t^2 + \frac{1}{4} c_{2\beta} M_Z^2 \mp \frac{1}{288}(3 - 8s_w^2)^2 \frac{M_Z^3}{m_t}\left(\frac{M_Z}{X_t}\right) + \mathcal{O}\left(\left(\frac{M_Z}{X_t}\right)^3\right),$$

$$m_{\tilde{t}_2}^2 = M_{Susy}^2 \pm m_t X_t + m_t^2 + \frac{1}{4} c_{2\beta} M_Z^2 \pm \frac{1}{288}(3 - 8s_w^2)^2 \frac{M_Z^3}{m_t}\left(\frac{M_Z}{X_t}\right) + \mathcal{O}\left(\left(\frac{M_Z}{X_t}\right)^3\right),$$

(C.1)

where the upper signs apply for $X_t > 0$, the lower signs for $X_t < 0$.

For the stop mixing matrix one obtains

$$\mathbf{U}_{\tilde{t},11} = \frac{1}{\sqrt{2}}\left[\mp 1 + \frac{1}{24}(3 - 8s_w^2)c_{2\beta}\frac{M_Z}{m_t}\left(\frac{M_Z}{X_t}\right) \pm \frac{1}{1152}(3 - 8s_w^2)^2 c_{2\beta}^2 \frac{M_Z^2}{m_t^2}\left(\frac{M_Z}{X_t}\right)^2\right.$$
$$\left. - \frac{1}{9216}(3 - 8s_w^2)^3 c_{2\beta}^3 \frac{M_Z^3}{m_t^3}\left(\frac{M_Z}{X_t}\right)^3 + \mathcal{O}\left(\left(\frac{M_Z}{X_t}\right)^4\right)\right],$$

$$\mathbf{U}_{\tilde{t},12} = \frac{1}{\sqrt{2}}\left[+1 \pm \frac{1}{24}(3 - 8s_w^2)c_{2\beta}\frac{M_Z}{m_t}\left(\frac{M_Z}{X_t}\right) - \frac{1}{1152}(3 - 8s_w^2)^2 c_{2\beta}^2 \frac{M_Z^2}{m_t^2}\left(\frac{M_Z}{X_t}\right)^2\right.$$
$$\left. \mp \frac{1}{9216}(3 - 8s_w^2)^3 c_{2\beta}^3 \frac{M_Z^3}{m_t^3}\left(\frac{M_Z}{X_t}\right)^3 + \mathcal{O}\left(\left(\frac{M_Z}{X_t}\right)^4\right)\right],$$

$$\mathbf{U}_{\tilde{t},21} = \frac{1}{\sqrt{2}}\left[\pm 1 + \frac{1}{24}(3-8s_w^2)c_{2\beta}\frac{M_Z}{m_t}\left(\frac{M_Z}{X_t}\right) \mp \frac{1}{1152}(3-8s_w^2)^2c_{2\beta}^2\frac{M_Z^2}{m_t^2}\left(\frac{M_Z}{X_t}\right)^2\right.$$
$$\left. - \frac{1}{9216}(3-8s_w^2)^3c_{2\beta}^3\frac{M_Z^3}{m_t^3}\left(\frac{M_Z}{X_t}\right)^3 + \mathcal{O}\left(\left(\frac{M_Z}{X_t}\right)^4\right)\right],$$

$$\mathbf{U}_{\tilde{t},22} = \frac{1}{\sqrt{2}}\left[+1 \mp \frac{1}{24}(3-8s_w^2)c_{2\beta}\frac{M_Z}{m_t}\left(\frac{M_Z}{X_t}\right) - \frac{1}{1152}(3-8s_w^2)^2c_{2\beta}^2\frac{M_Z^2}{m_t^2}\left(\frac{M_Z}{X_t}\right)^2\right.$$
$$\left. \pm \frac{1}{9216}(3-8s_w^2)^3c_{2\beta}^3\frac{M_Z^3}{m_t^3}\left(\frac{M_Z}{X_t}\right)^3 + \mathcal{O}\left(\left(\frac{M_Z}{X_t}\right)^4\right)\right]. \tag{C.2}$$

If $X_t = 0$, then $\mathbf{U}_{\tilde{t}} = \mathbb{1}$.

## C.2 Chargino sector

Expanding in the variable $x_\chi = M_Z/M_\chi$ yields the following expressions for the masses $(m_{\tilde{\chi}_1^\pm} < m_{\tilde{\chi}_2^\pm})$,

$$m_{\tilde{\chi}_1^\pm} = M_\chi\left(1 - \frac{1}{\sqrt{2}}c_w(c_\beta + s_\beta)x_\chi + \frac{1}{4}c_w^2(c_\beta - s_\beta)^2x_\chi^2 + \mathcal{O}(x_\chi^4)\right),$$
$$m_{\tilde{\chi}_2^\pm} = M_\chi\left(1 + \frac{1}{\sqrt{2}}c_w(c_\beta + s_\beta)x_\chi + \frac{1}{4}c_w^2(c_\beta - s_\beta)^2x_\chi^2 + \mathcal{O}(x_\chi^4)\right), \tag{C.3}$$

and mixing matrices,

$$\mathbf{U}_{11} = -\frac{1}{\sqrt{2}} + \frac{1}{4}c_w(s_\beta - c_\beta)x_\chi + \frac{1}{16\sqrt{2}}c_w^2(c_\beta - s_\beta)^2x_\chi^2 + \frac{3}{64}c_w^3(c_\beta - s_\beta)^3x_\chi^3 + \mathcal{O}(x_\chi^4),$$
$$\mathbf{U}_{12} = \frac{1}{\sqrt{2}} - \frac{1}{4}c_w(c_\beta - s_\beta)x_\chi - \frac{1}{16\sqrt{2}}c_w^2(c_\beta - s_\beta)^2x_\chi^2 + \frac{3}{64}c_w^3(c_\beta - s_\beta)^3x_\chi^3 + \mathcal{O}(x_\chi^4),$$
$$\mathbf{U}_{22} = \frac{1}{\sqrt{2}} + \frac{1}{4}c_w(c_\beta - s_\beta)x_\chi - \frac{1}{16\sqrt{2}}c_w^2(c_\beta - s_\beta)^2x_\chi^2 - \frac{3}{64}c_w^3(c_\beta - s_\beta)^3x_\chi^3 + \mathcal{O}(x_\chi^4),$$
$$\mathbf{U}_{21} = \mathbf{U}_{12}, \tag{C.4}$$

$$\mathbf{V}_{11} = -\frac{1}{\sqrt{2}} + \frac{1}{4}c_w(c_\beta - s_\beta)x_\chi + \frac{1}{16\sqrt{2}}c_w^2(c_\beta - s_\beta)^2x_\chi^2 - \frac{3}{64}c_w^3(c_\beta - s_\beta)^3x_\chi^3 + \mathcal{O}(x_\chi^4),$$
$$\mathbf{V}_{12} = \frac{1}{\sqrt{2}} + \frac{1}{4}c_w(c_\beta - s_\beta)x_\chi - \frac{1}{16\sqrt{2}}c_w^2(c_\beta - s_\beta)^2x_\chi^2 - \frac{3}{64}c_w^3(c_\beta - s_\beta)^3x_\chi^3 + \mathcal{O}(x_\chi^4),$$
$$\mathbf{V}_{22} = \frac{1}{\sqrt{2}} - \frac{1}{4}c_w(c_\beta - s_\beta)x_\chi - \frac{1}{16\sqrt{2}}c_w^2(c_\beta - s_\beta)^2x_\chi^2 + \frac{3}{64}c_w^3(c_\beta - s_\beta)^3x_\chi^3 + \mathcal{O}(x_\chi^4),$$
$$\mathbf{V}_{21} = \mathbf{V}_{12} \tag{C.5}$$

of the charginos (see Section 4.4).

Logarithmic contributions in Higgs self-energies proportional to $M_\chi$ cancel in the final expression. Therefore, to get all terms of the order $\mathcal{O}(x_\chi^0)$ in a consistent way, terms up to the order $\mathcal{O}(x_\chi^3)$ have to be kept, because e.g. in tadpole diagrams terms containing factors like $m_{\tilde{\chi}_1^\pm}^3 \propto x_Z^{-3}$ arise.

## C.3 Neutralino sector

The masses and mixing matrix of the neutralino sector (see Section 4.5) expanded in the variable $x_\chi = M_Z/M_\chi$ are given by $(m_{\tilde{\chi}_1^0} < m_{\tilde{\chi}_2^0} < m_{\tilde{\chi}_3^0} < m_{\tilde{\chi}_4^0})$

$$m_{\tilde{\chi}_1^0} = M_\chi \left( 1 - \frac{1}{\sqrt{2}}(c_\beta + s_\beta)x_\chi + \frac{1}{8}(c_\beta - s_\beta)^2 x_\chi^2 + \frac{1}{128\sqrt{2}} \frac{1 + 4s_{2\beta} + 5c_{4\beta}}{s_\beta + c_\beta} x_\chi^3 + \mathcal{O}(x_\chi^4) \right),$$

$$m_{\tilde{\chi}_2^0} = M_\chi,$$

$$m_{\tilde{\chi}_3^0} = M_\chi \left( 1 + \frac{1}{4}(c_\beta - s_\beta)^2 x_\chi^2 + \mathcal{O}(x_\chi^4) \right),$$

$$m_{\tilde{\chi}_4^0} = M_\chi \left( 1 + \frac{1}{\sqrt{2}}(c_\beta + s_\beta)x_\chi + \frac{1}{8}(c_\beta - s_\beta)^2 x_\chi^2 - \frac{1}{128\sqrt{2}} \frac{1 + 4s_{2\beta} + 5c_{4\beta}}{s_\beta + c_\beta} x_\chi^3 + \mathcal{O}(x_\chi^4) \right),$$

$$\tag{C.6}$$

$$\mathbf{N}_{11} = s_w \left( \frac{1}{\sqrt{2}} - \frac{1}{16} \frac{(c_\beta - s_\beta)^2}{c_\beta + s_\beta} x_\chi - \frac{1}{256\sqrt{2}} \frac{(c_\beta - s_\beta)^2 (2 + 15(c_\beta + s_\beta)^2)}{(c_\beta + s_\beta)} x_\chi^2 \right.$$
$$\left. - \frac{1}{8192} \frac{(c_\beta - s_\beta)^2 (396 s_{2\beta} - 125 c_{4\beta} + 247)}{(c_\beta + s_\beta)^3} x_\chi^3 \right) + \mathcal{O}(x_\chi^4),$$

$$\mathbf{N}_{12} = c_w \left( -\frac{1}{\sqrt{2}} + \frac{1}{16} \frac{(c_\beta - s_\beta)^2}{c_\beta + s_\beta} x_\chi + \frac{1}{256\sqrt{2}} \frac{(c_\beta - s_\beta)^2 (2 + 15(c_\beta + s_\beta)^2)}{(c_\beta + s_\beta)} x_\chi^2 \right.$$
$$\left. + \frac{1}{8192} \frac{(c_\beta - s_\beta)^2 (396 s_{2\beta} - 125 c_{4\beta} + 247)}{(c_\beta + s_\beta)^3} x_\chi^3 \right) + \mathcal{O}(x_\chi^4),$$

$$\mathbf{N}_{13} = \frac{1}{2} + \frac{1}{16\sqrt{2}} \frac{-1 + 4c_{2\beta} + s_{2\beta}}{c_\beta + s_\beta} x_\chi + \frac{1}{1024} \frac{-3 - 48c_{2\beta} + c_{4\beta} + 4s_{2\beta} - 40s_{4\beta}}{(c_\beta + s_\beta)^2} x_\chi^2$$
$$- \frac{1}{16384\sqrt{2}} \frac{-29s_{2\beta} + 528s_{4\beta} + 19s_{6\beta} + 140c_{2\beta} + 78c_{4\beta} - 284c_{6\beta} + 126}{(s_\beta + c_\beta)^3} x_\chi^3$$
$$+ \mathcal{O}(x_\chi^4),$$

$$\mathbf{N}_{14} = -\frac{1}{2} + \frac{1}{16\sqrt{2}} \frac{-1 - 4c_{2\beta} + s_{2\beta}}{c_\beta + s_\beta} x_\chi - \frac{1}{1024} \frac{-3 + 48c_{2\beta} + c_{4\beta} + 4s_{2\beta} + 40s_{4\beta}}{(c_\beta + s_\beta)^2} x_\chi^2$$
$$+ \frac{1}{16384\sqrt{2}} \frac{-29s_{2\beta} + 528s_{4\beta} + 19s_{6\beta} - 140c_{2\beta} + 78c_{4\beta} + 284c_{6\beta} + 126}{(s_\beta + c_\beta)^3} x_\chi^3$$
$$+ \mathcal{O}(x_\chi^4),$$

$$\mathbf{N}_{21} = c_w,$$

$$\mathbf{N}_{22} = s_w,$$

$$\mathbf{N}_{23} = 0,$$

$$\mathbf{N}_{24} = 0,$$

$$\mathbf{N}_{31} = is_w \left( \frac{1}{2\sqrt{2}}(c_\beta - s_\beta)x_\chi - \frac{1}{32\sqrt{2}}(c_\beta - s_\beta)(1 - 5s_{2\beta})x_\chi^3 \right) + \mathcal{O}(x_\chi^4),$$

$$\mathbf{N}_{32} = -ic_w \left( \frac{1}{2\sqrt{2}}(c_\beta - s_\beta)x_\chi - \frac{1}{32\sqrt{2}}(c_\beta - s_\beta)(1 - 5s_{2\beta})x_\chi^3 \right) + \mathcal{O}(x_\chi^4),$$

$$\mathbf{N}_{33} = i \left( \frac{1}{\sqrt{2}} + \frac{1}{16\sqrt{2}}(c_\beta - s_\beta)(-1 + 2c_{2\beta} + s_{2\beta})x_\chi^2 \right) + \mathcal{O}(x_\chi^4),$$

$$\mathbf{N}_{34} = i \left( \frac{1}{\sqrt{2}} - \frac{1}{16\sqrt{2}} (c_\beta - s_\beta)(1 + 2c_{2\beta} - s_{2\beta}) x_\chi^2 \right) + \mathcal{O}(x_\chi^4),$$

$$\mathbf{N}_{41} = s_w \left( -\frac{1}{\sqrt{2}} - \frac{1}{16} \frac{(c_\beta - s_\beta)^2}{c_\beta + s_\beta} x_\chi + \frac{1}{256\sqrt{2}} \frac{(c_\beta - s_\beta)^2 (2 + 15(c_\beta + s_\beta)^2)}{(c_\beta + s_\beta)} x_\chi^2 \right.$$
$$\left. -\frac{1}{8192} \frac{(c_\beta - s_\beta)^2 (396 s_{2\beta} - 125 c_{4\beta} + 247)}{(c_\beta + s_\beta)^3} x_\chi^3 \right) + \mathcal{O}(x_\chi^4),$$

$$\mathbf{N}_{42} = c_w \left( \frac{1}{\sqrt{2}} - \frac{1}{16} \frac{(c_\beta - s_\beta)^2}{c_\beta + s_\beta} x_\chi + \frac{1}{256\sqrt{2}} \frac{(c_\beta - s_\beta)^2 (2 + 15(c_\beta + s_\beta)^2)}{(c_\beta + s_\beta)} x_\chi^2 \right.$$
$$\left. +\frac{1}{8192} \frac{(c_\beta - s_\beta)^2 (396 s_{2\beta} - 125 c_{4\beta} + 247)}{(c_\beta + s_\beta)^3} x_\chi^3 \right) + \mathcal{O}(x_\chi^4),$$

$$\mathbf{N}_{43} = \frac{1}{2} - \frac{1}{16\sqrt{2}} \frac{-1 + 4c_{2\beta} + s_{2\beta}}{c_\beta + s_\beta} x_\chi + \frac{1}{1024} \frac{-3 - 48c_{2\beta} + c_{4\beta} + 4s_{2\beta} - 40s_{4\beta}}{(c_\beta + s_\beta)^2} x_\chi^2$$
$$+ \frac{1}{16384\sqrt{2}} \frac{-29 s_{2\beta} + 528 s_{4\beta} + 19 s_{6\beta} + 140 c_{2\beta} + 78 c_{4\beta} - 284 c_{6\beta} + 126}{(s_\beta + c_\beta)^3} x_\chi^3$$
$$+ \mathcal{O}(x_\chi^4),$$

$$\mathbf{N}_{44} = -\frac{1}{2} - \frac{1}{16\sqrt{2}} \frac{-1 - 4c_{2\beta} + s_{2\beta}}{c_\beta + s_\beta} x_\chi - \frac{1}{1024} \frac{-3 + 48c_{2\beta} + c_{4\beta} + 4s_{2\beta} + 40s_{4\beta}}{(c_\beta + s_\beta)^2} x_\chi^2$$
$$- \frac{1}{16384\sqrt{2}} \frac{-29 s_{2\beta} + 528 s_{4\beta} + 19 s_{6\beta} - 140 c_{2\beta} + 78 c_{4\beta} + 284 c_{6\beta} + 126}{(s_\beta + c_\beta)^3} x_\chi^3$$
$$+ \mathcal{O}(x_\chi^4). \tag{C.7}$$

Again, terms up to $\mathcal{O}(x_\chi^3)$ are kept because of diagrams involving factor like $m_{\tilde\chi^0}^3$.

## C.4   Higgs sector

If the mass of the A-boson $M_A$ is assumed to be much higher than the electroweak scale $\mathcal{O}(M_Z)$, the tree-level expressions for the Higgs-boson masses (see Section 4.6) can be expanded in the variable $x_A = M_Z/M_A$,

$$m_h^2 = M_A^2 \left( c_{2\beta}^2 x_A^2 + \mathcal{O}(x_A^3) \right),$$
$$m_H^2 = M_A^2 \left( 1 + s_{2\beta}^2 x_A^2 + \mathcal{O}(x_A^3) \right),$$
$$m_{H^\pm}^2 = M_A^2 \left( 1 + c_w^2 x_A^2 \right). \tag{C.8}$$

Also the relation between $\alpha$ and $\beta$ (see (4.47), (4.48)) can be expanded in the limit $M_A \gg M_Z$, resulting in the expressions

$$s_\alpha = -c_\beta + \frac{1}{2} s_\beta s_{4\beta} x_A^2 + \mathcal{O}(x_A^3),$$
$$c_\alpha = s_\beta + 2 s_\beta c_{2\beta} c_\beta^2 x_A^2 + \mathcal{O}(x_A^3). \tag{C.9}$$

All other possible trigonometric functions involving $\alpha$ are expanded similarly.

# Appendix D

# One-loop functions
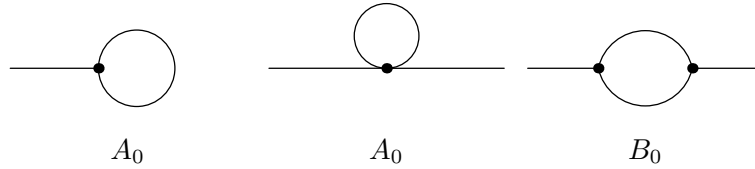


Figure D.1: Feynman diagrams of generic one-loop integrals (up to two-point function).

The loop functions used in this thesis (one-loop one- and two-point functions) are listed below (the corresponding generic topologies are displayed in Figure D.1),

$$A_0(m^2) = \mu^{4-D}\frac{16\pi^2}{i}\int\frac{d^Dk}{(2\pi)^D}\frac{1}{k^2 - m^2} =$$
$$= m^2(\Delta + 1 - \ln\frac{m^2}{\mu^2}), \tag{D.1a}$$

$$B_0(q^2, m_1^2, m_2^2) = \mu^{4-D}\frac{16\pi^2}{i}\int\frac{d^Dk}{(2\pi)^D}\frac{1}{(k^2 - m_1^2)((k+q)^2 - m_2^2)} =$$
$$= \Delta + \frac{m_1^2 - m_2^2 + p^2}{2p^2}\ln\frac{m_1^2}{\mu^2} + \frac{m_2^2 - m_1^2 + p^2}{2p^2}\ln\frac{m_2^2}{\mu^2} +$$
$$+ \frac{R}{2p^2}\left(\ln\frac{m_1^2 + m_2^2 - p^2 + R}{\mu^2} - \ln\frac{m_1^2 + m_2^2 - p^2 - R}{\mu^2}\right), \tag{D.1b}$$

$$B_\mu(q^2, m_1^2, m_2^2) = \mu^{4-D}\frac{16\pi^2}{i}\int\frac{d^Dk}{(2\pi)^D}\frac{k_\mu}{(k^2 - m_1^2)((k+q)^2 - m_2^2)} =$$
$$\equiv q_\mu B_1(p^2, m_1^2, m_2^2), \tag{D.1c}$$

$$B_{\mu\nu}(q^2, m_1^2, m_2^2) = \mu^{4-D}\frac{16\pi^2}{i}\int\frac{d^Dk}{(2\pi)^D}\frac{k_\mu k_\nu}{(k^2 - m_1^2)((k+q)^2 - m_2^2)} =$$
$$\equiv g_{\mu\nu}B_{00}(p^2, m_1^2, m_2^2) + q_\mu q_\nu B_{11}(p^2, m_1^2, m_2^2) \tag{D.1d}$$

with $R = \sqrt{(m_1^2 - m_2^2)^2 + p^2(p^2 - 2m_1^2 - 2m_2^2)}$. Note that $m^2$ has to be understood as $m^2 - i\epsilon$ (with $\epsilon > 0$ being infinitesimally small) to regulate singularities of the integrand. The functions

$B_1$ and $B_{00}$ are given by ($B_{11}$ does not appear in this thesis)

$$B_1(q^2, m_1^2, m_2^2) = \frac{1}{2p^2} \left[ A_0(m_1^2) - A_0(m_2^2) - (p^2 - m_2^2 + m_1^2) B_0(p^2, m_1^2, m_2^2) \right], \quad \text{(D.2a)}$$

$$B_{00}(q^2, m_1^2, m_2^2) = \frac{1}{2(3 - 2\epsilon)} \cdot$$
$$\left[ A_0(m_2^2) + 2m_1^2 B_0(p^2, m_1^2, m_2^2) + (p^2 - m_2^2 + m_1^2) B_1(p^2, m_1^2, m_2^2) \right]. \quad \text{(D.2b)}$$

In this way, all one-loop (one- and two-point) integrals can be expressed in terms of the scalar functions $A_0$ and $B_0$. This procedure is called Passarino-Veltman reduction [64].

# Appendix E

# Running of tan$\beta$ - numerical analysis

In Section 7.4, the issues concerning the running of $\tan\beta$ are discussed. The following strategies are proposed,

1. ignoring the running of $\tan\beta$ and identifying $t_\beta(m_t)$ with $t_\beta(M_S)$.

2. using an one-loop fixed-order expression to relate $t_\beta(m_t)$ to $t_\beta(M_S)$ (derived using the one-loop RGE in Eq. (7.15)).

3. using the one-loop RGE of $\tan\beta$ to relate $t_\beta(m_t)$ to $t_\beta(M_S)$.

4. using the two-loop RGE of $\tan\beta$ to relate $t_\beta(m_t)$ to $t_\beta(M_S)$ neglecting possible threshold corrections.

In this appendix, the different approaches are compared numerically.

In Figure E.1, $\Delta M_h$ is plotted against $M_S$ for $\tan\beta = 10$ and $X_t/M_S = 10$. Here, $\Delta M_h$ is defined by

$$\Delta M_h = M_h(\text{using method 1}) - M_h(\text{using method 2-4}). \tag{E.1}$$

As noted in Section 7.4, ignoring the running of $t_\beta$ introduces an error already at the one-loop level. Using the one-loop fixed-order formula

$$t_\beta(M_S) = t_\beta(m_t) - \frac{3}{2}kh_t^2(m_t)\frac{1 + t_\beta^2(m_t)}{t_\beta(m_t)}\ln\frac{M_S^2}{m_t^2}, \tag{E.2}$$

the error is corrected at the one-loop level shifting $M_h$ up by $\sim 0.1 - 0.2$ GeV. Running $\tan\beta$ between $Q = m_t$ and $Q = M_S$ using the one-loop RGE given in Eq. (7.15) increases $M_h$ again by up to $\sim 0.04$ GeV for $M_S \sim 20$ TeV. Using the two-loop RGE [56,57]

$$\frac{1}{\tan^2\beta}\frac{d\tan^2\beta}{dt} = -3k\tilde{h}_t^2 + k^2\left[9\tilde{h}_t^4 - \left(\frac{4}{3}g'^2 + 16g_3^2\right)\tilde{h}_t^2\right], \tag{E.3}$$

$M_h$ is only marginally shifted downwards ($< 0.01$ GeV). Of course possible threshold corrections as well as modifications of the RGE if passing below thresholds are ignored. Nevertheless, even this incomplete two-loop running should give a reliable estimate of the size of these NLL corrections. The minor impact shows that the two-loop running is most probably negligible.

In conclusion, all corrections found due to the running of $\tan\beta$ are smaller than 0.2 GeV and therefore within the theoretical errors of the whole calculation [31] negligible.
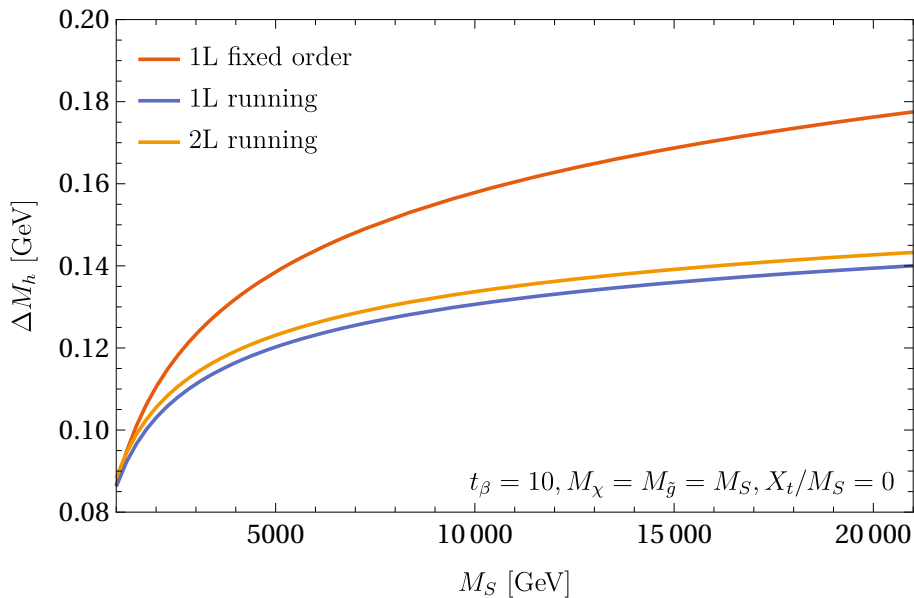


Figure E.1: Corrections of $M_h$ over $M_S$ for different ways to run $\tan\beta$ between $Q = m_t$ and $Q = M_S$ ($t_\beta = 10$).

Choosing a smaller value for $t_\beta(m_t)$ changes the situation (see Figure E.2 showing basically the same as in Figure E.1 but for $t_\beta(m_t) = 3$). Using method 2 decreases $M_h$ by up to $\sim 1.5$ GeV in comparison with method 1. This is a quite significant shift showing that the running of $\tan\beta$ is not negligible for small $t_\beta(m_t)$. If one-loop running is taken into account, $M_h$ is increased in comparison to method 2 by up to $\sim 0.3$ GeV. Two-loop running is again negligible.

The fact that the shift induced by one-loop running is of order $\mathcal{O}(100)$ MeV further justifies the approach chosen. The one-loop iterative solution shows that $\tan\beta$ has to be seen as a running quantity, because otherwise the one-loop Feynman-diagrammatic result is not reproduced. So, at least method 2 has to be used. Even if we assume that method 3, which is in some sense an extension of method 2, is used, is completely wrong, the induced error should still be well below the overall theoretical uncertainty [31].
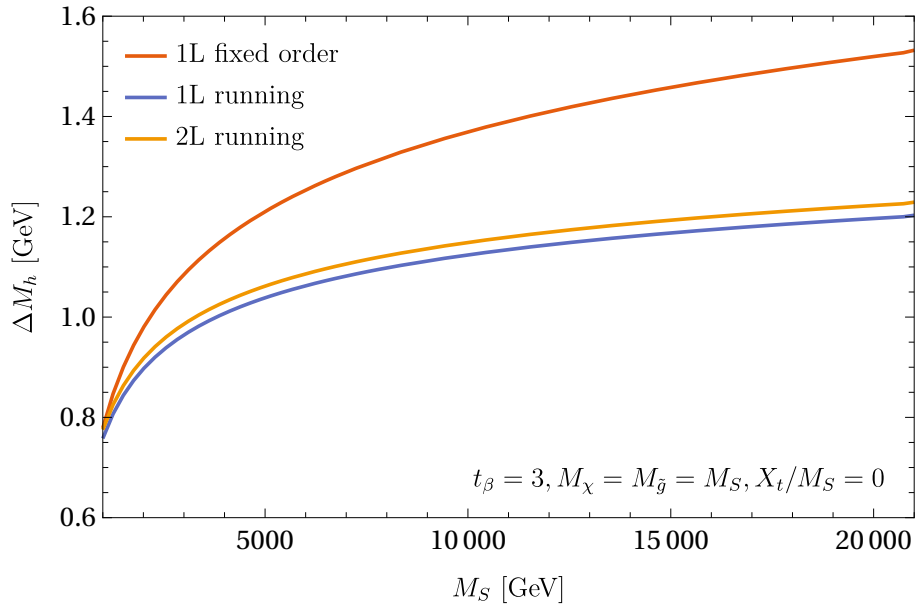
Figure E.2: Corrections of $M_h$ over $M_S$ for different ways to run $\tan\beta$ between $Q = m_t$ and $Q = M_S$ ($t_\beta = 3$).

# Appendix F

# Explicit 2- and 3-loop expressions

In this part of the appendix, analytic expressions obtained by solving the RGEs iteratively are given. They are derived in the special case that all sparticles share the common mass scale $M_S$ (i.e. $M_\chi = M_{\tilde{g}} = M_S$). The following abbreviations are used:

$$L \equiv \ln \frac{M_S^2}{m_t^2} \tag{F.1}$$

$$\hat{X}_t \equiv \frac{X_t^{\text{OS}}}{M_S} \tag{F.2}$$

The 2-loop leading logarithms contributing to the mass of the lightest Higgs-boson (including weak gauge couplings) are given by

$$(\Delta M_h^2)^{\text{2L,LL}} =$$

$$2v^2 \frac{L^2}{73728\pi} \Bigg\{ -55296\alpha_t^2 \big(16\alpha_s - 3\alpha_t\big)$$

$$+ \frac{4\alpha}{s_w^4 c_w^4} \bigg[ 24\Big( -2\big(745\alpha^2 + 54\alpha\alpha_t + 54\alpha_t^2\big)c_{4\beta} - 1544\alpha^2$$

$$+ 3\alpha_t c_{2\beta}\big(116\alpha - 48\alpha_s + 9\alpha_t\big) - 216\alpha\alpha_t c_{6\beta} + 3\alpha\big(22\alpha - 9\alpha_t\big)c_{8\beta} + 297\alpha\alpha_t - 102\alpha_t^2\Big)$$

$$+ 96c_{2w}\big(77\alpha^2 c_{4\beta} + 47\alpha^2 - 267\alpha\alpha_t c_{2\beta} + 54\alpha\alpha_t + 6\alpha_t^2\big)$$

$$+ \frac{2\alpha^2}{s_w^2}\big(9c_{4\beta} + 20\big)\big(4c_{4\beta} + 9c_{8\beta} + 211\big) + \frac{2\alpha^2}{c_w^2}\big(9c_{4\beta} - 82\big)\big(-164c_{4\beta} + 9c_{8\beta} - 101\big)$$

$$+ 72\alpha_t c_{4w}\Big(c_{2\beta}\big(44\alpha + 48\alpha_s - 9\alpha_t\big) + 18\alpha + 36\alpha_t c_{4\beta} + 34\alpha_t\Big) - 576\alpha_t^2 c_{6w}\bigg] \Bigg\}. \tag{F.3}$$

The corresponding 2-loop subleading logarithms (including weak gauge couplings) are given by

$$(\Delta M_h^2)^{\text{2L,NLL}} =$$

$$2v^2 \frac{L}{73728\pi} \frac{1}{s_w^4 c_w^4} \cdot$$

$$\Bigg\{ \frac{\alpha^3}{s_w^2}\big(91392s_{2\beta} + 22944s_{6\beta} - 864s_{10\beta} + 83569c_{4\beta} - 8694c_{8\beta} - 945c_{12\beta} - 167114\big)$$

$$+ \frac{\alpha^3}{c_w^2}\Big(-171904s_{2\beta} + 14176s_{6\beta} - 288s_{10\beta} + 40689c_{4\beta} + 23274c_{8\beta} - 945c_{12\beta} - 94250\Big)$$

$$+ 4\alpha c_{2w}\bigg[3\Big(16\big(716\alpha^2 - 16\alpha\alpha_s + 391\alpha\alpha_t - 8\alpha_t^2\big)$$

$$+ 192\alpha\Big(19(\alpha_t - \alpha)s_{2\beta} + 3\alpha_t s_{4\beta} + 14\alpha_t/t_\beta\Big) + 7\alpha_t\hat{X}_t^2\big(739\alpha + 66\alpha_t\big) - 45\alpha_t^2\hat{X}_t^4\Big)$$

$$- \alpha c_{4\beta}\Big(64\big(11\alpha - 9\alpha_t\big)s_{2\beta} + 704\alpha + 768\alpha_s - 2217\alpha_t\hat{X}_t^2 + 816\alpha_t\Big)\bigg]$$

$$+ 48c_{4w}\bigg[2\alpha^2\Big(80\alpha_s + \alpha_t\big(671 - 56\hat{X}_t^2\big)\Big) + \alpha\Big(c_{4\beta}\big(2\alpha(80\alpha_s - 8\alpha_t\hat{X}_t^2 - 13\alpha_t)$$

$$+ 3\alpha_t(80\alpha_s - 3\alpha_t(3\hat{X}_t^4 - 50\hat{X}_t^2 + 1))\big) + 24\alpha_t c_{2\beta}\big(3\alpha_t\hat{X}_t^2 - 2\alpha\big) + 192\alpha\alpha_t\Big(s_{2\beta} + \frac{1}{t_\beta}\Big)\Big)$$

$$+ \alpha\alpha_t\Big(240\alpha_s + \alpha_t\big(23\hat{X}_t^4 + 462\hat{X}_t^2 - 73\big)\Big)$$

$$+ 6\alpha_t^2\Big(32\alpha_s\big(3\hat{X}_t^2 - 2\big) + 3\alpha_t\big(\hat{X}_t^2 + 2\big)\big(\hat{X}_t^4 - 8\hat{X}_t^2 + 10\big)\Big)\bigg]$$

$$+ 8\bigg[48608\alpha^3 + 2\alpha\Big(3c_{4\beta}\big(-2128\alpha^2 + \alpha(480\alpha_s + 448\alpha_t\hat{X}_t^2 + 778\alpha_t)$$

$$+ 3\alpha_t\big(3\alpha_t(3\hat{X}_t^4 - 50\hat{X}_t^2 + 1) - 80\alpha_s\big)\Big)$$

$$- 216\alpha_t c_{2\beta}\big(\alpha_t\hat{X}_t^2 - 18\alpha\big) + 4\alpha\Big(9\alpha_t\big(3(\hat{X}_t^2 + 9)c_{8\beta} + 72c_{6\beta}$$

$$+ 4\big(33s_{2\beta} + 6s_{4\beta} + s_{6\beta} + 24/t_\beta\big)\big)$$

$$- 8\alpha(21s_{2\beta} + 29s_{6\beta} + 27c_{8\beta})\Big)\Big) + 12\alpha^2\Big(240\alpha_s + \alpha_t\big(2327 - 178\hat{X}_t^2\big)\Big)$$

$$- 6\alpha\alpha_t\Big(240\alpha_s + \alpha_t\big(20\hat{X}_t^2(\hat{X}_t^2 + 24) - 73\big)\Big) - 27\alpha_t^2\Big(32\alpha_s\big(3\hat{X}_t^2 - 2\big)$$

$$+ 3\alpha_t\big(\hat{X}_t^2 + 2\big)\big(\hat{X}_t^4 - 8\hat{X}_t^2 + 10\big)\Big)\bigg]$$

$$- 72\alpha_t^2 c_{8w}\bigg[2\alpha\big(\hat{X}_t^2 - 6\big)\hat{X}_t^2 + 32\alpha_s\big(3\hat{X}_t^2 - 2\big) + 3\alpha_t\big(\hat{X}_t^2 + 2\big)\big(\hat{X}_t^4 - 8\hat{X}_t^2 + 10\big)\bigg]$$

$$- 78\alpha\alpha_t^2\hat{X}_t^2\big(\hat{X}_t^2 - 6\big)c_{10w}$$

$$+ 6\alpha\alpha_t c_{6w}\bigg[2\hat{X}_t^2\big(91\alpha - 501\alpha_t\big) + 26\alpha\hat{X}_t^2 c_{4\beta} + 103\alpha_t\hat{X}_t^4 + 256\alpha_t\bigg]\bigg\}. \tag{F.4}$$

Neglecting the weak gauge couplings, a compact expressions for the leading and subleading logarithms up to the 3-loop level can be given,

$$\big(\Delta M_h^2\big)^{\text{1L-3L,LL+NLL}} =$$

$$= M_{h,tree}^2 + m_t^2\bigg\{\frac{3\alpha_t}{\pi}L$$

$$+ \frac{3\alpha_t}{8\pi^2}\big[3\alpha_t - 16\alpha_s\big]L^2$$

$$+ \frac{\alpha_t}{16\pi^2}\bigg[\alpha_s\Big(64 - 96\hat{X}_t^2\Big) - 3\alpha_t\Big(20 - 6\hat{X}_t^2 - 6\hat{X}_t^4 + \hat{X}_t^6\Big)\bigg]L+$$

$$+\frac{\alpha_t}{64\pi^3}\left[736\alpha_s^2 - 240\alpha_s\alpha_t - 99\alpha_t^2\right]L^3+$$
$$-\frac{\alpha_t}{512\pi^3}\left[64\alpha_s^2\left(254 - 36\hat{X}_t^2 + \hat{X}_t^4\right) + 96\alpha_s\alpha_t\left(-84 + 18\hat{X}_t^2 + 18\hat{X}_t^4 + \hat{X}_t^6\right)\right.$$
$$\left.+9\alpha_t^2\left(320 + 306\hat{X}_t^2 - 63\hat{X}_t^4 - 4\hat{X}_t^6 + 3\hat{X}_t^8\right)\right]L^2\Bigg\}. \tag{F.5}$$

All couplings appearing in the presented expressions have to be evaluated at $Q = m_t$.

# Bibliography

[1] D. Hanneke, S. Fogwell, and G. Gabrielse. New Measurement of the Electron Magnetic Moment and the Fine Structure Constant. *Phys.Rev.Lett.*, 100:120801, 2008, arXiv:0801.1134.

[2] T. Aoyama, M. Hayakawa, T. Kinoshita, and M. Nio. Tenth-Order QED Contribution to the Electron g-2 and an Improved Value of the Fine Structure Constant. *Phys.Rev.Lett.*, 109:111807, 2012, arXiv:1205.5368.

[3] P. W. Higgs. Broken Symmetries and the Masses of Gauge Bosons. *Phys.Rev.Lett.*, 13:508–509, 1964.

[4] P. W. Higgs. Broken symmetries, massless particles and gauge fields. *Phys.Lett.*, 12:132–133, 1964.

[5] F. Englert and R. Brout. Broken Symmetry and the Mass of Gauge Vector Mesons. *Phys.Rev.Lett.*, 13:321–323, 1964.

[6] G. Aad et al. Observation of a new particle in the search for the Standard Model Higgs boson with the ATLAS detector at the LHC. *Phys.Lett.*, B716:1–29, 2012, arXiv:1207.7214.

[7] S. Chatrchyan et al. Observation of a new boson at a mass of 125 GeV with the CMS experiment at the LHC. *Phys.Lett.*, B716:30–61, 2012, arXiv:1207.7235.

[8] G. Aad et al. Combined Measurement of the Higgs Boson Mass in $pp$ Collisions at $\sqrt{s} = 7$ and 8 TeV with the ATLAS and CMS Experiments. 2015, arXiv:1503.07589.

[9] J. P. Miller, E. de Rafael, and B. L. Roberts. Muon (g-2): Experiment and theory. *Rept.Prog.Phys.*, 70:795, 2007, hep-ph/0703049.

[10] B. Pontecorvo. Mesonium and anti-mesonium. *Sov.Phys.JETP*, 6:429, 1957.

[11] B. Pontecorvo. Neutrino Experiments and the Problem of Conservation of Leptonic Charge. *Sov.Phys.JETP*, 26:984–988, 1968.

[12] P. H. Chankowski, S. Pokorski, and J. Rosiek. Complete on-shell renormalization scheme for the minimal supersymmetric Higgs sector. *Nucl.Phys.*, B423:437–496, 1994, hep-ph/9303309.

[13] A. Dabelstein. The One loop renormalization of the MSSM Higgs sector and its application to the neutral scalar Higgs masses. *Z.Phys.*, C67:495–512, 1995, hep-ph/9409375.

[14] D. M. Pierce, J. A. Bagger, K. T. Matchev, and R. Zhang. Precision corrections in the minimal supersymmetric standard model. *Nucl.Phys.*, B491:3–67, 1997, hep-ph/9606211.

[15] S. Heinemeyer, W. Hollik, and G. Weiglein. Precise prediction for the mass of the lightest Higgs boson in the MSSM. *Phys.Lett.*, B440:296–304, 1998, hep-ph/9807423.

[16] S. Heinemeyer, W. Hollik, and G. Weiglein. QCD corrections to the masses of the neutral CP - even Higgs bosons in the MSSM. *Phys.Rev.*, D58:091701, 1998, hep-ph/9803277.

[17] S. Heinemeyer, W. Hollik, and G. Weiglein. The Masses of the neutral CP - even Higgs bosons in the MSSM: Accurate analysis at the two loop level. *Eur.Phys.J.*, C9:343–366, 1999, hep-ph/9812472.

[18] S. Heinemeyer, W. Hollik, and G. Weiglein. The Mass of the lightest MSSM Higgs boson: A Compact analytical expression at the two loop level. *Phys.Lett.*, B455:179–191, 1999, hep-ph/9903404.

[19] S. Heinemeyer, W. Hollik, H. Rzehak, and G. Weiglein. High-precision predictions for the MSSM Higgs sector at O(alpha(b) alpha(s)). *Eur.Phys.J.*, C39:465–481, 2005, hep-ph/0411114.

[20] R. Zhang. Two loop effective potential calculation of the lightest CP even Higgs boson mass in the MSSM. *Phys.Lett.*, B447:89–97, 1999, hep-ph/9808299.

[21] J. R. Espinosa and R. Zhang. MSSM lightest CP even Higgs boson mass to O(alpha(s) alpha(t)): The Effective potential approach. *JHEP*, 0003:026, 2000, hep-ph/9912236.

[22] G. Degrassi, P. Slavich, and F. Zwirner. On the neutral Higgs boson masses in the MSSM for arbitrary stop mixing. *Nucl.Phys.*, B611:403–422, 2001, hep-ph/0105096.

[23] R. Hempfling and A. H. Hoang. Two loop radiative corrections to the upper limit of the lightest Higgs boson mass in the minimal supersymmetric model. *Phys.Lett.*, B331:99–106, 1994, hep-ph/9401219.

[24] A. Brignole, G. Degrassi, P. Slavich, and F. Zwirner. On the two loop sbottom corrections to the neutral Higgs boson masses in the MSSM. *Nucl.Phys.*, B643:79–92, 2002, hep-ph/0206101.

[25] A. Dedes, G. Degrassi, and P. Slavich. On the two loop Yukawa corrections to the MSSM Higgs boson masses at large tan beta. *Nucl.Phys.*, B672:144–162, 2003, hep-ph/0305127.

[26] M. S. Carena, M. Quiros, and C. E. M. Wagner. Effective potential methods and the Higgs mass spectrum in the MSSM. *Nucl.Phys.*, B461:407–436, 1996, hep-ph/9508343.

[27] J. A. Casas, J. R. Espinosa, M. Quiros, and A. Riotto. The Lightest Higgs boson mass in the minimal supersymmetric standard model. *Nucl.Phys.*, B436:3–29, 1995, hep-ph/9407389.

[28] A. Brignole, G. Degrassi, P. Slavich, and F. Zwirner. On the O(alpha(t)**2) two loop corrections to the neutral Higgs boson masses in the MSSM. *Nucl.Phys.*, B631:195–218, 2002, hep-ph/0112177.

[29] J. R. Espinosa and R. Zhang. Complete two loop dominant corrections to the mass of the lightest CP even Higgs boson in the minimal supersymmetric standard model. *Nucl.Phys.*, B586:3–38, 2000, hep-ph/0003246.

[30] S. Heinemeyer, W. Hollik, and G. Weiglein. FeynHiggs: A Program for the calculation of the masses of the neutral CP even Higgs bosons in the MSSM. *Comput.Phys.Commun.*, 124:76–89, 2000, hep-ph/9812320.

[31] G. Degrassi, S. Heinemeyer, W. Hollik, P. Slavich, and G. Weiglein. Towards high precision predictions for the MSSM Higgs sector. *Eur.Phys.J.*, C28:133–143, 2003, hep-ph/0212020.

[32] H. E. Haber and R. Hempfling. The Renormalization group improved Higgs sector of the minimal supersymmetric model. *Phys.Rev.*, D48:4280–4309, 1993, hep-ph/9307201.

[33] H. E. Haber, R. Hempfling, and A. H. Hoang. Approximating the radiatively corrected Higgs mass in the minimal supersymmetric model. *Z.Phys.*, C75:539–554, 1997, hep-ph/9609331.

[34] M. S. Carena, H. E. Haber, S. Heinemeyer, W. Hollik, C. E. M. Wagner, et al. Reconciling the two loop diagrammatic and effective field theory computations of the mass of the lightest CP - even Higgs boson in the MSSM. *Nucl.Phys.*, B580:29–57, 2000, hep-ph/0001002.

[35] G. F. Giudice and A. Strumia. Probing High-Scale and Split Supersymmetry with Higgs Mass Measurements. *Nucl.Phys.*, B858:63–83, 2012, arXiv:1108.6077.

[36] E. Bagnaschi, G. F. Giudice, P. Slavich, and A. Strumia. Higgs Mass and Unnatural Supersymmetry. *JHEP*, 1409:092, 2014, arXiv:1407.4081.

[37] P. Draper, G. Lee, and C. E. M. Wagner. Precise Estimates of the Higgs Mass in Heavy SUSY. *Phys.Rev.*, D89(5):055023, 2014, arXiv:1312.5743.

[38] J. P. Vega and G. Villadoro. SusyHD: Higgs mass Determination in Supersymmetry. 2015, arXiv:1504.05200.

[39] T. Hahn, S. Heinemeyer, W. Hollik, H. Rzehak, and G. Weiglein. High-Precision Predictions for the Light CP -Even Higgs Boson Mass of the Minimal Supersymmetric Standard Model. *Phys.Rev.Lett.*, 112(14):141801, 2014, arXiv:1312.4937.

[40] M. E. Peskin and D. V. Schroeder. An Introduction to quantum field theory. *Addison-Wesley Publishing Company*, 1995.

[41] K. A. Olive et al. Review of Particle Physics. *Chin.Phys.*, C38:090001, 2014.

[42] S. R. Coleman and J. Mandula. All Possible Symmetries of the S Matrix. *Phys.Rev.*, 159:1251–1256, 1967.

[43] R. Haag, J. T. Lopuszanski, and M. Sohnius. All Possible Generators of Supersymmetries of the s Matrix. *Nucl.Phys.*, B88:257, 1975.

[44] S. P. Martin. A Supersymmetry primer. *Adv.Ser.Direct.High Energy Phys.*, 21:1–153, 2010, hep-ph/9709356.

[45] H. P. Nilles. Supersymmetry, Supergravity and Particle Physics. *Phys.Rept.*, 110:1–162, 1984.

[46] G. F. Giudice and R. Rattazzi. Theories with gauge mediated supersymmetry breaking. *Phys.Rept.*, 322:419–499, 1999, hep-ph/9801271.

[47] M. Frank, T. Hahn, S. Heinemeyer, W. Hollik, H. Rzehak, et al. The Higgs Boson Masses and Mixings of the Complex MSSM in the Feynman-Diagrammatic Approach. *JHEP*, 0702:047, 2007, hep-ph/0611326.

[48] T. Takagi. *Japanese J.Math.*, 1:83, 1927.

[49] S.Y. Choi, J. Kalinowski, Gudrid A. Moortgat-Pick, and P.M. Zerwas. Analysis of the neutralino system in supersymmetric theories. *Eur.Phys.J.*, C22:563–579, 2001, hep-ph/0108117.

[50] I. Jack and D. R. T. Jones. Regularization of supersymmetric theories. *Adv.Ser.Direct.High Energy Phys.*, 21:494–513, 2010, hep-ph/9707278.

[51] A. Denner. Techniques for calculation of electroweak radiative corrections at the one loop level and results for W physics at LEP-200. *Fortsch.Phys.*, 41:307–420, 1993, arXiv:0709.1075.

[52] A. Freitas and D. Stöckinger. Gauge dependence and renormalization of tan beta. pages 657–661, 2002, hep-ph/0210372.

[53] T. Hahn. Generating Feynman diagrams and amplitudes with FeynArts 3. *Comput.Phys.Commun.*, 140:418–431, 2001, hep-ph/0012260.

[54] H. E. Haber and R. Hempfling. Can the mass of the lightest Higgs boson of the minimal supersymmetric model be larger than m(Z)? *Phys.Rev.Lett.*, 66:1815–1818, 1991.

[55] C. Groß, T. Hahn, S. Heinemeyer, F. von der Pahlen, H. Rzehak, et al. New Developments in FormCalc 8.4. 2014, arXiv:1407.0235.

[56] M. Sperling, D. Stöckinger, and A. Voigt. Renormalization of vacuum expectation values in spontaneously broken gauge theories. *JHEP*, 1307:132, 2013, arXiv:1305.1548.

[57] M. Sperling, D. Stöckinger, and A. Voigt. Renormalization of vacuum expectation values in spontaneously broken gauge theories: Two-loop results. *JHEP*, 1401:068, 2014, arXiv:1310.7629.

[58] J. R. Espinosa and I. Navarro. Radiative corrections to the Higgs boson mass for a hierarchical stop spectrum. *Nucl.Phys.*, B615:82–116, 2001, hep-ph/0104047.

[59] T. Fritzsche, S. Heinemeyer, H. Rzehak, and C. Schappacher. Heavy Scalar Top Quark Decays in the Complex MSSM: A Full One-Loop Analysis. *Phys.Rev.*, D86:035014, 2012, arXiv:1111.7289.

[60] D. Buttazzo, G. Degrassi, P. P. Giardino, G. F. Giudice, F. Sala, et al. Investigating the near-criticality of the Higgs boson. *JHEP*, 1312:089, 2013, arXiv:1307.3536.

[61] P. Slavich. Presentation at "The 9th Workshop of the LHC Higgs Cross Section Working Group", 22-24 January 2015 - CERN, URL: https://indico.cern.ch/event/331452.

[62] B. Schrempp and M. Wimmer. Top quark and Higgs boson masses: Interplay between infrared and ultraviolet physics. *Prog.Part.Nucl.Phys.*, 37:1–90, 1996, hep-ph/9606386.

[63] T. Hahn. Routines for the diagonalization of complex matrices. *arXiv*, 2006, physics/0607103.

[64] G. Passarino and M. J. G. Veltman. One Loop Corrections for e+ e- Annihilation Into mu+ mu- in the Weinberg Model. *Nucl.Phys.*, B160:151, 1979.